AFOSR-TN-59-595

ASTIA Doc. No. AD 217 182

CALIFORNIA INSTITUTE OF TECHNOLOGY

Antenna Laboratory

Technical Report No. 19

ASYMMETRICALLY EXCITED ELECTROMAGNETIC RADIATION FROM CIRCULAR CYLINDERS OF FINITE LENGTH AND PROLATE SPHEROIDS

by

Hans H. Kuehl

Research supported by the

U. S. Air Force Office of Scientific Research

June 1959

ABSTRACT

The far zone radiation from two types of asymmetrically excited systems is considered. The first is a finite cylinder excited by an electric dipole in the radial direction near the cylinder. The second is a prolate spheroid excited by a narrow belt of electric field around the surface of the spheroid. In both cases the body considered is perfectly conducting and the excitation is not necessarily centered at the midplane of the body. In the case of the finite cylinder excited by a radial dipole, an approximate method is used in which the current on the finite cylinder is taken to be identical with the current which would exist on an infinite cylinder under the same excitation. This approximation is shown to be valid analytically and experimentally if the cylinder is not short. The analytic and experimental results are compared for two cylinder lengths. The turnstile antenna mounted on a finite cylinder is considered analytically and the modification of the radiation by the cylinder is exhibited. In the case of the prolate spheroid excited by a narrow belt of electric field, experimental results are compared to analytic expressions. The differences between the experimental and analytic results are considered. The considerations in obtaining accurate experimental results in both asymmetrically excited systems are discussed.

ACKNOWLEDGEMENTS

The author wishes to express his indebtedness to Professor C. H. Papas for his guidance and encouragement throughout the course of this research.

The author is grateful to Dr. C. P. Wells of Michigan State University for the use of the computed results of the asymmetrically fed spheroidal antenna. Thanks are due to Mr. Cavour Yeh for valuable assistance with the computational and experimental portion of this research, to Miss Adelheid A. Hohenlohe for the preparation of the figures, and to Mrs. Ruth Stratton for the typing of the text. The author acknowledges the Western Data Processing Center at the University of California at Los Angeles for the use of the computing facilities.

TABLE OF CONTENTS

1. INTRODUCTION

The two radiating systems to be examined here have three properties in common; the asymmetrical position of the excitation, the rotational symmetry of the excited body about an axis and the finite length of the excited body in the axial direction. The systems considered here are the cylinder of finite length excited by a radial dipole and the prolate spheroidal antenna excited by an electric field impressed across a belt on the surface of the spheroid. The asymmetry of the first case is due to the fact that the exciting dipole is not necessarily situated in the plane equidistant from the two ends of the finite cylinder, and in the second case because the exciting belt is not necessarily in the equatorial plane of the prolate spheroid.

Asymmetrically excited antennas exhibit certain properties not found in the corresponding symmetrically excited counterparts. Perhaps the most important is the asymmetry of the radiation patterns. In the cases treated here the radiation pattern is not symmetrical about the midplane of the system, whereas the symmetrically excited case must necessarily produce a symmetrical pattern. Thus the gain of an asymmetrically excited antenna may be greater than the symmetrical case since a radiation lobe on one side of the midplane may be greater than a lobe on the opposite side, whereas they must be identical for the symmetrical case. The asymmetrical case may also possess more desirable impedance properties (1).

The radiating systems considered here are of interest theoretically and also have practical application. Perhaps the most

important practical use is in communication with space vehicles. In order to obtain meaningful information via electromagnetic waves from space vehicles, it is often necessary to know the radiation pattern and polarization in the far zone. However, the radiation of the antennas on the vehicle may be greatly modified by the presence of the vehicle itself. Commonly used antennas on satellites and missiles are slots or radial linear antennas which are similar to the gap and radial dipole treated here. Also, the body of the satellite or missile usually can be approximated by the finite cylinder or spheroid. Thus the results given here can be used to predict the modification of the antenna radiation pattern by the space vehicle on which it is mounted.

The problem of the finite cylinder excited by a radial dipole is quite similar to the problem of a prolate spheroid excited by a radial dipole if the eccentricity is near unity. The radiation from either configuration is expected to be quite similar. Thus one might expect that the spheroidal problem should be attacked because a constant value of one coordinate defines the spheroid, whereas the finite cylinder is specified by a constant value of the radial coordinate over one region and a constant value of the axial coordinate over two regions leading to mathematical difficulties when the boundary conditions are to be satisfied. However, the spheroidal approach leads to considerable mathematical difficulties. The spheroidal coordinate system possesses the unfortunate property that expressions for the electromagnetic field cannot be found in spheroidal coordinates in the manner utilized in simpler coordinate systems.

The problem is to find solutions to the vector Helmholtz equation $\nabla^2 \underline{F} + k^2 \underline{F} = 0$ and difficulty arises from the fact that the vector

Helmholtz equation is not separable in spheroidal coordinates. In the vector case separability is defined in a different manner than in the scalar case (2). Separability of the vector Helmholtz equation in a particular coordinate system is defined as the process of breaking the vector solution into three components which are defined in a particular manner and are derived from the scalar Helmholtz equation. In other words, separability of the vector Helmholtz equation is possible if solutions can be found by applying certain vector operators to the solution of the scalar Helmholtz equation in that coordinate system. It can be shown (2) that of the eleven coordinate systems which allow separation of the scalar Helmholtz equation, only six allow separation of the vector Helmholtz equation. These are: rectangular, circular cylindrical, elliptic cylindrical, parabolic cylindrical, spherical, and conical coordinates. It can be shown that it is still possible to form general solutions in spheroidal coordinates using the rectangular solutions of the scalar Helmholtz equation. However, when this is done, the matching of boundary conditions becomes so complicated as to be almost impossible.

It is for these reasons that the finite cylinder was chosen rather than the spheroid with dipole excitation, since at least relatively simple solutions to the vector Helmholtz equation are known, although the difficulty of the boundary conditions remains. This is overcome by using an approximation described in Chap. 2 .

There is one special case where the vector Helmholtz equation can be solved in spheroidal coordinates in a manner such that boundary conditions can be easily satisfied. This is the case where the

solution is independent of ϕ, the angle of rotation about the axis of symmetry. For this reason a spheroid was chosen as the asymmetrically driven body rather than a cylinder when the excitation is an axially symmetric belt field since the solution must be independent of ϕ .

The problem of the radial dipole near an infinite conducting cylinder has received the attention of various authors. Carter (3) derived expressions for the far zone radiation from dipoles of various orientations near an infinite conducting cylinder using the principle of reciprocity. In a later paper, Lucke (4) obtained essentially the same results using the Green's function method. Moullin (5) has related results in his book and LePage, Harrington and Schlecht (6), (7) and Walsh (8) consider similar problems.

The ϕ-independent prolate spheroidal antenna has been considered by numerous authors. Forced oscillation of a prolate spheroid was first considered by Page and Adams (9) who treated the case of a thin spheroid driven by a plane wave whose electric field was parallel to the major axis. Chu and Stratton (10) attacked the case of the center-fed prolate spheroidal antenna by different methods and obtained curves of input impedance. A detailed analysis of the aspects of the same problem was carried out by Ryder (11) who based his treatment in part upon earlier work of Page and Adams (9). In later papers, Page (12) treated the more general vector wave equation and extended his previous results. Flammer (13) considered the problem of a spheroidal monopole antenna which is formed when the inner conductor of a coaxial line is extended into free space in the form of half a prolate spheroid, while the outer conductor is spread out into

a conducting plane. The radiation from an electric dipole located at the tip of a prolate spheroid has been computed by Hatcher and Leitner (14). Recently Myers (15) computed the radiation from an asymmetrically fed prolate spheroidal antenna excited by a belt of impressed field. The theoretical results of Myers are compared here to experimental results in Chap. 5.

It is the purpose of the present work to investigate the two asymmetrically excited systems described above. The case of the cylinder excited by a radial dipole is treated analytically and experimentally. The case of the asymmetrically excited spheroid is treated largely from an experimental aspect.

2. FINITE CYLINDER EXCITED BY A RADIAL ELECTRIC DIPOLE: THEORY

The effect of a finite perfectly conducting cylinder on the far zone radiation of a radial electric dipole is considered in this chapter. The boundary conditions at the ends of the cylinder introduce serious mathematical difficulties but through the use of the solution for an infinite cylinder, it is shown that an approximate solution can be obtained if the cylinder is not very short.

2.1 The Infinite Cylinder Excited by a Radial Dipole

Since the current distribution and far zone field expressions for the infinite cylinder excited by a radial dipole will be used later, these expressions will be derived in this section. The far zone field has been given by Carter (3) who made use of the principle of reciprocity and by Lucke (4) who used the Green's function method. The Green's function approach will be used here and in addition to the far zone field, the current distribution on the cylinder will be derived.

The infinite cylinder of radius a and excited by a radial dipole at radius b is shown in Fig. 2.1. The Green's function method leads to expressions for the fields within a region in terms of the currents and charges in the region and the fields on the bounding surface of the region. The necessary relations are given by Stratton (16), p. 466. The kernel in the equations given by Stratton is the free space Green's function but it may be shown that they are also valid with the kernel equal to any Green's function. With this modification the equations for the electric and magnetic fields within a region V bounded by a surface S are (time

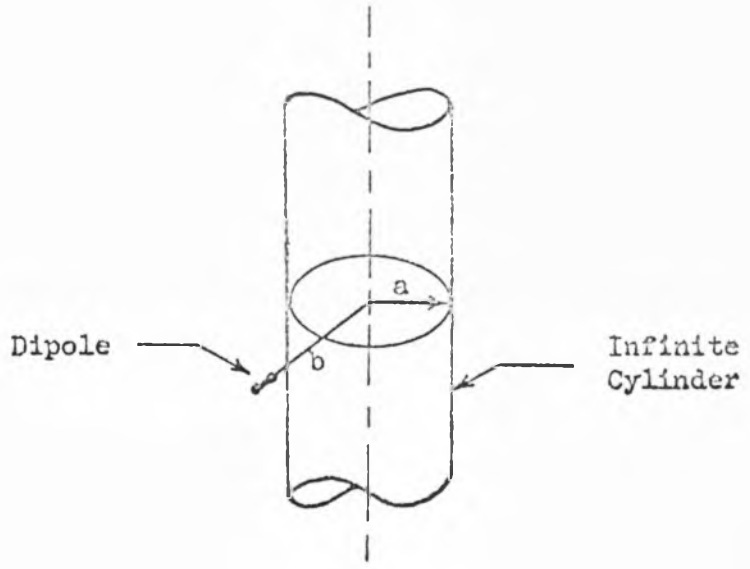

Figure 2.1. Infinite Cylinder with Radial Electric Dipole

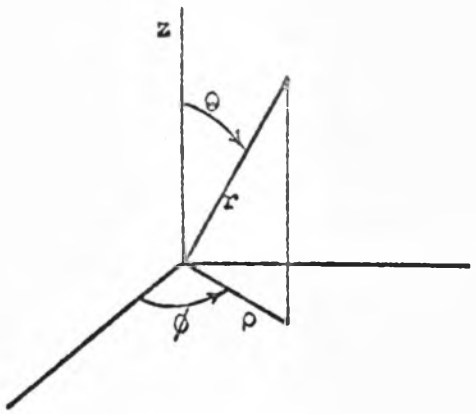

Figure 2.2. Coordinate System

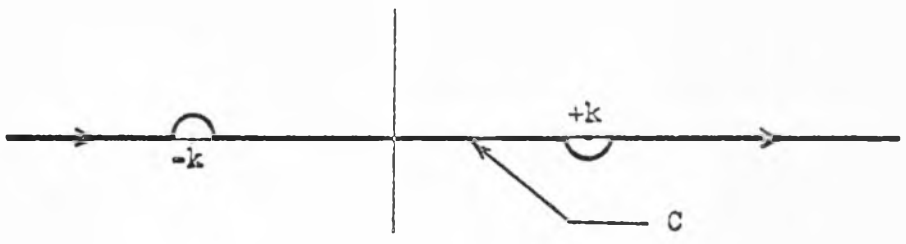

Figure 2.3. Contour of Integration in α Plane

dependence $e^{-i\omega t}$)

$$\underline{E}(r) = \int_V [i\omega\mu\, \underline{J}(\underline{r}')G(\underline{r},\underline{r}') + (1/\epsilon)\rho(\underline{r}')\nabla' G(\underline{r},\underline{r}')]\, dv'$$

$$- \int_S \Big\{ i\omega\mu[\underline{n} \times \underline{H}(\underline{r}')]G(\underline{r},\underline{r}') + [\underline{n} \times \underline{E}(\underline{r}')] \times \nabla' G(\underline{r},\underline{r}') + [\underline{n} \cdot \underline{E}(\underline{r}')]\, \nabla' G(\underline{r},\underline{r}') \Big\}\, da' \qquad (2.1)$$

$$\underline{H}(r) = \int_V [J(\underline{r}') \times \nabla' G(\underline{r},\underline{r}')]dv' + \int_S \Big\{ i\omega\epsilon[\underline{n} \times \underline{E}(\underline{r}')]G(\underline{r},\underline{r}')$$

$$- [\underline{n} \times \underline{H}(\underline{r}')] \times \nabla' G(\underline{r},\underline{r}') - [\underline{n} \cdot \underline{H}(\underline{r}')]\, \nabla' G(\underline{r},\underline{r}') \Big\}\, da' \qquad (2.2)$$

in which $\underline{J}(\underline{r}')$ is the current density, $\rho(\underline{r}')$ is the charge density, ϵ and μ are the permittivity and permeability, $\underline{n}$ is the outward normal unit vector, ∇' is the gradient with respect to the primed coordinates and $G(\underline{r},\underline{r}')$ satisfies

$$(\nabla^2 + k^2)G(\underline{r},\underline{r}') = -\delta(\underline{r} - \underline{r}') \quad . \qquad (2.3)$$

$\delta(\underline{r} - \underline{r}')$ is the three-dimensional Dirac delta function and $k = \omega\sqrt{\mu\epsilon}$. The properties of $G(\underline{r},\underline{r}')$ and $\delta(\underline{r} - \underline{r}')$ are discussed by Borgnis and Papas (17). In order to simplify equations 2.1 and 2.2, one is free to assign arbitrary boundary conditions to $G(\underline{r},\underline{r}')$. If the boundary conditions $G_1(\underline{r},\underline{r}') = 0$ when $\rho' = a$ and $\partial G_2(\underline{r},\underline{r}')/\partial\rho' = 0$ when $\rho' = a$ are used in equations 2.1 and 2.2 respectively where the coordinate system is shown in Fig. 2.2,

equations 2.1 and 2.2 become

$$E_z(\underline{r}) = \int_V \left[i\omega\mu \, J_z(\underline{r}')G_1(\underline{r},\underline{r}') + (1/\epsilon)\rho(\underline{r}')(\partial/\partial z')G_1(\underline{r},\underline{r}') \right] dv' \quad (2.4)$$

$$H_z(\underline{r}) = \int_V \left[\underline{J}(\underline{r}') \times \nabla' G_2(\underline{r},\underline{r}') \right]_z dv' \quad (2.5)$$

where use has been made of the fact that $\underline{n} \times \underline{E}(\underline{r}') = 0$ at the perfectly conducting cylinder.

The Green's functions as given by Lucke (4) are for $\rho' < \rho$

$$G_1(\underline{r},\underline{r}') = (i/8\pi) \int_C \sum_{m=-\infty}^{\infty} e^{im(\phi-\phi')} e^{i\alpha(z-z')} \frac{H_m(\beta\rho)}{H_m(\beta a)} \left[J_m(\beta\rho')H_m(\beta a) - H_m(\beta\rho')J_m(\beta a) \right] d\alpha \quad (2.6)$$

$$G_2(\underline{r},\underline{r}') = (i/8\pi) \int_C \sum_{m=-\infty}^{\infty} e^{im(\phi-\phi')} e^{i\alpha(z-z')} \frac{H_m(\beta\rho)}{H_m'(\beta a)} \left[J_m(\beta\rho')H_m'(\beta a) - H_m(\beta\rho')J_m'(\beta a) \right] d\alpha \quad (2.7)$$

where primes indicate differentiation with respect to the argument, $H_m(x)$ is the Hankel function of the first kind of argument x, $\beta = \sqrt{k^2 - \alpha^2}$ and the contour of integration C is shown in Fig. 2.3. To determine the far zone fields the far zone approximations for G_1 and G_2 are used. These are evaluated from a result given by Papas (18) and upon substitution of these expressions into equations 2.4 and 2.5 and integrating, the far zone expressions for E_z and H_z for a dipole at $\rho' = b$, $\phi' = 0$, $z' = 0$ are obtained as follows.

$$E_z = - \frac{iMk^2 e^{ikr} \cos\theta \sin\theta}{4\pi\epsilon r} \sum_{m=0}^{\infty} (-i)^m \epsilon_m \cos m\phi \left[\frac{1}{H_m(ka \sin\theta)} \right]$$

$$\times \left[H_m(ka \sin\theta) J'_m(kb \sin\theta) - J_m(ka \sin\theta) H'_m(kb \sin\theta) \right] \qquad (2.8)$$

$$H_z = - \frac{i\omega M e^{ikr}}{2\pi br} \sum_{m=1}^{\infty} (-i)^m m \sin m\phi \left[\frac{1}{H'_m(ka \sin\theta)} \right]$$

$$\times \left[H'_m(ka \sin\theta) J_m(kb \sin\theta) - H_m(kb \sin\theta) J'_m(ka \sin\theta) \right] . \qquad (2.9)$$

In these equations M is the dipole moment of the electric dipole, b is its distance from the axis, a is the radius of the cylinder, and $\epsilon_m = 1$ when $m = 0$ and 2 when $m \neq 0$. The far zone field is completely determined by equations 2.8 and 2.9. For the case of the dipole at the surface of the cylinder, $b = a$ and using the Wronskian relation

$$H_m(x)\, J'_m(x) - J_m(x)\, H'_m(x) = - \frac{2i}{\pi x} \qquad (2.10)$$

one obtains

$$E_z = - \frac{Mke^{ikr} \cos\theta}{2\pi^2 a\epsilon r} \sum_{m=0}^{\infty} (-i)^m \epsilon_m \frac{\cos m\phi}{H_m(ka \sin\theta)} \qquad (2.11)$$

$$H_z = \frac{M\omega e^{ikr}}{ka^2 \pi^2 r \sin\theta} \sum_{m=1}^{\infty} (-i)^m m \frac{\sin m\phi}{H'_m(ka \sin\theta)} . \qquad (2.12)$$

The two components of electric field in the far zone are determined from the relations

$$E_\theta = -E_z/\sin\theta = \frac{Mkc^{ikr}\cos\theta}{2\pi^2 a\,\epsilon r \sin\theta} \sum_{m=0}^{\infty} (-i)^m \epsilon_m \frac{\cos m\phi}{H_m(ka\sin\theta)} \qquad (2.13)$$

$$E_\phi = \sqrt{\mu/\epsilon}\; H_z/\sin\theta = \frac{Me^{ikr}}{\pi^2 a^2 \epsilon r \sin^2\theta} \sum_{m=1}^{\infty} (-i)^m m \frac{\sin m\phi}{H'_m(ka\sin\theta)} . \qquad (2.14)$$

It is of interest to consider the radiation pattern for the case ka = .6317 since a finite cylinder of this radius is discussed later. The patterns of E_θ and E_ϕ in the half plane $\phi = \pi/2$ are shown in Figs. 2.4 and 2.5. It is seen that E_θ actually becomes infinite if $\theta = 0$. Since the cylinder is infinite, however, θ can never take on the value $\theta = 0$. The limiting value of θ is that defined by $\sin\theta = a/r$ since for this value the point of observation is on the surface of the cylinder. It appears from equation 2.14 that E_ϕ approaches the value $-Mk^2 e^{ikr}\sin\phi/2\pi\epsilon r$ as θ approaches zero. This, of course, cannot be true, since E_ϕ is tangential to the cylinder as θ approaches zero and therefore must vanish. Actually, it does vanish on the cylinder and the trouble arises from the fact that the limit of equation 2.14 as θ approaches zero is not equal to the value of E_ϕ at $\theta = 0$. It is easy to show that E_ϕ is actually zero at $\rho = a$ by using equation A3.10 and equations 2.17 and 2.18. Thus equation 2.14 can be used at any point in the far zone except at the

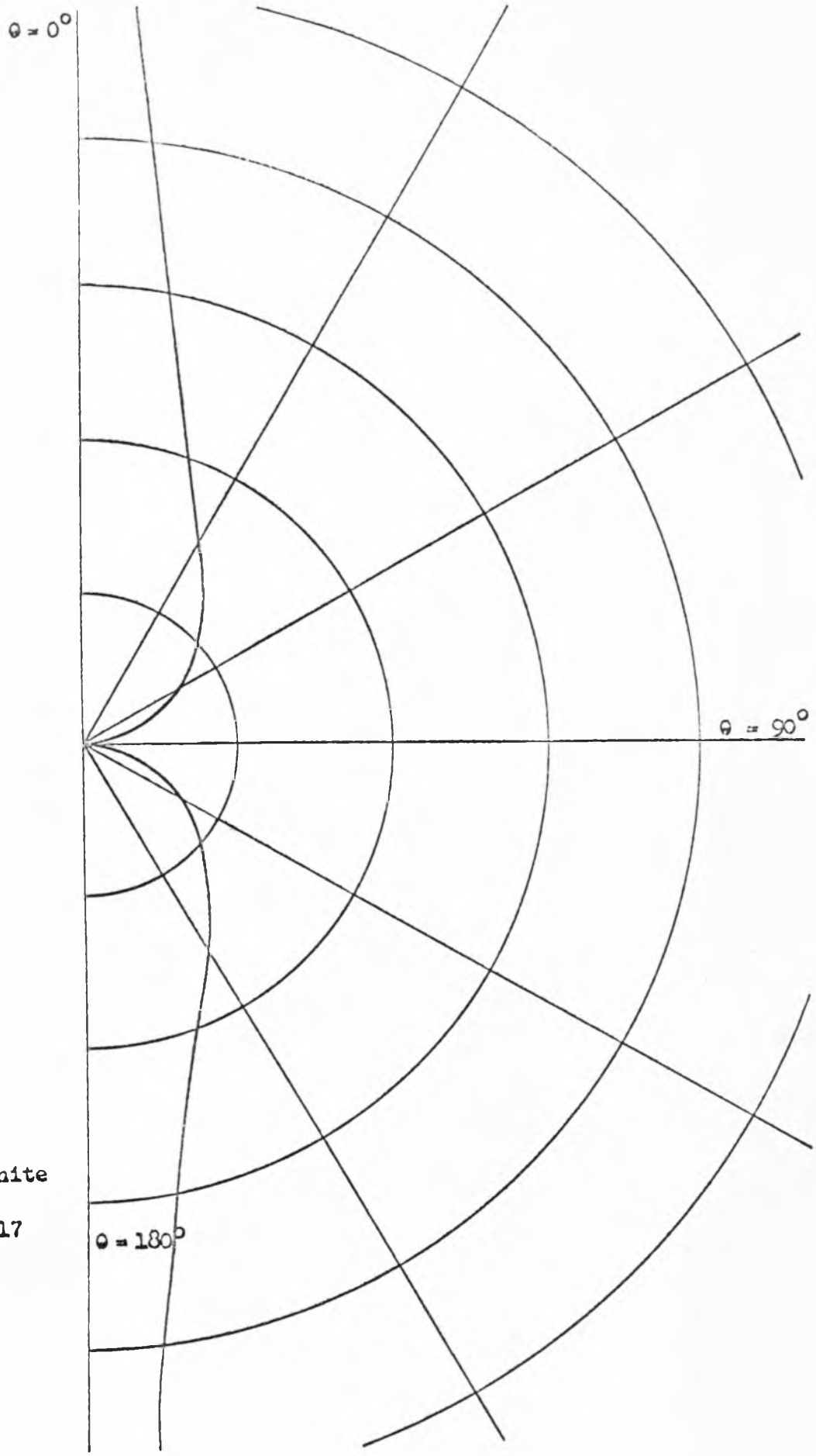

Figure 2.4.

E_θ for Infinite Cylinder.

ka = kb = .6317

ϕ = 90°

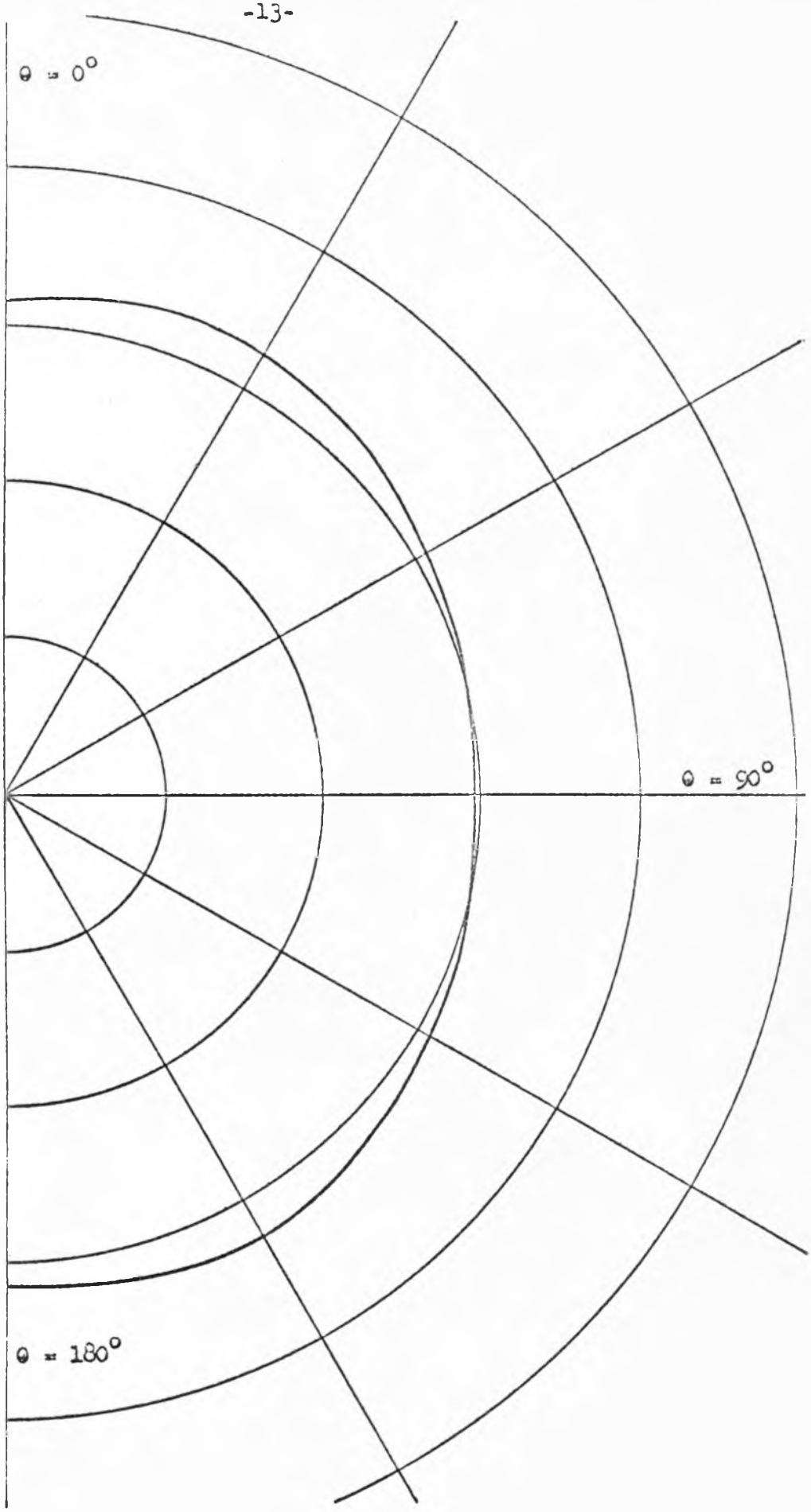

Figure 2.5
E_ϕ for Infinite Cylinder
ka = kb = .6317
$\phi = 90°$

surface of the cylinder where its value is zero. This peculiar type of behavior is encountered in other places such as in the expression for the field about an infinitely thin wire where the expressions appear to yield a finite value for the tangential field at the wire. This is discussed by Schelkunoff (21), and it is shown that the field actually is zero at the wire, the discrepancy arising from the fact that the limit of the function as the wire is approached is not equal to the function at the wire. Precisely this behavior is also exhibited by E_ϕ of the infinite cylinder at $\rho = a$.

If the radiation from a very long but finite cylinder is desired, the expressions for the infinite cylinder can furnish some information. However, these expressions must be used with care. The expression for E_θ obviously cannot be used in the region near $\theta = 0$ because of the singularity there. In the region not near $\theta = 0$, the results are still of questionable validity because the limits of θ within which the infinite cylinder expression can be used with accuracy are not known. The radiation from a finite cylinder will be derived later and the lobes which become evident in the pattern for E_θ are not evident at all in the pattern for the infinite cylinder. The expression for E_ϕ of the infinite cylinder approximates the corresponding expression for the long finite cylinder more closely than in the case of E_θ if the discontinuous behavior discussed above is not included. This is justified, since the discontinuous nature is due

to the infinite extent of the cylinder. The agreement between the infinite and finite cylinder expressions for E_ϕ may be observed in Figs. 2.5 and 2.11. The closer agreement in the case of E_ϕ is due to the manner in which the currents on the cylinder decrease with z. E_θ has the surface current K_z as its source on the cylinder, while E_ϕ has K_ϕ as its source and it is shown later that K_ϕ decreases faster with z than K_z. Thus E_ϕ is due more to currents near the origin than E_θ and thus its pattern is less dependent on the length of the cylinder.

The current distribution on the cylinder is calculated in a similar manner except that far zone approximations cannot be used. First E_z and H_z at the cylinder are determined and the current on the cylinder is derived from these components of the field. The proper Green's functions needed are those valid for $\rho < \rho'$. These are obtained from equations 2.6 and 2.7 by interchanging ρ and ρ'. Thus for $\rho < \rho'$

$$G_1(\underline{r},\underline{r}') = (i/8\pi) \int_C \sum_{m=-\infty}^{\infty} e^{im(\phi-\phi')}\, e^{i\alpha(z-z')}\, \frac{H_m(\beta\rho')}{H_m(\beta a)} \left[J_m(\beta\rho)H_m(\beta a) - H_m(\beta\rho)J_m(\beta a) \right] d\alpha \qquad (2.15)$$

$$G_2(\underline{r},\underline{r}') = (i/8\pi) \int_C \sum_{m=-\infty}^{\infty} e^{im(\phi-\phi')}\, e^{i\alpha(z-z')}\, \frac{H_m(\beta\rho')}{H_m'(\beta a)} \left[J_m(\beta\rho)H_m'(\beta a) - H_m(\beta\rho)J_m'(\beta a) \right] d\alpha \,. \qquad (2.16)$$

Substituting this expression for G_1 into equation 2.4 and integrating over the dipole, one obtains

$$E_z = \frac{M}{8\pi\epsilon} \int_C \sum_{m=-\infty}^{\infty} e^{im\phi} \beta\alpha\, e^{i\alpha z} \left[H_m(\beta a) J_m(\beta\rho) - H_m(\beta\rho) J_m(\beta a) \right] \frac{H_m'(\beta b)}{H_m(\beta a)}\, d\alpha \,. \tag{2.17}$$

Using equations 2.16 and 2.5 one obtains

$$H_z = -\frac{i\omega M}{8\pi b} \int_C \sum_{m=-\infty}^{\infty} m e^{im\phi} e^{i\alpha z} \left[J_m(\beta\rho) H_m'(\beta a) - H_m(\beta\rho) J_m'(\beta a) \right] \frac{H_m(\beta b)}{H_m'(\beta a)}\, d\alpha \,. \tag{2.18}$$

As shown in Appendix 3, H_ϕ is determined from E_z and H_z through the relation

$$H_\phi = \frac{i}{2\pi} \int_{-\infty}^{\infty} \frac{1}{\beta^2} \left\{ \omega\epsilon \frac{\partial \bar{E}_z(\alpha)}{\partial\rho} + \frac{\alpha}{\rho} \frac{\partial \bar{H}_z(\alpha)}{\partial\phi} \right\} e^{i\alpha z}\, d\alpha \tag{2.19}$$

where $\bar{E}_z(\alpha)$ and $\bar{H}_z(\alpha)$ are the Fourier transforms of E_z and H_z. From equations 2.17 and 2.18, $\bar{E}_z(\alpha)$ and $\bar{H}_z(\alpha)$ are given by

$$\bar{E}_z(\alpha) = \frac{M}{4\epsilon} \sum_{m=-\infty}^{\infty} e^{im\phi}\, \beta\alpha \left[H_m(\beta a) J_m(\beta\rho) - H_m(\beta\rho) J_m(\beta a) \right] \frac{H_m'(\beta b)}{H_m(\beta a)} \tag{2.20}$$

$$\bar{H}_z(\alpha) = -\frac{i\omega M}{4b} \sum_{m=-\infty}^{\infty} m e^{im\phi} \left[J_m(\beta\rho) H_m'(\beta a) - H_m(\beta\rho) J_m'(\beta a) \right] \frac{H_m(\beta b)}{H_m'(\beta a)} \,. \tag{2.21}$$

Thus from equation 2.19, one finds that H_ϕ at the cylinder $\rho = a$ is given by

$$H_\phi(\rho=a) = \frac{M\omega}{4\pi^2} \sum_{m=-\infty}^{\infty} \left\{ \int_C \frac{\alpha}{\beta a} \left[\frac{H_m'(\beta b)}{H_m(\beta a)} - \frac{m^2}{\beta^2 ab} \frac{H_m(\beta b)}{H_m'(\beta a)} \right] e^{i\alpha z}\, d\alpha \right\} e^{im\phi} \,. \tag{2.22}$$

From equation 2.18, H_z at $\rho = a$ is

$$H_z(\rho=a) = \frac{M\omega}{4\pi^2 b} \sum_{m=-\infty}^{\infty} m \left\{ \int_C \frac{1}{\beta a} \frac{H_m(\beta b)}{H_m'(\beta a)} e^{i\alpha z} \, d\alpha \right\} e^{im\phi} \quad . \tag{2.23}$$

The surface current densities on the cylinder are then

$$K_z = H_\phi(\rho=a) \qquad K_\phi = -H_z(\rho=a) \tag{2.24}$$

and the currents on the cylinder are completely determined.

2.2 The Finite Cylinder Excited by a Radial Dipole; The Method of Approximation

The determination of the far zone field of a finite cylinder, i.e., a cylinder not of infinite extent in the $\pm z$ direction, when excited by a radial electric dipole presents greater difficulty than the case of the infinite cylinder. The case of the finite cylinder involves complicated boundary conditions in that the tangential electric field must vanish over parts of two different coordinate surfaces. As shown in Fig. 2.6, the tangential field must vanish at $\rho = a$ for $-\ell_1 < z < \ell_2$ and also at $z = \ell_2, -\ell_1$ for $\rho < a$. These boundary conditions introduce considerable complications and usually the solutions to problems of this sort involve some method of approximation.

In order to carry out an approximate solution to this problem the current distribution on the finite cylinder will be taken identical to the distribution on the infinite cylinder. In other words, the current distribution on the infinite cylinder is determined. Then as shown in

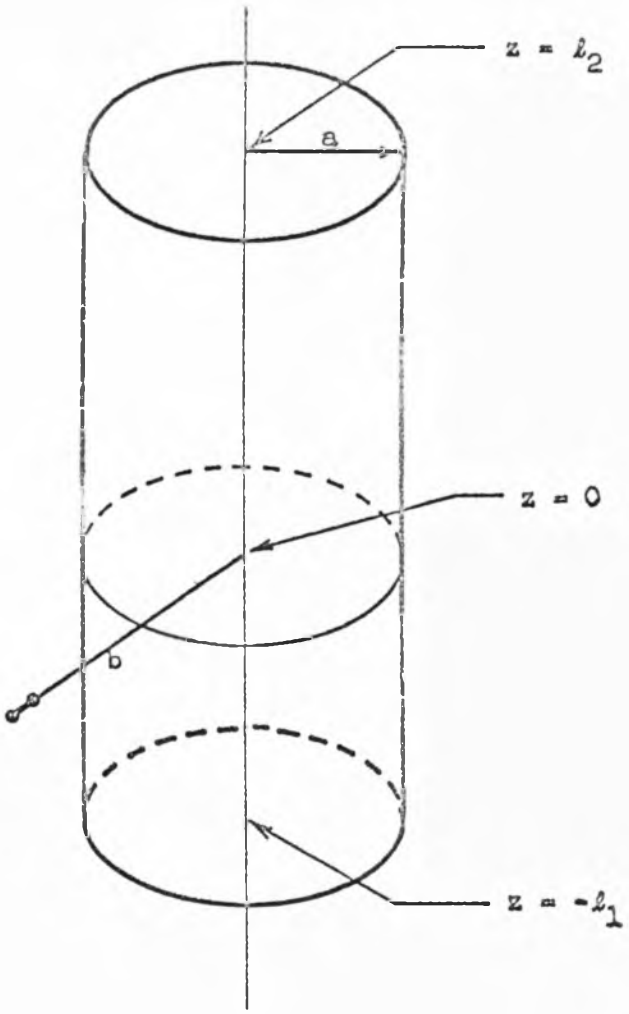

Figure 2.6. Finite Cylinder with Radial Electric Dipole

Fig. 2.7, the portions of the infinite cylinder above $z = \ell_2$ and below $z = -\ell_1$ are removed and the current on the remaining portion of the cylinder is assumed unchanged. The far zone field of this unchanged portion of the current between $-\ell_1$ and ℓ_2 is then computed and added to the field of the dipole to obtain an expression for the total far zone field of the configuration.

Actually, of course, the current distribution on the remaining portion of the cylinder is changed when the upper and lower portions of the infinite cylinder are removed. However, it will now be shown that this modification of the current will be small if ℓ_1 and ℓ_2 are not short compared to a wavelength.

It is evident that the regions where the greatest perturbation of the current distribution from the infinite cylinder distribution exists are regions II and III of Fig. 2.7 which are the regions near the ends. In these regions the physical conditions have changed greatly since an abrupt discontinuity now exists where a smooth surface existed previously. The current in region I will not be affected as greatly because it is determined largely by the dipole field which is very strong in this region. However, the large change of the currents in regions II and III will not have a large effect on the far zone field if these currents are small relative to the currents in region I. The region II and III currents will, in fact, be small if the current distribution on the infinite cylinder has decreased by a large factor at $z = \ell_2$ and $-\ell_1$ from the value near $z = 0$ where the dipole is located since the region I and II currents on the finite cylinder are of the same order of magnitude as the region I and II

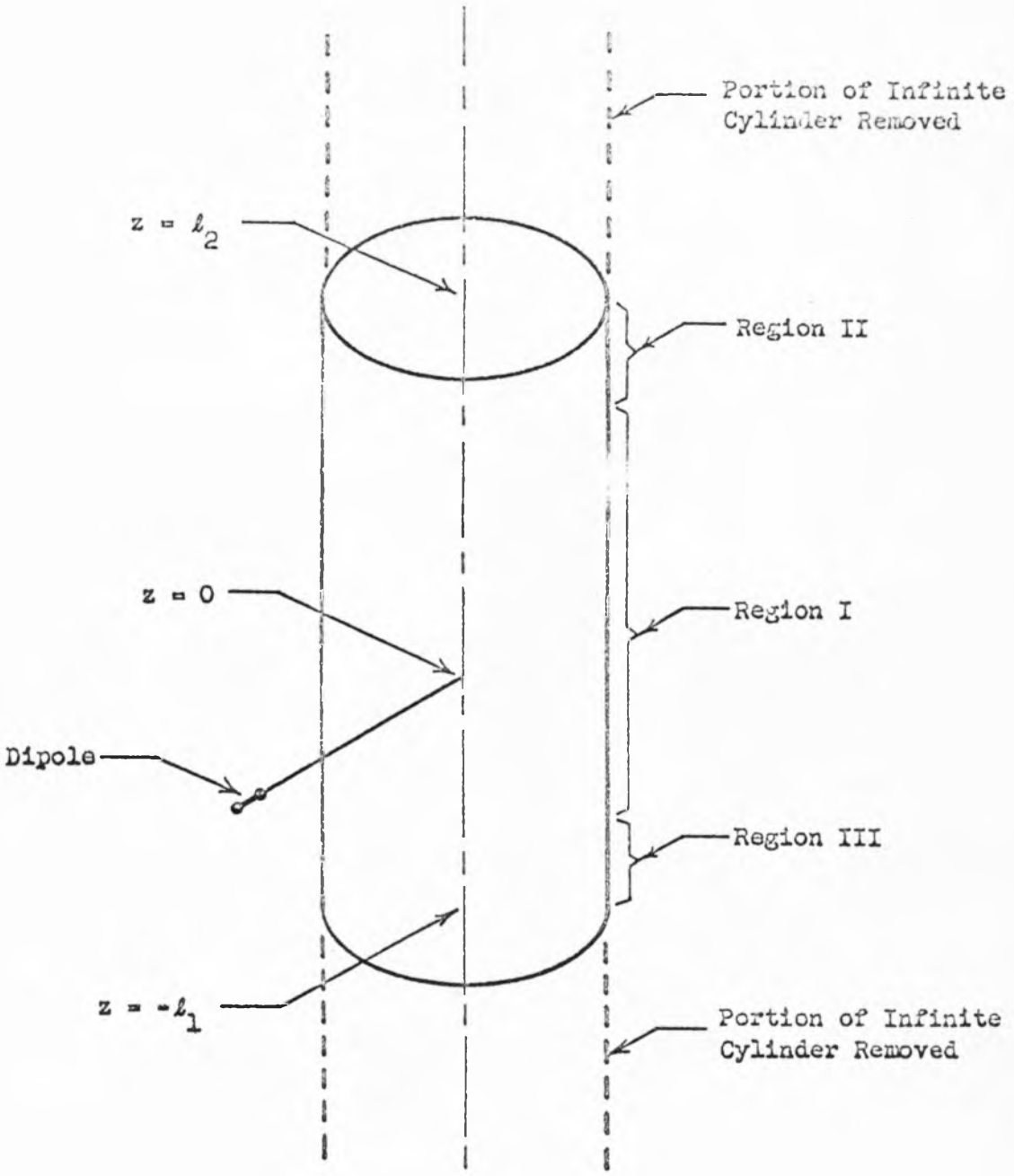

Figure 2.7. Finite Cylinder Divided into Regions for Approximate Analysis.

currents on the infinite cylinder. It is relatively simple to show that the current does decrease rapidly with z as one moves away from the dipole. Only the case of the dipole at the surface of the cylinder, i.e., $b = a$, will be considered. It is necessary to examine the current distribution for large z, for under this condition a simple expression may be obtained and the rapidly decreasing behavior is exhibited. Instead of examining equations 2.22 and 2.23 for large z it is simpler to use equations 2.11 and 2.12, since the condition of large z is already contained in them. The ϕ component of surface current can be derived from the expression for H_z at the cylinder. From equation 2.12 H_z in the far zone is

$$H_z = \frac{M\omega e^{ikr}}{ka^2\pi^2 \sin\theta\, r} \sum_{m=1}^{\infty} (-i)^m m \frac{\sin m\phi}{H_m'(ka \sin\theta)} \quad . \tag{2.25}$$

At a large distance from the origin at the surface of the cylinder

$$\sin\theta = \frac{a}{\sqrt{z^2 + a^2}} \approx \frac{a}{z} \tag{2.26}$$

so that the argument of H_m' in equation 2.25 is small. Using the small argument approximation for the Hankel functions it is found that for $m > 0$

$$H_m'(x) \approx i\, 2^m\, m!/\pi x^{m+1} \quad . \tag{2.27}$$

Using equations 2.27, 2.26 and noting that $r \approx z$, the expression for H_z at the cylinder for large z is

$$H_z(\rho=a) = -\frac{M\omega ka \sin\phi\, e^{ikz}}{2\pi z^2} \tag{2.28}$$

where only the large leading term of the series has been retained. Since the surface current density $K_\phi = -H_z(\rho=a)$ it is indeed true that this component of current decreases rapidly with z, i.e., $K_\phi \propto 1/z^2$.

To obtain the corresponding expression for $H_\phi(\rho=a)$ use is made of the fact that in the far zone in free space

$$H_\phi = \sqrt{\frac{\epsilon_o}{\mu_o}}\, E_\theta = -\sqrt{\frac{\epsilon_o}{\mu_o}}\, \frac{E_z}{\sin\theta} \quad . \tag{2.29}$$

Thus using equation 2.11 for E_z, H_ϕ becomes for large z

$$H_\phi = \sqrt{\frac{\epsilon_o}{\mu_o}}\, \frac{Mk\cos\theta\, e^{ikr}}{2\pi^2\epsilon_o ar\sin\theta} \sum_{m=0}^{\infty} (-i)^m \epsilon_m \frac{\cos m\phi}{H_m(ka\sin\theta)} \quad . \tag{2.30}$$

Using equation 2.26 and the small argument approximation for the Hankel function one obtains for H_ϕ at the cylinder for large z

$$H_\phi(\rho=a) = \frac{iM\omega\, e^{ikz}}{4\pi a^2 \ell n\left(\frac{2z}{\gamma ka^2}\right)} \tag{2.31}$$

where again the leading term of the series is retained. In equation 2.31, $\gamma = 1.781072$. Since $K_z = H_\phi(\rho=a)$, equation 2.31 shows that K_z decreases quite rapidly although not as fast as K_ϕ. Thus it is shown that at least for large z the currents on the infinite cylinder attenuate rapidly so that the region II and III currents of Fig. 2.7 are small compared to those near $z = 0$ as long as ℓ_1 and ℓ_2 are large.

It remains to be shown that the currents in region I will not be

greatly perturbed when the upper and lower sections of the infinite cylinder are removed. The currents in the regions $z > \ell_2$ and $z < -\ell_1$ impress a field on region I before their removal and when this field is removed the currents on the remaining portion of the cylinder must redistribute in order to maintain the proper boundary conditions at the surface. This redistribution will be a small effect only if the fields in region I due to the currents above $z = \ell_2$ and below $z = -\ell_1$ are small. The fact that the currents are small above ℓ_2 and below $-\ell_1$ does not guarantee that the field in region I due to these currents is small, because the field is an integrated effect. However, it will now be demonstrated that at least for large ℓ_1 and ℓ_2 the fields in region I due to currents above $z = \ell_2$ and below $z = -\ell_1$ are small.

The magnitude of the fields near $z = 0$ due to currents above $z = \ell_2$ will be computed. For large ℓ_2 the currents are given by equations 2.28 and 2.31. The field due to K_ϕ will be derived first. From equation 2.28

$$K_\phi = \frac{M\omega ka \sin \phi \, e^{ikz}}{2\pi z^2} \quad . \tag{2.32}$$

This current flows circumferentially around the cylinder and it is convenient in computing the radiation to consider this distribution as a distribution of current loops with radius a starting at $z = \ell_2$ and extending to infinity. It can be shown easily that the radiation field along the negative z axis of a loop of radius a, carrying a current $I_o \sin \phi$ located in the plane $z = 0$ is

$$E_\phi = \frac{i\, I_o \omega \mu_o a \sin\phi\, e^{ik|z|}}{4|z|} \quad . \tag{2.33}$$

Thus the field at $z = 0$ due to a section of the current of equation 2.32 of length dz at z is

$$dE_\phi = \frac{i(K_\phi dz)\omega\mu_o a \sin\phi\, e^{ikz}}{4z} = \frac{iM\omega^2\mu_o k a^2 \sin\phi\, e^{i2kz} dz}{8\pi z^3} \quad . \tag{2.34}$$

The total field at $z = 0$ is then

$$\int dE_\phi = E_\phi = \frac{iM\omega^2\mu_o k a^2 \sin\phi}{8\pi} \int_{\ell_2}^{\infty} \frac{e^{i2kz}}{z^3}\, dz \quad . \tag{2.35}$$

Integrating, one obtains

$$E_\phi = \frac{iM\omega^2\mu_o k a^2 \sin\phi}{8\pi} \left\{ \frac{e^{i2k\ell_2}}{2\ell_2^2} + \frac{ike^{i2k\ell_2}}{\ell_2} \right.$$
$$\left. -2k^2 \left[-Ci(2k\ell_2) + i\left(\frac{\pi}{2} - Si(2k\ell_2)\right) \right] \right\} \quad . \tag{2.36}$$

Since ℓ_2 is large $Ci(2k\ell_2) \approx -\sin(2k\ell_2)/(2k\ell_2)$ and $Si(2k\ell_2) \approx \pi/2 - \cos(2k\ell_2)/(2k\ell_2)$ so that

$$E_\phi = \frac{iM\omega^2\mu_o k a^2 \sin\phi\, e^{i2k\ell_2}}{16\pi\, \ell_2^2} \tag{2.37}$$

demonstrating that E_ϕ is small, of the order of $1/\ell_2^2$. The other component of current is from equation 2.31

$$K_z = \frac{iM\omega\, e^{ikz}}{4\pi a^2\, \ell n\left(\frac{2z}{\gamma k a^2}\right)} \quad . \tag{2.38}$$

This current flows in the axial direction and in order to compute the

field, can be replaced by a distribution of dipoles parallel to the z-axis at $\rho = a$. It is known that both E_θ and H_ϕ vanish along the axis of a dipole so that these components do not contribute in region I of the cylinder. However, there is an E_r in the axial direction of a dipole which is given in the $\theta = \pi$ direction by

$$E_r = \frac{imk}{2\pi\epsilon_o} \frac{e^{ikr}}{r^2} \tag{2.39}$$

where m is the dipole moment. The equivalent dipole moment of a ring of current in the axial direction of axial length dz is

$$m = \frac{i}{\omega} (2\pi a K_z \, dz) \tag{2.40}$$

so that the field at $z = 0$ due to this ring of axial current is from equation 2.39

$$dE_z = \frac{K_z \, ka \, e^{ikz} \, dz}{\omega \, \epsilon_o \, z^2} \quad . \tag{2.41}$$

Substituting for K_z from equation 2.38 and integrating to find the total field from the z component of current above $z = \ell_2$ one obtains

$$E_z = \frac{iMk}{4\pi\epsilon_o a} \int_{\ell_2}^{\infty} \frac{e^{i2kz} \, dz}{z^2 \ell n(\frac{2}{\gamma} \frac{z}{ka}^2)} \quad . \tag{2.42}$$

The magnitude of the integral in equation 2.42 is less than the magnitude of

$$\int_{\ell_2}^{\infty} \frac{dz}{z^2 \ell n(\frac{2z}{\gamma ka}^2)} \tag{2.43}$$

because of the oscillatory nature of e^{i2kz}. But

$$\int_{\ell_2}^{\infty} \frac{dz}{z^2 \ln\left(\frac{2z}{\gamma k a^2}\right)} = -\frac{2}{\gamma k a^2}\, Ei\left(-\ln\left(\frac{2\ell_2}{\gamma k a^2}\right)\right) \tag{2.44}$$

where $-Ei(-x) = \int_x^{\infty} \frac{e^{-x}}{x}\, dx$. Since ℓ_2 is large, an asymptotic expression for $-Ei(-x)$ can be used to give

$$\int_{\ell_2}^{\infty} \frac{dz}{z^2 \ln\left(\frac{2z}{\gamma k a^2}\right)} \approx \frac{1}{\ell_2 \ln\left(\frac{2\ell_2}{\gamma k a^2}\right)} \quad . \tag{2.45}$$

Therefore

$$|E_z| < \frac{Mk}{4\pi\epsilon_o a\, \ell_2 \ln\left(\frac{2\ell_2}{\gamma k a^2}\right)} \tag{2.46}$$

showing that $|E_z|$ in region I due to currents above $z = \ell_2$ are small, of the order of $1/\ell_2 \ln\left(\frac{2\ell_2}{\gamma k a^2}\right)$. The fields due to the currents below $z = -\ell_1$ exhibit similar properties.

It should be noted that although the currents above $z = \ell_2$ and below $z = -\ell_1$ cause a small field in region I, the field in other directions is not necessarily small. It was shown above that E_θ and H_ϕ due to K_z vanishes in region I but this is not true in other directions. Thus it would not be a good approximation to leave the currents above $z = \ell_2$ and below $z = -\ell_1$ in place even though the currents on these portions are small since their radiation fields are appreciable in directions other than the axial direction.

To summarize, the reason for using the current distribution of the infinite cylinder for the problem of the finite cylinder is that

the currents which contribute most to the radiation (region I) are modified very little while the currents which are perturbed to a larger extent (regions II and III) contribute little to the radiation field because of their small magnitude.

The preceding statements hold for ℓ_1 and ℓ_2 large. Exact lower limits for ℓ_1 and ℓ_2 beyond which the approximation described fails are difficult to determine because of the complexity of the functions involved. However, experimental results are compared to theoretical results in Chap. 4 to give an idea of the error for certain values of ℓ_1 and ℓ_2 .

2.3 The Finite Cylinder Excited by a Radial Dipole; The Approximate Solution

The far zone radiation field of the radial dipole near a finite cylinder will now be derived using the approximation discussed in section 2.2. The physical configuration and coordinate systems are shown in Fig. 2.8. The field is to be calculated at an arbitrary point P . The field due to the current on the cylinder will first be derived and the dipole field will be added to give the total field. The far zone ϕ-component of electric field due to a current density $\underline{J}$ is (19)

$$E_\phi = \frac{i\omega\mu_o e^{ikr}}{4\pi r} \int_V \underline{J}(\rho',\phi',z') \cdot \underline{e}_\phi \, e^{-ik\underline{r}'\cdot\underline{e}_r} \, dV' \qquad (2.47)$$

where $\underline{e}_\phi$ and $\underline{e}_r$ are unit vectors in the ϕ and r directions respectively, the integration is over the primed coordinates and includes the volume occupied by the source current. For a surface

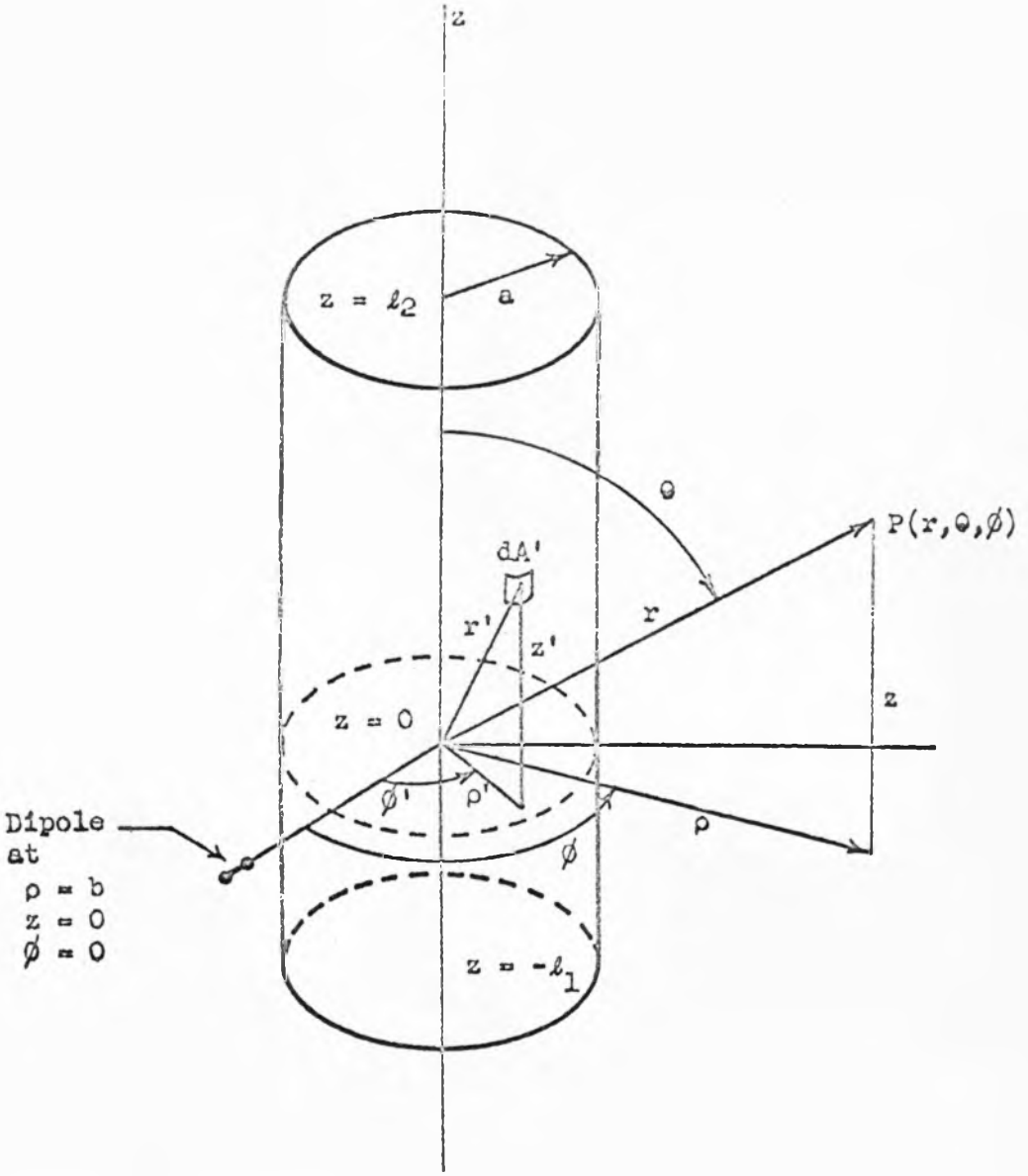

Figure 2.8. Finite Cylinder with Dipole and Coordinate Systems

current density $\underline{K}$ flowing over an area A , equation 2.47 becomes

$$E_\phi = \frac{i\omega\mu_o e^{ikr}}{4\pi r} \int_A \underline{K}(\rho',\phi',z') \cdot \underline{e}_\phi \, e^{ik\underline{r}' \cdot \underline{e}_r} \, dA' \quad . \tag{2.48}$$

For the cylinder of Fig. 2.8, $dA' = ad\phi'dz'$ and

$$\underline{r}' \cdot \underline{e}_r = a\cos(\phi'-\phi)\sin\theta + z'\cos\theta \tag{2.49}$$

$$\underline{K} \cdot \underline{e}_\phi = K_\phi \cos(\phi'-\phi) = -H_z(\rho'=a)\cos(\phi'-\phi) \tag{2.50}$$

so that equation 2.48 becomes

$$E_\phi = -\frac{i\omega\mu_o a\, e^{ikr}}{4\pi r} \int_{-\ell_1}^{\ell_2}\int_0^{2\pi} H_z(\rho'=a)\cos(\phi'-\phi) \times e^{-ik[a\cos(\phi'-\phi)\sin\theta + z'\cos\theta]} \, d\phi'dz' \quad . \tag{2.51}$$

$H_z(\rho'=a)$ is obtained from equation 2.23. Observing that $H_m(\beta b)/H_m'(\beta a) = H_{-m}(\beta b)/H_{-m}'(\beta a)$, equation 2.23 may be written

$$H_z(\rho'=a) = \frac{i\,M\omega}{2\pi^2 b} \sum_{m=1}^{\infty} m\left[\int_C \frac{1}{\beta a} \frac{H_m(\beta b)}{H_m'(\beta a)} e^{i\alpha z'} d\alpha\right] \sin m\phi' \quad . \tag{2.52}$$

Substituting equation 2.52 into equation 2.51, one obtains

$$E_\phi = \frac{M\omega^2\mu_o a e^{ikr}}{8\pi^3 r\, b} \sum_{m=1}^{\infty} m \int_0^{2\pi} \sin m\phi' \cos(\phi'-\phi) e^{-ika\cos(\phi'-\phi)\sin\theta} \, d\phi' \times \int_{-\ell_1}^{\ell_2}\int_C \frac{H_m(\beta b)}{\beta a\, H_m'(\beta a)} e^{i\alpha z'} e^{-ikz'\cos\theta} \, d\alpha \, dz' \quad . \tag{2.53}$$

It can be shown after considerable manipulation and use of the formula (20)

$$J_n(x) = \frac{(i)^{-n}}{2\pi} \int_0^{2\pi} e^{ix\cos\phi}\, e^{in\phi}\, d\phi \tag{2.54}$$

that the first integral in equation 2.53 ,

$$\int_0^{2\pi} \sin m\phi' \cos(\phi'-\phi)\, e^{-ika\cos(\phi'-\phi)\sin\theta}\, d\phi'$$

$$= 2\pi(-i)^{m-1} \sin m\phi\, J_m'(ka\sin\theta) \quad . \tag{2.55}$$

Thus equation 2.53 becomes

$$E_\phi = \frac{M\omega^2\mu_o a\, e^{ikr}}{4\pi^2 r\, b} \sum_{m=1}^{\infty} m(-i)^{m-1} \sin m\phi J_m'(ka\sin\theta)$$

$$\times \int_{-\ell_1}^{\ell_2} \int_C \frac{H_m(\beta b)}{\beta a\, H_m'(\beta a)}\, e^{i\alpha z'}\, e^{-ikz'\cos\theta}\, d\alpha\, dz' \quad . \tag{2.56}$$

Since the contour is as shown in Fig. 2.3 and since $\beta = \sqrt{k^2 - \alpha^2}$ is an even function of α one can write

$$\int_{-\ell_1}^{\ell_2} \int_C \frac{H_m(\beta b)}{\beta a H_m'(\beta a)}\, e^{i\alpha z'}\, e^{-ikz'\cos\theta} d\alpha\, dz'$$

$$= 2\int_{-\ell_1}^{\ell_2} \int_0^{\infty} \frac{H_m(\beta b)}{\beta a\, H_m'(\beta a)} \cos\alpha z'\, e^{-ikz'\cos\theta}\, d\alpha\, dz' \tag{2.57}$$

where the indentation at $\alpha = k$ is understood in the second integral. Interchanging the integral signs in equation 2.57 and carrying out the

integral with respect to z', equation 2.57 becomes

$$2\int_0^\infty \frac{H_m(\beta b)}{\beta a\, H_m'(\beta a)} \left[\frac{e^{i\ell_2(\alpha - k\cos\theta)} - e^{-i\ell_1(\alpha - k\cos\theta)}}{2i(\alpha - k\cos\theta)} - \frac{e^{-i\ell_2(\alpha + k\cos\theta)} - e^{i\ell_1(\alpha + k\cos\theta)}}{2i(\alpha + k\cos\theta)} \right] d\alpha \,. \quad (2.58)$$

To simplify this expression, let

$$\ell_2 = \ell + \Delta \,, \qquad \ell_1 = \ell - \Delta \,. \quad (2.59)$$

Then after considerable manipulation equation 2.58 becomes

$$4e^{-ik\Delta\cos\theta} \int_0^\infty \frac{H_m(\beta b)}{\beta a\, H_m'(\beta a)} \times \left\{ \frac{\cos(\Delta\alpha)\,[\alpha \sin(\ell\alpha)\cos(k\ell\cos\theta) - k\cos\theta\cos(\ell\alpha)\sin(k\ell\cos\theta)]}{(\alpha^2 - k^2\cos\theta)} + \frac{i\sin(\Delta\alpha)\,[k\cos\theta\sin(\ell\alpha)\cos(k\ell\cos\theta) - \alpha\cos(\ell\alpha)\sin(k\ell\cos\theta)]}{(\alpha^2 - k^2\cos^2\theta)} \right\} d\alpha \quad (2.60)$$

Letting $\alpha = kh$, equation 2.60 becomes

$$\frac{4e^{-ik\cos\theta}}{ka} \int_0^\infty \frac{H_m(kb\sqrt{1-h^2})}{\sqrt{1-h^2}\, H_m'(ka\sqrt{1-h^2})} \times \left\{ \frac{\cos(k\Delta h)[\cos(k\ell\cos\theta)h\sin(k\ell h) - \cos\theta\sin(k\ell\cos\theta)\cos(k\ell h)]}{(h^2 - \cos^2\theta)} - \frac{i\sin(k\Delta h)[\cos\theta\cos(k\ell\cos\theta)\sin(k\ell h) - \sin(k\ell\cos\theta)h\cos(k\ell h)]}{(h^2 - \cos^2\theta)} \right\} dh \quad (2.61)$$

Letting the integral in 2.61 be represented by $\psi_m(ka,kb,k\Delta,k\ell,\cos\theta)$, the expression for E_ϕ becomes

$$E_\phi = \frac{iM\omega^2\mu_o e^{ikr} e^{-ik\Delta\cos\theta}}{\pi^2 kb\, r} \sum_{m=1}^{\infty} (-i)^m m \sin m\phi\, J'_m(ka\sin\theta) \times \psi_m(ka,kb,k\Delta,k\ell,\cos\theta) \quad . \quad (2.62)$$

The far zone E_ϕ of the dipole alone is

$$E_{\phi dipole} = -\frac{M\omega^2\mu_o \sin\phi\, e^{-ikb\sin\theta\cos\phi}\, e^{ikr}}{4\pi r} \quad (2.63)$$

so that the total ϕ component of the far zone field is

$$E_{\phi TOT} = -\frac{M\omega^2\mu_o e^{ikr}}{\pi r}\left[\frac{\sin\phi\, e^{-ikb\sin\theta\cos\phi}}{4} - \frac{ie^{-ik\Delta\cos\theta}}{\pi kb}\sum_{m=1}^{\infty}(-i)^m m\sin m\phi\, J'_m(ka\sin\theta)\psi_m(ka,kb,k\Delta,k\ell,\cos\theta)\right] \quad (2.64)$$

The far zone θ-component of electric field due to a current density $\underline{J}$ is (19)

$$E_\theta = \frac{i\omega\mu_o e^{ikr}}{4\pi r}\int_V \underline{J}(\rho',\phi',z')\cdot\underline{e}_\theta\, e^{-ik\underline{r}'\cdot\underline{e}_r}\, dV' \quad (2.65)$$

where $\underline{e}_\theta$ and $\underline{e}_r$ are unit vectors in the θ and r directions respectively, the integration is over the primed coordinates and includes the volume occupied by the source current. For surface currents $\underline{K}$,

equation 2.65 becomes

$$E_\theta = \frac{i\omega\mu_o e^{ikr}}{4\pi r} \int_A \underline{K} \cdot \underline{e}_\theta \; e^{-ik\underline{r}'} \cdot \underline{e}_r \, dA' \quad . \tag{2.66}$$

For the cylinder of Fig. 2.8, $dA' = a d\phi' \; dz'$ and

$$\underline{K} \cdot \underline{e}_\theta = -K_z \sin\theta = -H_\phi(\rho'=a) \sin\theta \; . \tag{2.67}$$

Using equations 2.49 and 2.67, equation 2.66 becomes

$$E_\theta = -\frac{i\omega\mu_o \, ae^{ikr}}{4\pi r} \int_{-\ell_1}^{\ell_2} \int_0^{2\pi} H_\phi(\rho'=a) \sin\theta e^{-ik[a\cos(\phi'-\phi)\sin\theta + z'\cos\theta]} \, d\phi' dz' \tag{2.68}$$

$H_\phi(\rho'=a)$ is obtained from equation 2.22. Since $H'_m(\beta b)/H_m(\beta a) = H'_{-m}(\beta b)/H_{-m}(\beta a)$, equation 2.22 can be written

$$H_\phi(\rho'=a) = \frac{M\omega}{4\pi^2} \sum_{m=0}^{\infty} \epsilon_m \left\{ \int_C \frac{\alpha}{\beta a} \frac{H'_m(\beta b)}{H_m(\beta a)} - \frac{m^2}{\beta^2 ab} \frac{H_m(\beta b)}{H'_m(\beta a)} \; e^{i\alpha z'} d\alpha \right\} \cos m\phi' \; . \tag{2.69}$$

Substituting equation 2.69 into equation 2.68 one obtains

$$E_\theta = -\frac{i M \omega^2 \mu_o a \sin\theta e^{ikr}}{16\pi^3 r} \sum_{m=0}^{\infty} \epsilon_m \int_0^{2\pi} \cos m\phi' e^{-ika\cos(\phi'-\phi)\sin\theta} \, d\phi'$$

$$\times \int_{-\ell_1}^{\ell_2} \int_C \frac{\alpha}{\beta a} \left[\frac{H'_m(\beta b)}{H_m(\beta a)} - \frac{m^2}{\beta^2 ab} \frac{H_m(\beta b)}{H'_m(\beta a)} \right] e^{i\alpha z'} \, e^{-ikz'\cos\theta} \, d\alpha \, dz' . \tag{2.70}$$

It can be shown using equation 2.54 that the first integral in equation 2.70,

$$\int_0^{2\pi} \cos m\phi' e^{-ika\cos(\phi'-\phi)\sin\theta} d\phi' = 2\pi(-i)^m \cos m\phi\, J_m(ka\sin\theta) \quad . \quad (2.71)$$

Thus equation 2.70 becomes

$$E_\theta = -\frac{iM\omega^2\mu_o a \sin\theta\, e^{ikr}}{8\pi^2 r} \sum_{m=0}^{\infty} \epsilon_m (-i)^m \cos m\phi\, J_m(ka\sin\theta)$$

$$\times \int_{-\ell_1}^{\ell_2} \int_C \frac{\alpha}{\beta a}\left[\frac{H_m'(\beta b)}{H_m(\beta a)} - \frac{m^2}{\beta^2 ab}\frac{H_m(\beta b)}{H_m'(\beta a)}\right] e^{i\alpha z'} e^{-ikz'\cos\theta}\, d\alpha\, dz' \quad . (2.72)$$

Because β is an even function of α the double integral in equation 2.72 may be written

$$2i\int_{-\ell_1}^{\ell_2}\int_0^{\infty} \frac{\alpha}{\beta a}\left[\frac{H_m'(\beta b)}{H_m(\beta a)} - \frac{m^2}{\beta^2 ab}\frac{H_m(\beta b)}{H_m'(\beta a)}\right] \sin\alpha z'\, e^{-ikz'\cos\theta}\, d\alpha\, dz' \quad (2.73)$$

where the indentation in the contour at $\alpha = k$ is understood. Interchanging the integral signs, integrating with respect to z', defining ℓ and Δ as in equation 2.59, and letting $\alpha = kh$, the expression for E_θ becomes

$$E_\theta = -\frac{iM\omega^2\mu_o \sin\theta\, e^{ikr}\, e^{-ik\Delta\cos\theta}}{2\pi^2 r} \sum_{m=0}^{\infty} \epsilon_m (-i)^m \cos m\phi\, J_m(ka\sin\theta)$$

$$\times \Upsilon_m(ka, kb, k\Delta, k\ell, \cos\theta) \quad (2.74)$$

where

$$\gamma_m(ka,kb,k\Delta,k\ell,\cos\theta) = \int_0^\infty \frac{h}{\sqrt{1-h^2}}\left[\frac{H_m'(kb\sqrt{1-h^2})}{H_m(ka\sqrt{1-h^2})} - \frac{m^2 H_m(kb\sqrt{1-h^2})}{(1-h^2)kakbH_m'(ka\sqrt{1-h^2})}\right]$$

$$\times\left\{\frac{\cos(k\Delta h)[\cos(k\ell\cos\theta)\cos\theta\,\sin(k\ell h) - \sin(k\ell\cos\theta)h\cos(k\ell h)]}{(h^2-\cos^2\theta)}\right.$$

$$\left.+\frac{i\,\sin(k\Delta h)[\cos(k\ell\cos\theta)h\,\sin(k\ell h) - \cos\theta\,\sin(k\ell\cos\theta)\cos(k\ell h)]}{(h^2-\cos^2\theta)}\right\}dh. \tag{2.75}$$

The far zone E_θ of the dipole alone is

$$E_{\theta dipole} = \frac{M\omega^2\mu_o\cos\theta\cos\phi\, e^{-ikb\sin\theta\cos\phi}\, e^{ikr}}{4\pi r} \tag{2.76}$$

so that the total θ component of the far zone field is

$$E_{\theta TOT} = \frac{M\omega^2\mu_o e^{ikr}}{2\pi r}\left[\frac{\cos\theta\cos\phi\, e^{-ikb\sin\theta\cos\phi}}{2} - \frac{i\sin\theta e^{-ik\Delta\cos\theta}}{\pi}\right.$$

$$\left.\times\sum_{m=0}^{\infty}\epsilon_m(-i)^m\cos m\phi\, J_m(ka\sin\theta)\gamma_m(ka,kb,k\Delta,k\ell,\cos\theta)\right]. \tag{2.77}$$

Equations 2.64 and 2.77 completely determine the far zone field of a finite cylinder excited by a radial electric dipole.

It should be noted that in deriving equations 2.64 and 2.77, fields due to currents which flow on the end plates of the cylinder have been neglected. This is a good approximation for long cylinders because the currents which flow on the end plates are of the same order of magnitude as the currents which flow near the ends of the cylinder on the cylindrical surface itself. These currents were shown to be small in section 2.2 and should modify the radiation

pattern noticeably only near the minima.

Because of the complexity of the expressions for $\psi_m(ka,kb,k\Delta,k\ell,\cos\theta)$ and $\gamma_m(ka,kb,k\Delta,k\ell,\cos\theta)$, they are most easily evaluated with the aid of an electronic computer.* The method of numerical evaluation is discussed in Appendix 2. It is possible to obtain values for $\psi_m(ka,kb,k\Delta,k\ell,\cos\theta)$ and $\gamma_m(ka,kb,k\Delta,k\ell,\cos\theta)$ for a complete radiation pattern in a relatively short time by computing both quantities on the same computing program.

2.4 Radiation Patterns for the Finite Cylinder

With the computed values of $\psi_m(ka,kb,k\Delta,k\ell,\cos\theta)$ and $\gamma_m(ka,kb,k\Delta,k\ell,\cos\theta)$, the radiation at any point in the far zone can be computed by means of equations 2.64 and 2.77. The nature of the radiation patterns is exhibited in Fig. 2.9 for the case of $kb = ka = .6317$, $k\Delta = 2.618$, $k\ell = 5\pi/2$ which corresponds to a diameter of about $\lambda/5$, a total cylinder length of 2.5λ and the dipole a distance of about $.4\lambda$ from the midplane of the cylinder. Fig. 2.9 shows $E_{\theta TOT}$ in the half planes $\phi = 0^\circ$, 60°, 120°, and 180°. The direction of the longer portion of the cylinder is toward the top of the page. The general shape of the patterns is similar throughout the entire range from $\phi = 0^\circ$ to $\phi = 180^\circ$ although distinct quantitative differences occur. At $\phi = 0^\circ$ the two large lobes are maximum. As ϕ increases the large lobes decrease and gradually bend away from the

*The I.B.M. 709 computing facilities at the Western Data Processing Center and at Hughes Aircraft Company were used.

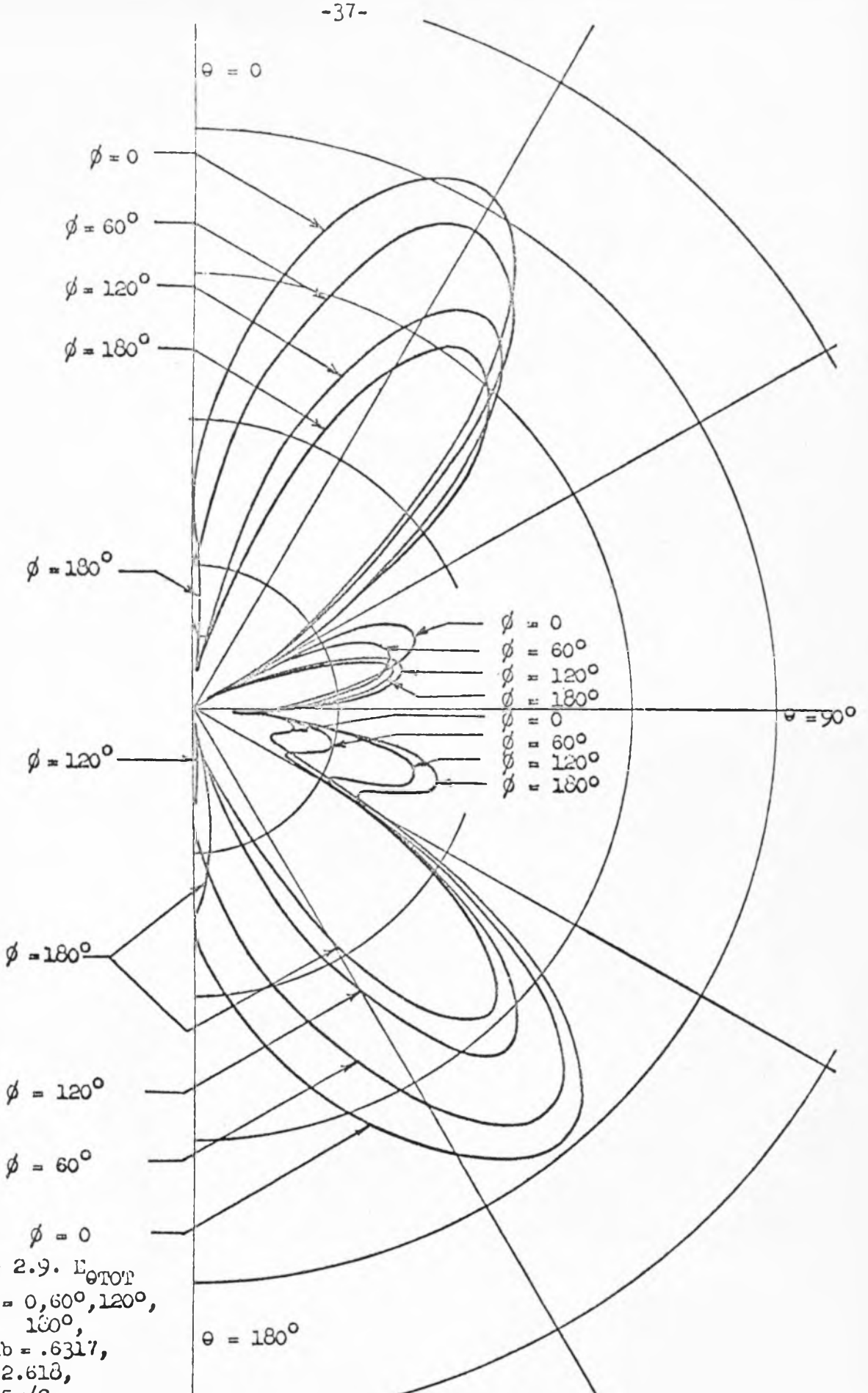

Figure 2.9. $E_{\theta TOT}$ for $\phi = 0, 60°, 120°, 180°$, $ka = kb = .6317$, $k\Delta = 2.618$, $k\ell = 5\pi/2$

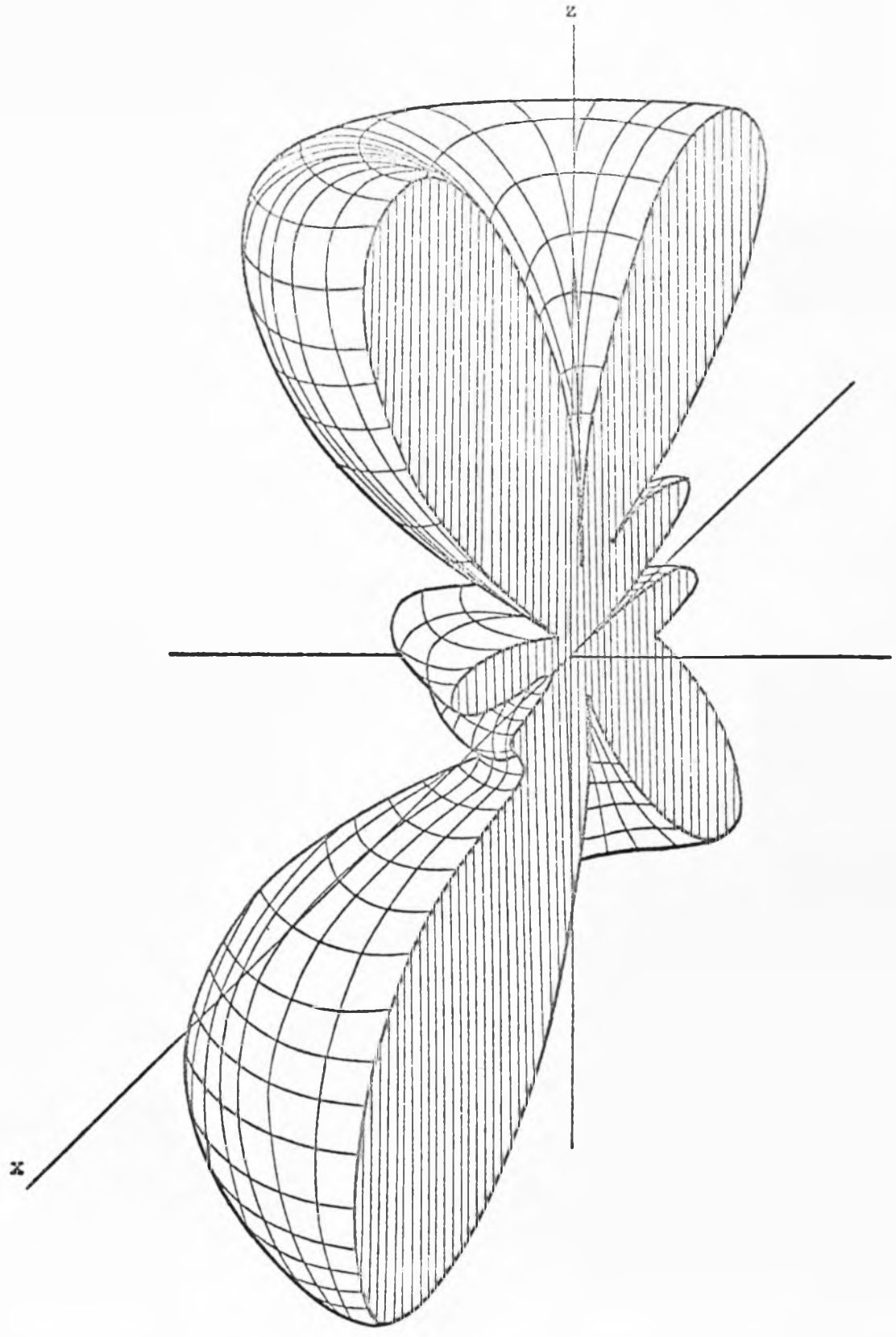

Figure 2.10. Relief of E_{TOT} in Region $-180^{\circ} \leq \phi \leq 0$ for Cylinder at Origin with Axis in z direction and Dipole in x direction. $ka = kb = .6317$, $k\Delta = 2.618$, $k\ell = 5\pi/2$.

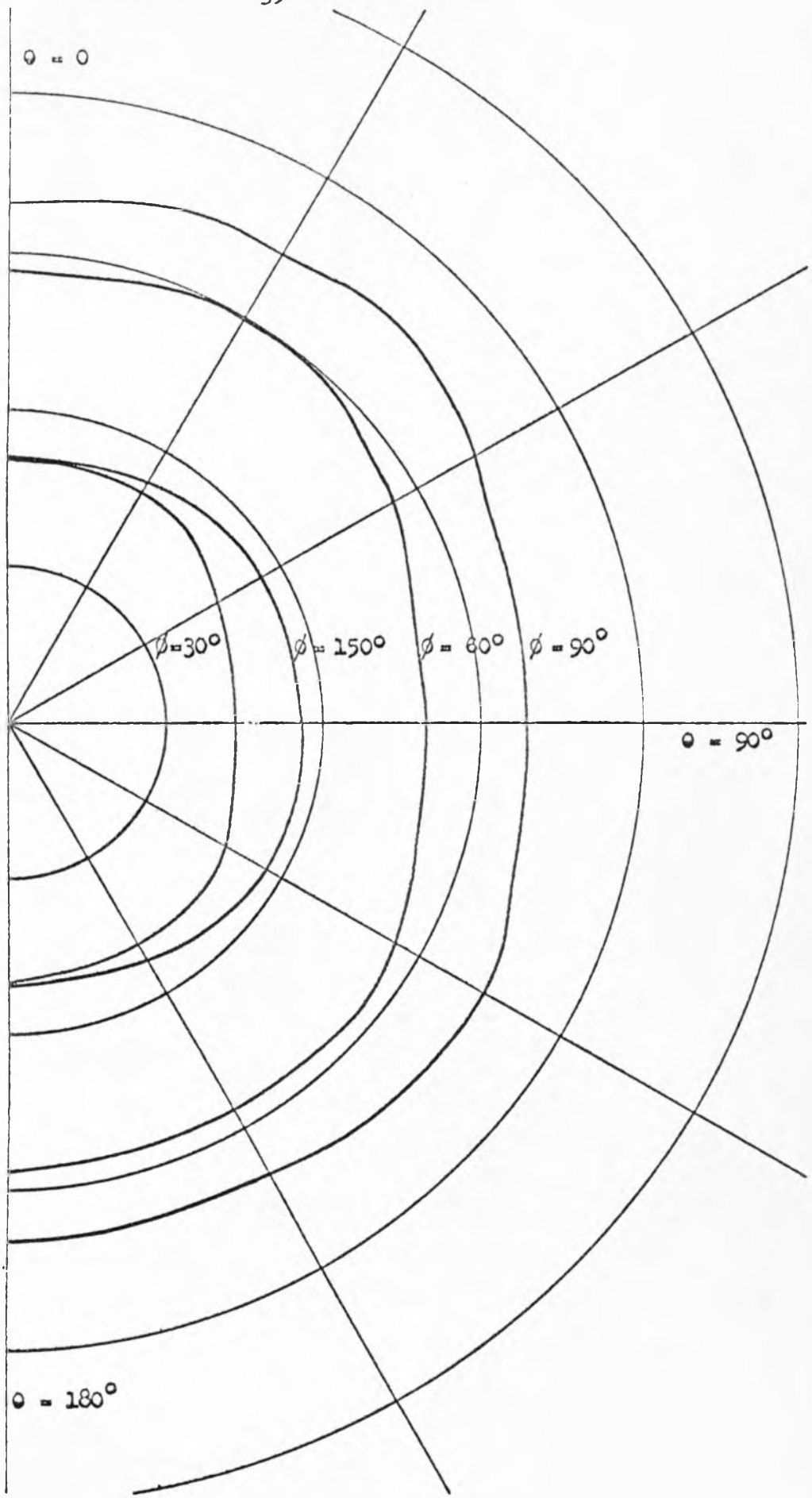

Figure 2.11

$E_{\phi TOT}$ for

$\phi = 30°, 60°, 90°$
$150°.$

$ka = kb = .6317,$

$k\Delta = 2.618,$

$kl = 5\pi/2$

axis of the cylinder. The small lobe near $\theta = 80^\circ$ stays approximately constant in amplitude but the small lobe near $\theta = 110^\circ$ increases as ϕ increases. The asymmetrical nature of the lobes should be noted; the pattern is not symmetrical about $\theta = 90^\circ$. The direction of the largest main lobe is always nearest the direction of the longer portion of the cylinder. A relief of the $E_{\theta TOT}$ pattern is shown in Fig. 2.10 for the region $-180^\circ \leq \phi \leq 0$. The cylinder axis is in the z direction and the dipole points in the x direction. $E_{\phi TOT}$ in the half planes $\phi = 30^\circ, 60^\circ, 90^\circ, 150^\circ$ for the same cylinder is shown in Fig. 2.11. $E_{\phi TOT}$ is zero for $\phi = 0^\circ, 180^\circ$ and the radiation patterns are almost circular for other values of ϕ. As ϕ increases from $\phi = 0^\circ$ to 180°, $E_{\phi TOT}$ increases; reaches a maximum at $\phi = 90^\circ$, and then decreases to zero at 180°. As in the case of $E_{\theta TOT}$ the patterns are qualitatively of similar shape for different values of ϕ. Because of this property, only patterns in the half plane $\phi = 90^\circ$ will be considered in the following and the pattern for other values of ϕ should show behavior similar to that of Figs. 2.9 and 2.11, i.e., the major lobes of $E_{\theta TOT}$ decrease and bend and $E_{\phi TOT}$ increases from zero to a maximum at 90° and then decreases to zero as ϕ increases from 0° to 180°. For larger cylinder radii than those discussed here this behavior probably does not always occur since the greater number of terms in the series of equations 2.64 and 2.77 which must be used modify the patterns more as ϕ increases. The pattern of $E_{\theta TOT}$ for $\phi = 90^\circ$ for the cylinder of Figs. 2.9 and 2.11 is shown in Fig. 2.12. A pattern of $E_{\theta TOT}$ for the same cylinder but with the dipole closer to one end than the previous

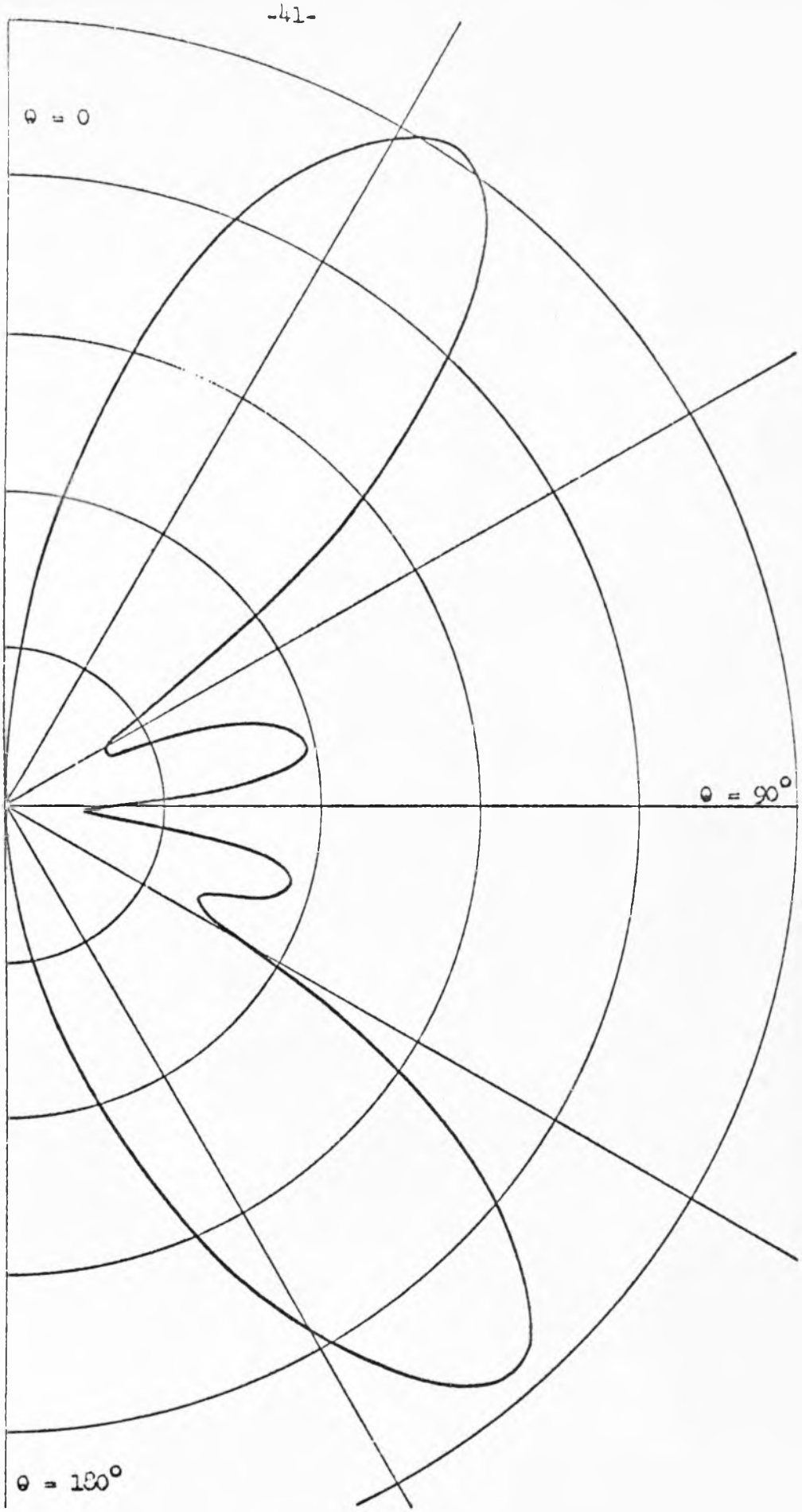

Figure 2.12.

$E_{\theta TOT}$ for
$\phi = 90°$
$ka = kb = .6317$,
$k\Delta = 2.618$,
$k\ell = 5\pi/2$

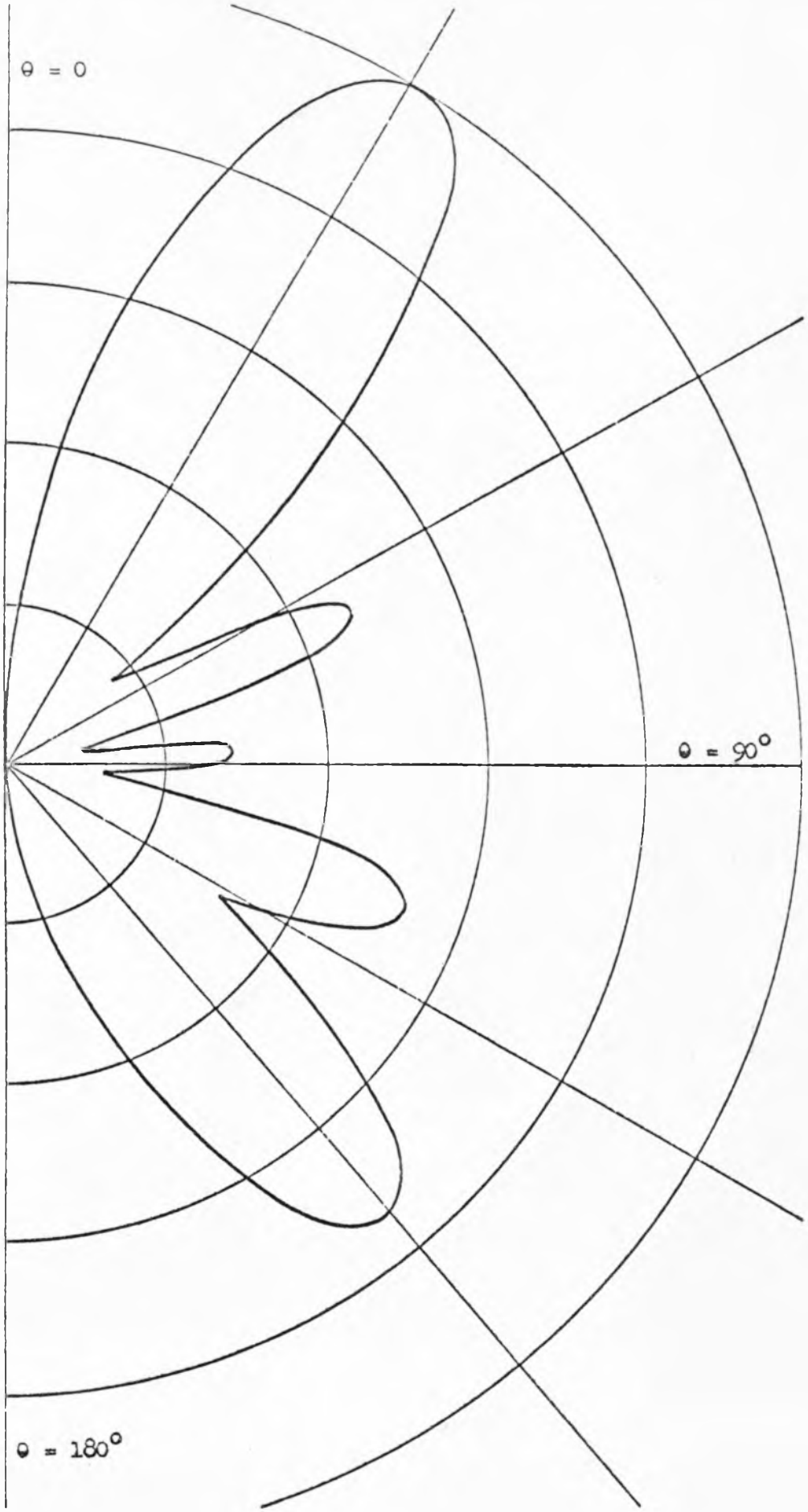

Figure 2.13

$E_{\theta TOT}$ for
$\phi = 90°$
$ka = kb = .6317$,
$k\Delta = 5.236$,
$k\ell = 5\pi/2$

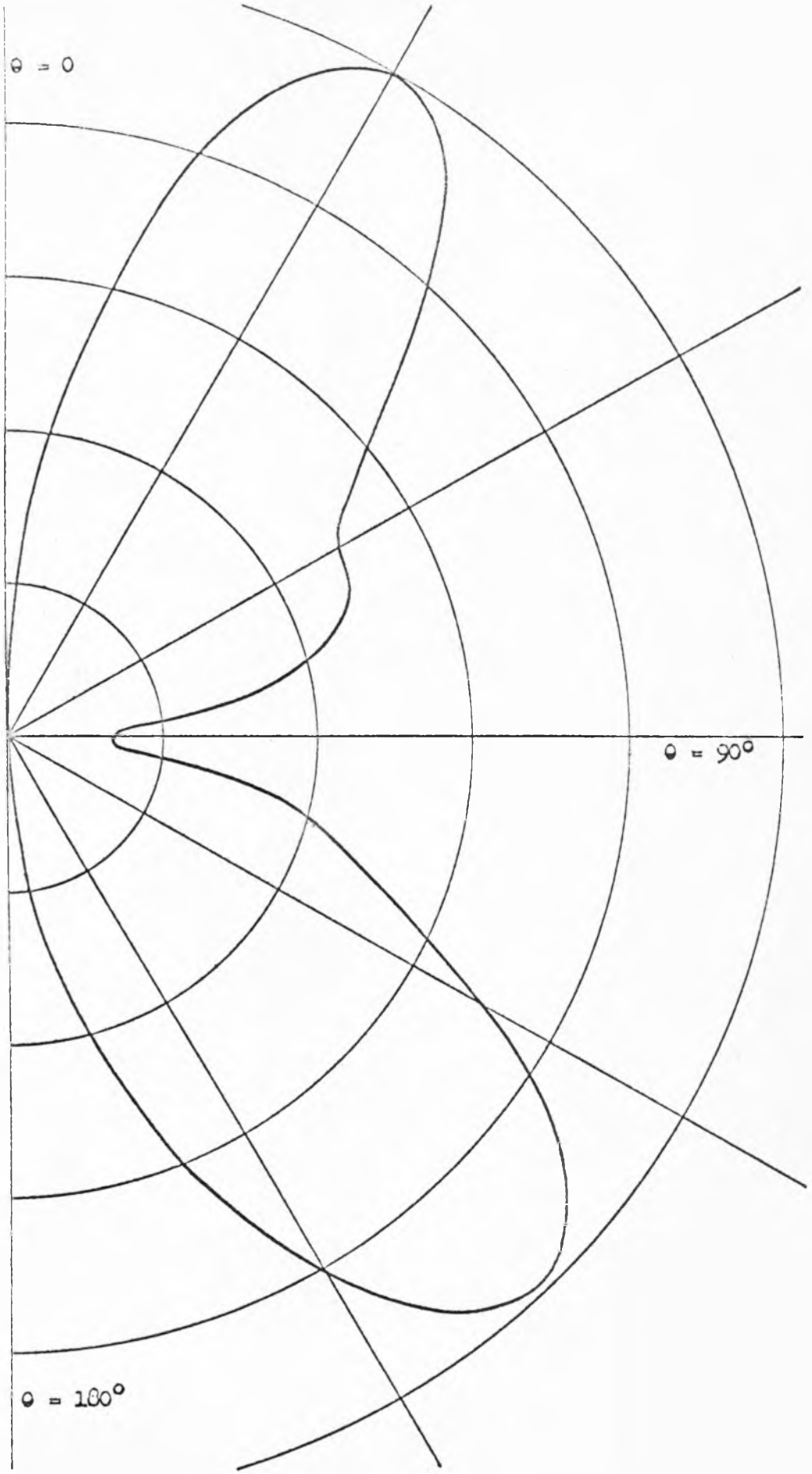

Figure 2.14

$E_{\theta TOT}$ for
$\phi = 90°$

$ka = kb = 2.0$,
$k\Delta = 2.618$,
$kl = 5\pi/2$

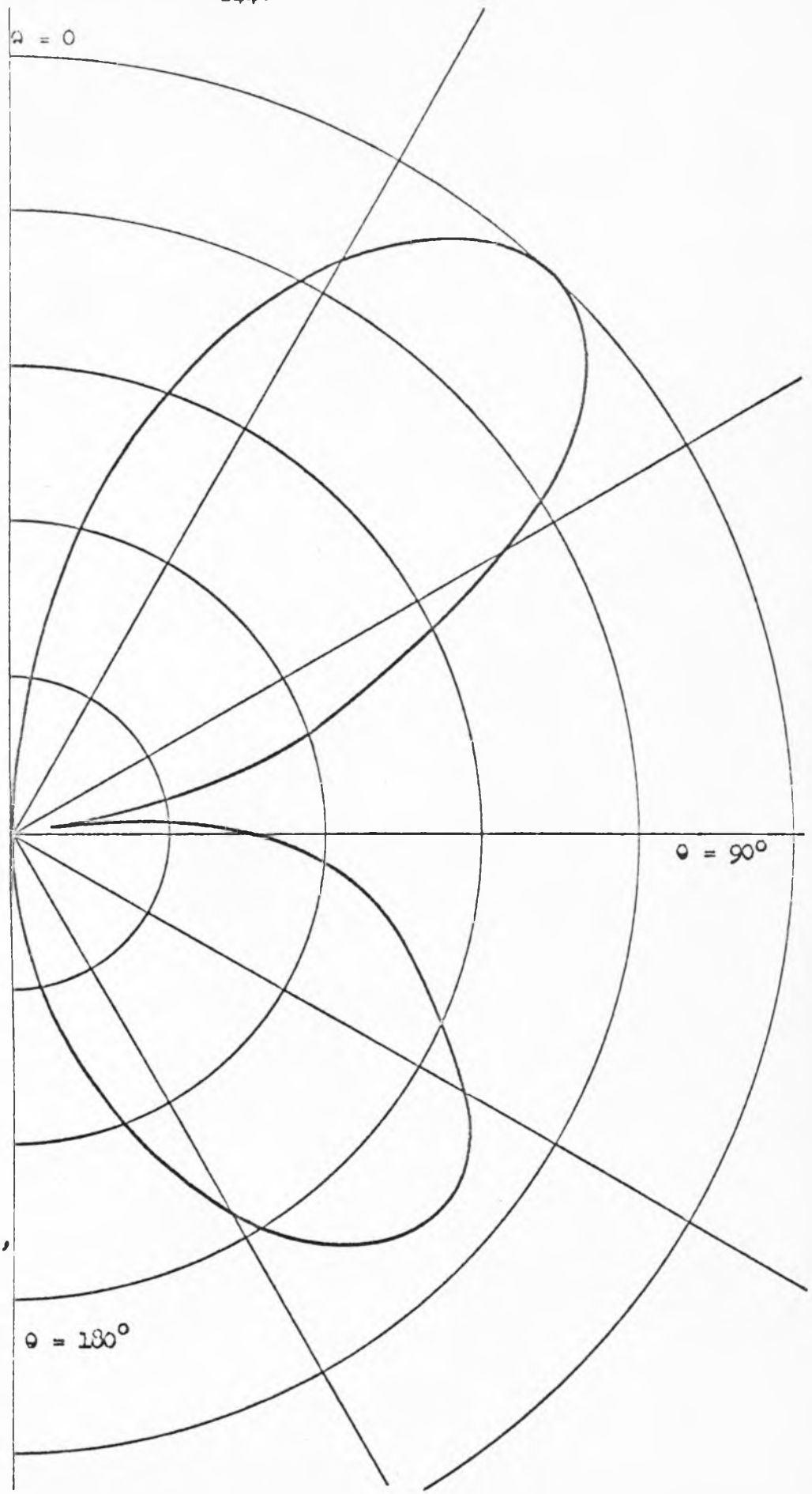

Figure 2.15
$E_{\theta TOT}$ for
$\phi = 90°$
$ka = kb = .6317$,
$k\Delta = 1.309$,
$k\ell = (5/4)\pi$

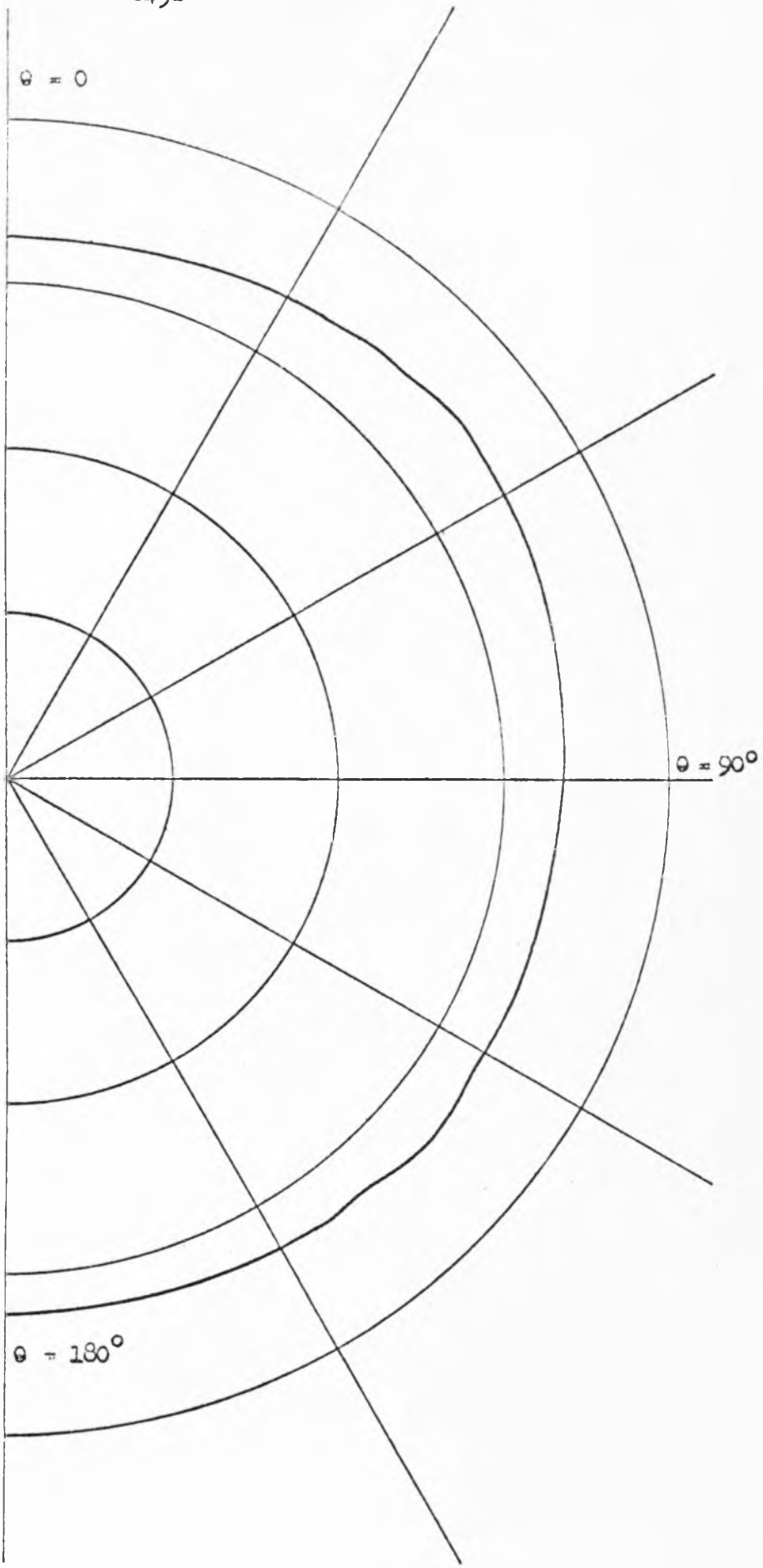

Figure 2.16

$E_{\phi TOT}$ for $\phi = 90^\circ$

$ka = kb = .6317$

$k\Delta = 1.309$

$k\ell = 5\pi/4$

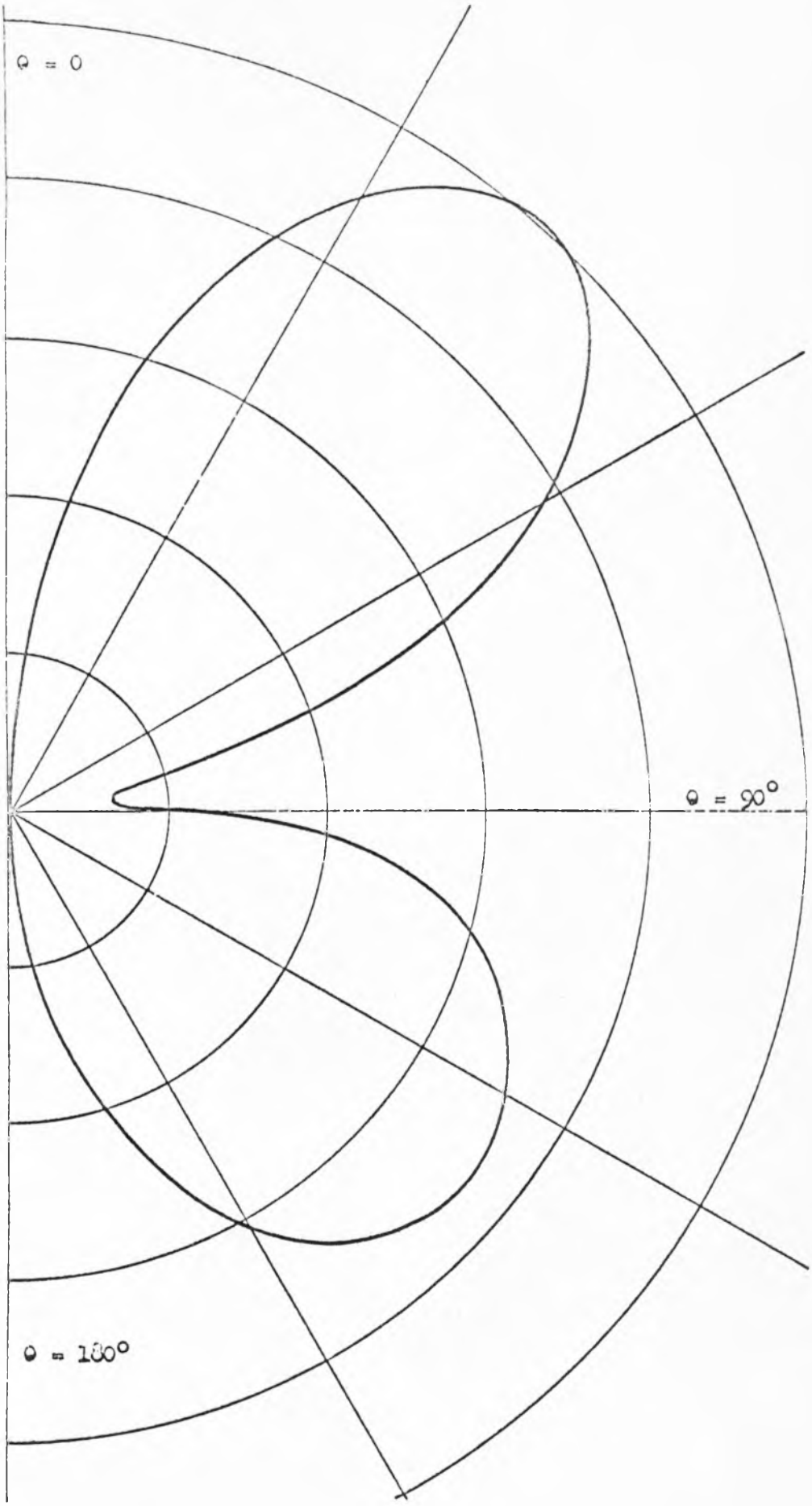

Figure 2.17.
$E_{\theta TOT}$ for
$\phi = 90°$.
$ka = kb = 2.0$,
$k\Delta = 1.309$
$k\ell = 5\pi/4$

case is shown in Fig. 2.13. In this figure $k\Delta = 5.236$ which corresponds to the dipole located at a distance of about $.4\lambda$ from the end of the cylinder. Locating the dipole nearer the end causes the largest lobe to move closer to the axis of the cylinder and also introduces a new lobe near $\theta = 90^{\circ}$. The asymmetry of the pattern is also increased. $E_{\phi TOT}$, however, does not change appreciably.

The effects of increasing the radius of the cylinder is exhibited in Fig. 2.14. This is the $E_{\theta TOT}$ pattern corresponding to a configuration of identical dimensions to the cylinder and dipole location of Fig. 2.12 except that the radius has been increased from $ka = .6317$ to $ka = 2.0$ which corresponds to a diameter of about $.6\lambda$. The main effect is the broadening of the lobes and the filling of the deep minima which occur in the case of smaller cylinder diameter. These changes are due largely to the increased magnitude of the higher order terms in the series of equation 2.77. The $E_{\phi TOT}$ pattern is not shown since it is not greatly modified.

$E_{\theta TOT}$ for a shorter cylinder is shown in Fig. 2.15 which is for $kb = ka = .6317$, $k\ell = 3.927$, $k\Delta = 1.309$. This corresponds to a diameter of about $\lambda/5$, a total cylinder length of 1.25λ and the dipole a distance of about $.2\lambda$ from the midplane of the cylinder. The small lobes of the pattern of the longer cylinder are not present. $E_{\phi TOT}$ for this cylinder is shown in Fig. 2.16. $E_{\theta TOT}$ for a cylinder of larger radius but the same length and dipole location is shown in Fig. 2.17. The lobes are again broadened as in the previous case.

2.5 The Turnstile Antenna

A very commonly used antenna consists of four radial dipoles placed at $\phi = 0, \pi/2, \pi,$ and $3\pi/2$, being energized so that the phase of each dipole is $\pi/2$ less than the preceding one as one proceeds from $\phi = 0$ to $\phi = 2\pi$. Thus in Fig. 2.18, dipole 1 has current $I_o \cos \omega t$, dipole 2 has $I_o \cos (\omega t - \pi/2)$, dipole 3 has $I_o \cos(\omega t - \pi)$, and dipole 4 has $I_o \cos(\omega t - 3\pi/2)$. This antenna has the property that it has an omnidirectional pattern of horizontal polarization in the plane $\theta = \pi/2$ if the dipoles are at the origin. An antenna of this type is called a turnstile antenna. In practice quarter wave antennas are used but since the far zone radiation of a quarter wave antenna and a dipole differs only by a few percent, the two cases are quite similar.

In practice the four dipoles must always be supported by a suitable structure and usually a cylindrical support is used as in Fig. 2.19. If the cylindrical support is conducting, it may modify the radiation pattern considerably. It is, however, a relatively simple matter to calculate the radiation from the configuration of Fig. 2.19 from the expressions derived in section 2.3. It is necessary to add the far zone radiation from the four dipoles with the proper phase relationship. From equation 2.64 the field due to the dipole at $\phi = 0$ and the cylinder is

$$E_{\phi TOT} = -\frac{M\omega^2\mu_o e^{ikr}}{4\pi r}\left[\sin\phi\, e^{-ika \sin\theta \cos\phi} - \frac{4ie^{-ik\Delta\cos\theta}}{\pi ka} \times \sum_{m=1}^{\infty} (-i)^m m\, A_m \sin m\phi\right] \qquad (2.78)$$

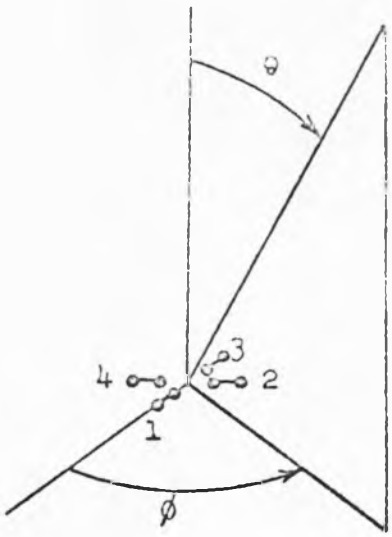

Figure 2.18. Turnstile Antenna

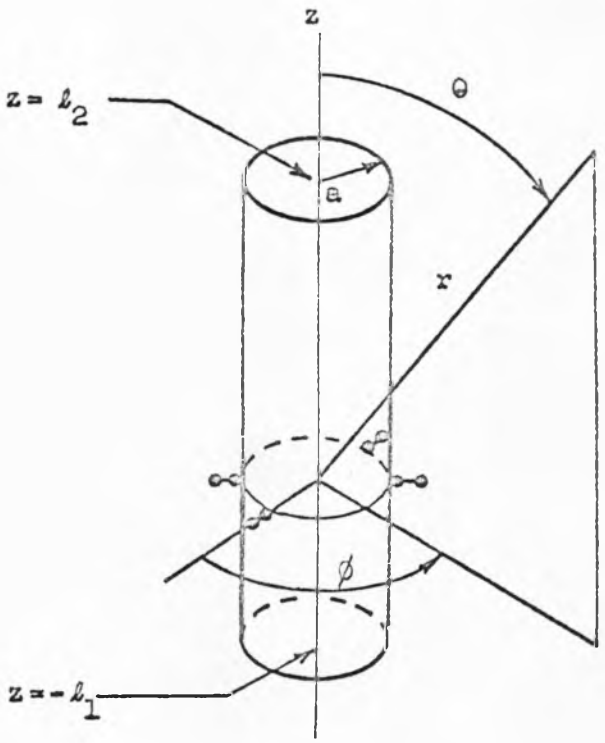

Figure 2.19. Turnstile Antenna with Cylinder

where b has been placed equal to a since the dipole is at the surface of the cylinder. Also $A_m = J'_m(ka \sin\theta)\, \psi_m(ka, ka, k\Delta, k\ell, \cos\theta)$. Adding the fields due to each dipole with the proper spatial and phase relation, one obtains

$$E_\phi = -\frac{M\omega^2\mu_o e^{ikr}}{4\pi r}\left\{\sin\phi\, e^{-ika\sin\theta\cos\phi} - \frac{i4e^{-ik\Delta\cos\theta}}{\pi ka}\sum_{m=1}^{\infty}(-i)^m m A_m \sin m\phi\right.$$

$$-i\sin(\phi+\tfrac{\pi}{2})e^{-ika\sin\theta\cos(\phi+\frac{\pi}{2})} - \frac{i(-i)4e^{-ik\Delta\cos\theta}}{\pi ka}\sum_{m=1}^{\infty}(-i)^m m A_m \sin m(\phi+\tfrac{\pi}{2})$$

$$-\sin(\phi+\pi)e^{-ika\sin\theta\cos(\phi+\pi)} + \frac{i4e^{-ik\Delta\cos\theta}}{\pi ka}\sum_{m=1}^{\infty}(-i)^m m A_m \sin m(\phi+\pi)$$

$$+i\sin(\phi+\tfrac{3\pi}{2})e^{-ika\sin\theta\cos(\phi+\frac{3\pi}{2})} - \frac{i(i)4e^{-ik\Delta\cos\theta}}{\pi ka}$$

$$\left.\times\sum_{m=1}^{\infty}(-i)^m m A_m \sin m(\phi+\tfrac{3\pi}{2})\right\}. \qquad (2.79)$$

After simplification, equation 2.79 becomes

$$E_\phi = -\frac{M\omega^2\mu_o e^{ikr}}{2\pi r}\left\{\sin\phi\cos(ka\sin\theta\cos\phi)\right.$$

$$-i\cos\phi\cos(ka\sin\theta\sin\phi) + \frac{i4e^{-ik\Delta\cos\theta}}{\pi ka}\sum_{m=1}^{\infty}(2m-1)A_{2m-1}$$

$$\left.\times e^{i(-1)^{m+1}(2m-1)\phi}\right\}. \qquad (2.80)$$

Using equation 2.77 in a similar manner the expression for E_θ is

$$E_\theta = \frac{M\omega^2\mu_o e^{ikr}}{2\pi r}\left\{\cos\theta\cos\phi\cos(ka\sin\theta\cos\phi) + i\cos\theta\sin\phi\cos(ka\sin\theta\sin\phi)\right.$$

$$\left. - \frac{4\sin\theta e^{-ik\Delta\cos\theta}}{\pi}\sum_{m=1}^{\infty}(-1)^{m+1}B_{2m-1}e^{i(-1)^{m+1}(2m-1)\phi}\right\} \qquad (2.81)$$

where $B_m = J_m(ka \sin\theta)\gamma_m(ka,ka,k\Delta,k\ell,\cos\theta)$.

The plane $\theta = \pi/2$ is of interest for turnstile antennas. If the dipoles are at the origin, E_ϕ is constant with ϕ, and E_θ is zero in this plane. However, if they are moved outward radially the pattern of E_ϕ is no longer omnidirectional and if a conducting cylinder is present, the pattern is further modified. This effect is shown in Fig. 2.20 for a rather short cylinder of small diameter. The smaller pattern is of the dipoles alone at a distance a from the origin. This pattern is approximately doubled by the currents on the cylinder. There is also an E_θ present in this plane which is not present in the absence of the cylinder. In Fig. 2.21 is shown the pattern of E_ϕ for a cylinder of larger diameter but of the same length. In this case the deep minima of dipole pattern disappear upon introduction of the cylinder.

2.6 The Long Cylinder of Small Radius

An interesting solution can be obtained in closed form for the special case of a long finite cylinder of small radius. The method of approximation discussed in section 2.2 is again used, but a different method is used in the derivation of the far zone field. Because the length of the cylinder is assumed to be very long in this section, the analytic expressions for the currents which flow on the portions of the infinite cylinder above ℓ_2 and below $-\ell_1$, which are not to be included in the calculation for the field of the finite cylinder, have a very simple form. They are just the currents derived in section 2.2 which are valid for large z. Thus, to derive an expression for the fields of a very long finite cylinder, the

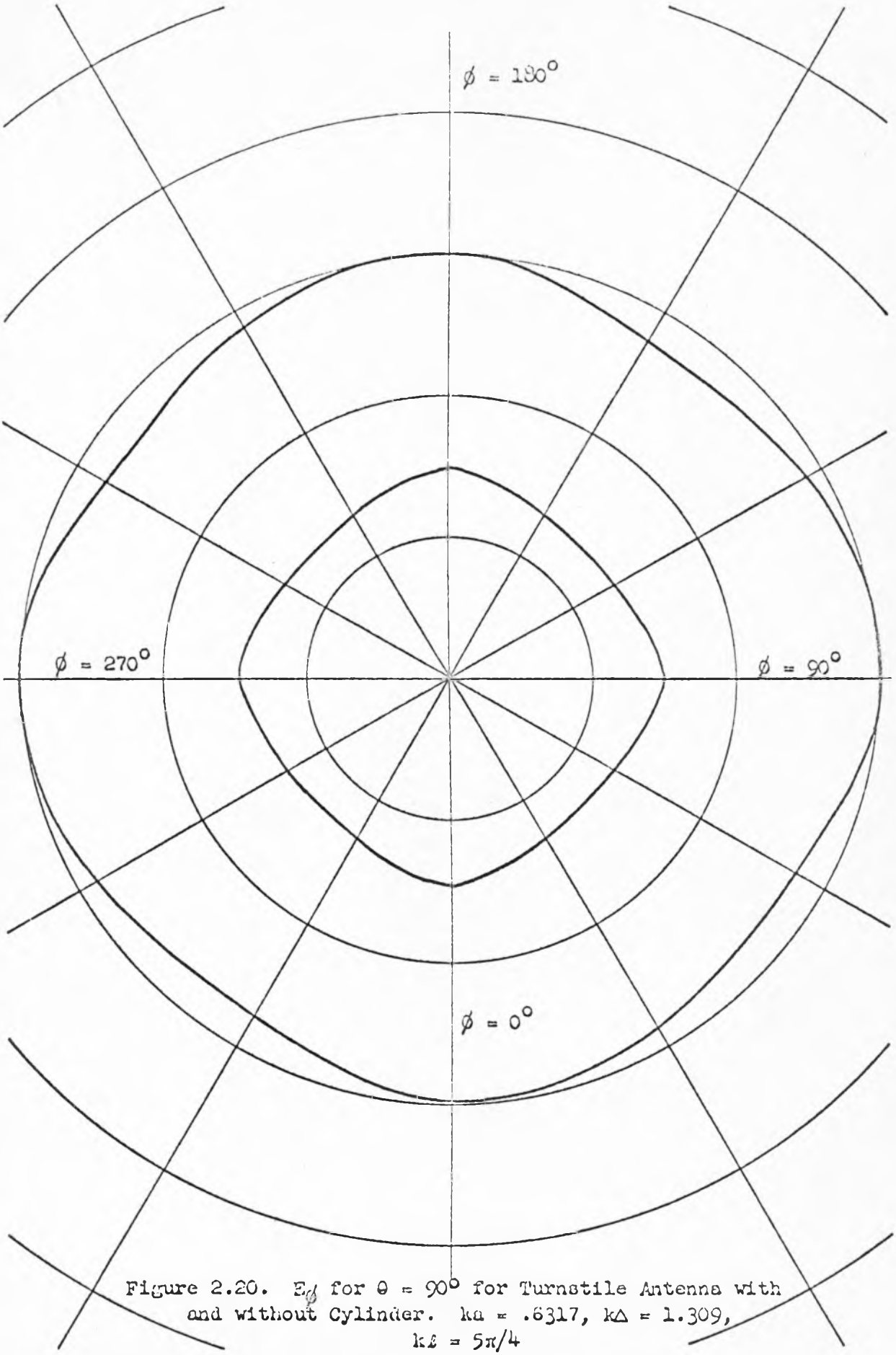

Figure 2.20. E_ϕ for $\theta = 90^\circ$ for Turnstile Antenna with and without Cylinder. $ka = .6317$, $k\Delta = 1.309$, $k\ell = 5\pi/4$

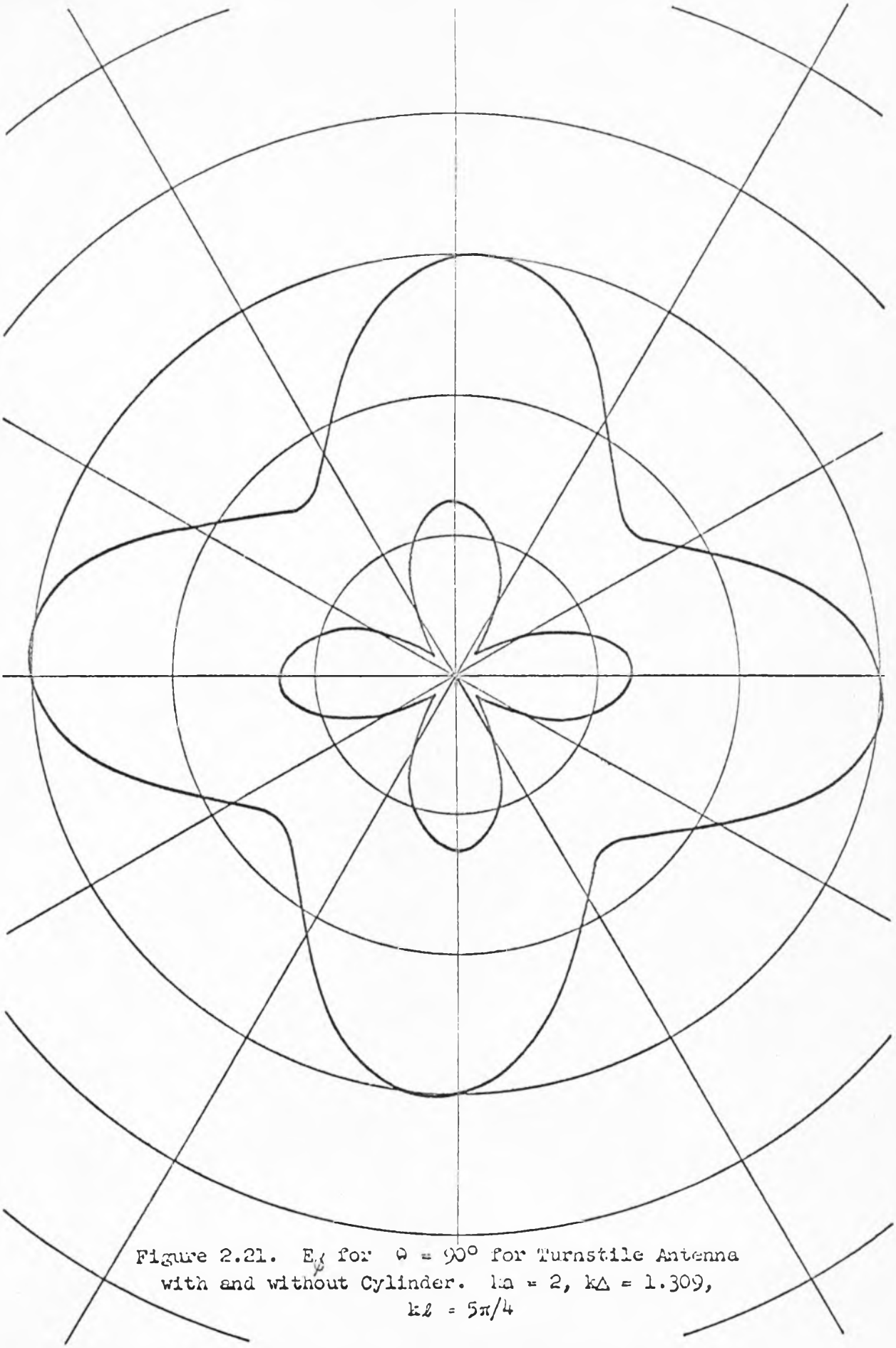

Figure 2.21. E_ϕ for $\theta = 90^\circ$ for Turnstile Antenna with and without Cylinder. $ka = 2$, $k\Delta = 1.309$, $k\ell = 5\pi/4$

partial field due to the analytically simple currents above ℓ_2 and below $-\ell_1$ on the infinite cylinder is calculated and then subtracted from the complete field of the infinite cylinder. In this way the definite integrals, ψ_m and γ_m, described in section 2.3, are avoided since the fields are calculated in an indirect manner without explicitly considering the currents on the cylinder near the origin.

The field of an infinite cylinder with dipole excitation at $b = a$ is given in equations 2.13 and 2.14. For small ka, the leading term in the series is retained and the small argument approximations for the Hankel functions are used to yield in free space

$$E_\theta = \frac{Mk\, e^{ikr} \cos\theta}{i4\pi\epsilon_0 ar \sin\theta\, \ell n(\frac{\gamma\, ka \sin\theta}{2})} \tag{2.82}$$

$$E_\phi = -\frac{Mk^2 e^{ikr} \sin\phi}{2\pi\epsilon_0 r} \tag{2.83}$$

where $\gamma = 1.781072$. For very small ka, E_ϕ becomes negligible compared to E_θ and therefore only E_θ will be considered in the following.

The current on the infinite cylinder for large z is, from equation 2.31

$$I_z = 2\pi a K_z = \frac{iM\omega e^{ikz}}{2a\, \ell n(\frac{2kz}{\gamma k^2 a^2})} = \frac{iM\omega e^{ikz}}{2a\left[\ell n(kz) - \ell n(\frac{\gamma k^2 a^2}{2})\right]} . \tag{2.84}$$

ka is assumed small enough so that $\ell n(kz)$ can be neglected with

respect to $\ell n(\frac{\gamma k^2 a^2}{2})$ in the denominator of equation 2.84. For this condition equation 2.84 becomes

$$I_z = -\frac{iM\omega e^{ikz}}{2a\ \ell n(\frac{\gamma k^2 a^2}{2})} \tag{2.85}$$

which shows that the current is sinusoidal for small ka. This current flows above ℓ_2 and below $-\ell_1$ and it is now necessary to obtain the field produced by it. Schelkunoff (21) gives a solution originally discovered by Manneback, which is the correct one in this case. The solution is valid for a semi-infinite thin wire and in spherical coordinates it is

$$E_\theta = \sqrt{\frac{\mu_o}{\epsilon_o}}\ \frac{I(t - r\sqrt{\mu_o\epsilon_o})(1+\cos\theta)}{4\pi r \sin\theta} \quad . \tag{2.86}$$

I(t) is the current at the end of the wire at the origin and the wire extends from the origin along the radius, $\theta = 0$, to infinity. For the case of the wire beginning at $z = \ell_2$ instead of at the origin carrying the current given in equation 2.85, equation 2.86 becomes

$$E_\theta = \frac{Mke^{ik\ell_2(1-\cos\theta)}\ e^{ikr}\ (1+\cos\theta)}{i8\pi\epsilon_o ar \sin\theta\ \ell n(\frac{\gamma k^2 a^2}{2})} \quad . \tag{2.87}$$

Equation 2.87 holds if the distance to the point of observation, r , is large compared to ℓ_2. Similarly, the field due to the currents below $-\ell_1$ is given by

$$E_\theta = - \frac{Mke^{ik\ell_1(1+\cos\theta)} e^{ikr}(1-\cos\theta)}{i8\pi\epsilon_o ar \sin\theta \, \ell n(\frac{\gamma k^2 a^2}{2})} \quad . \tag{2.88}$$

The solution for the finite cylinder of length $\ell_1 + \ell_2$ is then given by

$$E_\theta = \frac{Mk\, e^{ikr}}{i4\pi\epsilon_o ar \sin\theta} \left[\frac{\cos\theta}{\ell n(\frac{\gamma ka \sin\theta}{2})} - \frac{e^{ik\ell_2(1-\cos\theta)}(1+\cos\theta)}{2\,\ell n(\frac{\gamma k^2 a^2}{2})} + \frac{e^{ik\ell_1(1+\cos\theta)}(1-\cos\theta)}{2\,\ell n(\frac{\gamma k^2 a^2}{2})} \right] \tag{2.89}$$

where the field due to the currents above ℓ_2 and below $-\ell_1$ has been subtracted from the field of the infinite cylinder. The singularity which occurs along the axis in the case of the infinite cylinder (section 2.1) is now eliminated in equation 2.89 since at the surface of the infinite cylinder, $\sin\theta \approx a/z$, $\cos\theta \approx 1$ and $r \approx z$, so that equation 2.89 becomes

$$E_\theta = \frac{Mke^{ikr}}{i4\pi\epsilon_o a^2} \left[\frac{1}{\ell n(\frac{\gamma k^2 a^2}{2kz})} - \frac{1}{\ell n(\frac{\gamma k^2 a^2}{2})} \right] \quad . \tag{2.90}$$

Since it was assumed previously that $\ell n\, kz$ can be neglected with respect to $\ell n(\frac{\gamma k^2 a^2}{2})$, equation 2.90 can be written

$$E_\theta = \frac{Mke^{ikr}}{i4\pi\epsilon_o a^2} \left[\frac{1}{\ell n(\frac{\gamma k^2 a^2}{2})} - \frac{1}{\ell n(\frac{\gamma k^2 a^2}{2})} \right] = 0 \quad . \tag{2.91}$$

A similar result is found at $\theta = \pi$ so that the singularity has been

removed at the axis. Thus equation 2.89 is a simple expression for the far zone field of a long finite cylinder of small radius and is valid anywhere in the far zone.

3. THE ASYMMETRICALLY FED PROLATE SPHEROIDAL ANTENNA; THEORY

Another basic type of asymmetrically excited radiating system is the usual asymmetrically excited antenna. This consists of a cylinder, prolate spheroid, or any elongated body of revolution excited by a tangential belt of electric field which is not necessarily centered at the midplane of the body. The prolate spheroid is treated here for the following reasons. No experimental study of asymmetrically excited prolate spheroids had been done in the past, and since the facilities of the antenna range described in Appendix 1 are well suited to measurement of isolated antennas, i.e., with no external connecting transmission line, this study could be advantageously pursued. Also since an exact analytical solution is possible for the prolate spheroid, at least for the case when the form of the impressed belt field is known, any discrepancy between measured and theoretical radiation patterns evidently stems from an incorrect assumption for the mathematical form of the impressed field. Thus the measured radiation pattern yields information about this assumption. This is considered further in Chap. 5. From a practical standpoint, the asymmetrically fed cylindrical antenna is more important. However, even if the solution for the finite cylinder were desired rather than the solution of the prolate spheroid, the approximation involved in replacing the cylinder by the spheroid is probably better than the approximations one must use in solving the integral equation for the finite cylinder (11). Actually, the asymmetrically fed spheroid has practical importance in its own right because it is a good approximation to a commonly used satellite antenna.

It should be noted that the prolate spheroid was not treated for the configuration of Chap. 2 because as discussed in Chap. 1, extreme mathematical difficulties arise due to the ϕ-dependence of the problem.

3.1 The Mathematical Solution for the Asymmetrically Fed Prolate Spheroidal Antenna

The analytic solution of the asymmetrically fed prolate spheroid will now be presented. The analysis follows that of Schelkunoff (21) and Myers (15).

The prolate spheroidal coordinate system is shown in Fig. 3.1. The radial variable is u and the two angular variables are v and ϕ. A particular value of u, v, and ϕ determines a particular point in space by means of the equations

$$\frac{z^2}{u^2} + \frac{x^2}{u^2-1} + \frac{y^2}{u^2-1} = L^2 \tag{3.1}$$

$$\frac{z^2}{v^2} - \frac{x^2}{1-v^2} - \frac{y^2}{1-v^2} = L^2 \tag{3.2}$$

$$\phi = \phi \quad . \tag{3.3}$$

$2L$ is the interfocal distance.

The intersection of the spheroid defined by equation 3.1 and the hyperboloid defined by equation 3.2 and the half-plane defined by equation 3.3 locates a point in the coordinate system.

For a field which is circularly symmetric about the z axis, Maxwell's equations become with $\exp(-i\omega t)$ time dependence

$$L\left(\frac{u^2 - v^2}{1 - v^2}\right)^{1/2} E_u = \frac{i}{\omega \epsilon_o \rho} \frac{\partial(\rho H_\phi)}{\partial v} \tag{3.4}$$

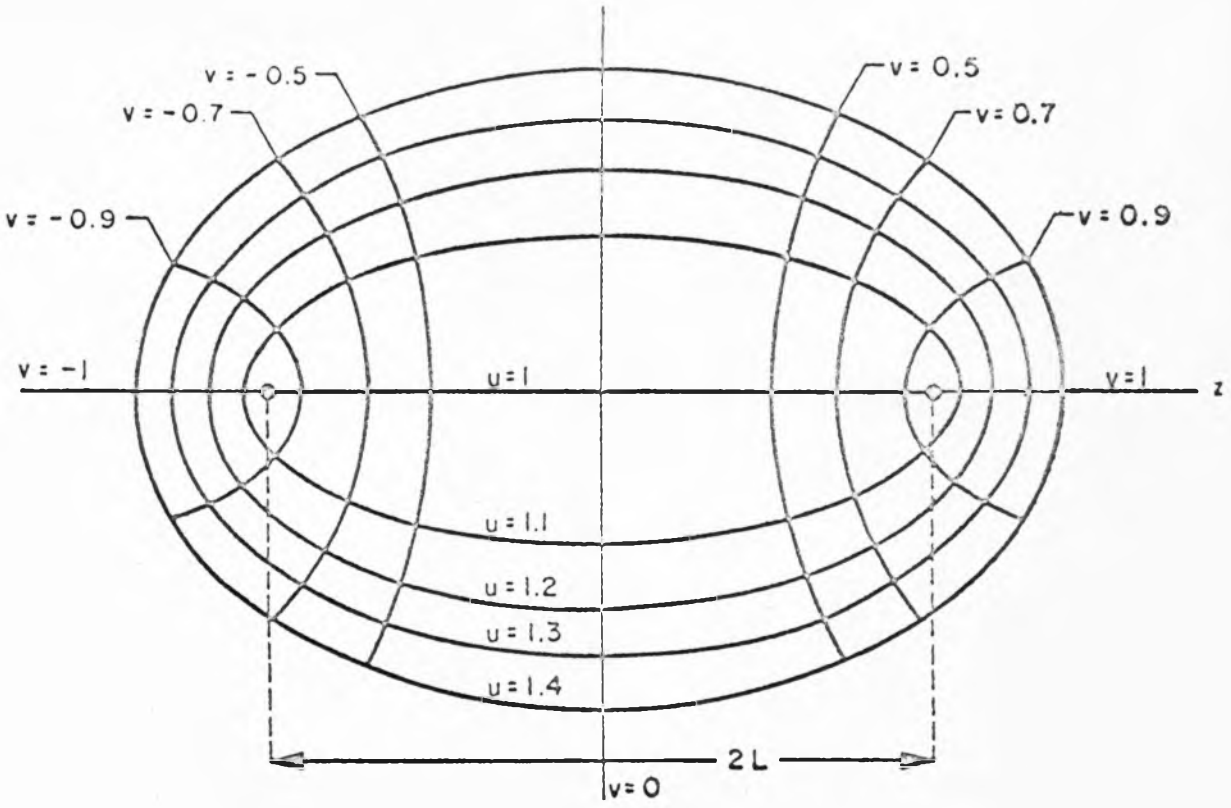

Figure 3.1. Prolate Spheroidal Coordinate System

$$L\left(\frac{u^2 - v^2}{u^2 - 1}\right)^{1/2} E_v = \frac{1}{i\omega\epsilon_o \rho} \frac{\partial(\rho H_\phi)}{\partial u} \tag{3.5}$$

$$\frac{\partial}{\partial u}\left[L\left(\frac{u^2 - v^2}{1 - v^2}\right)^{1/2} E_v\right] - \frac{\partial}{\partial v}\left[L\left(\frac{u^2 - v^2}{u^2 - 1}\right)^{1/2} E_u\right]$$

$$= i\omega\mu_o L^2\left(\frac{u^2 - v^2}{u^2 - 1}\right)^{1/2} \left(\frac{u^2 - v^2}{1 - v^2}\right)^{1/2} H_\phi \tag{3.6}$$

$$L\left(\frac{u^2 - v^2}{1 - v^2}\right)^{1/2} H_u = \frac{1}{i\omega\mu_o \rho} \frac{\partial}{\partial v}(\rho E_\phi) \tag{3.7}$$

$$L\left(\frac{u^2 - v^2}{u^2 - 1}\right)^{1/2} H_v = \frac{i}{\omega\mu_o \rho} \frac{\partial}{\partial u}(\rho E_\phi) \tag{3.8}$$

$$\frac{\partial}{\partial u}\left[L\left(\frac{u^2 - v^2}{1 - v^2}\right)^{1/2} H_v\right] - \frac{\partial}{\partial v}\left[L\left(\frac{u^2 - v^2}{u^2 - 1}\right)^{1/2} H_u\right]$$

$$= -i\omega\epsilon_o L^2\left(\frac{u^2 - v^2}{u^2 - 1}\right)^{1/2} \left(\frac{u^2 - v^2}{1 - v^2}\right)^{1/2} E_\phi \tag{3.9}$$

where

$$\rho = L(u^2 - 1)^{1/2} (1 - v^2)^{1/2} \quad . \tag{3.10}$$

It will be noticed that the first three Maxwell equations involve E_u, E_v and H_ϕ while the last three involve H_u, H_v and E_ϕ. For the case to be considered here as shown in Fig. 3.2, the excitation is an applied tangential electric field E_v across a narrow belt, and it is clear that only E_u, E_v and H_ϕ will be present. Thus the only equations needed are equations 3.4, 3.5, and 3.6. Letting

$$A = \rho H_\phi \tag{3.11}$$

the fields are

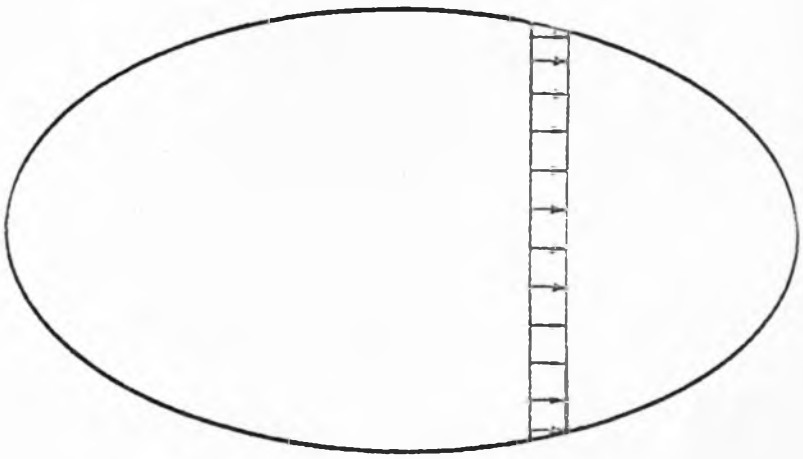

Figure 3.2. Prolate Spheroidal Antenna Showing Applied Field

$$E_u = \frac{i\eta}{kL^2}\left[(u^2-1)(u^2-v^2)\right]^{-1/2}\frac{\partial A}{\partial v} \tag{3.12}$$

$$E_v = -\frac{i\eta}{kL^2}\left[(1-v^2)(u^2-v^2)\right]^{-1/2}\frac{\partial A}{\partial u} \tag{3.13}$$

$$H_\phi = \frac{1}{L}\left[(u^2-1)(1-v^2)\right]^{-1/2} A \tag{3.14}$$

where $\eta = \sqrt{\mu_o/\epsilon_o}$ and $k = \omega\sqrt{\mu_o\epsilon_o}$. Substitution of equation 3.11 into equation 3.6 yields the differential equation for A

$$(u^2-1)\frac{\partial^2 A}{\partial u^2} + (1-v^2)\frac{\partial^2 A}{\partial v^2} + k^2L^2(u^2-v^2)A = 0 \quad . \tag{3.15}$$

Upon substituting $A = U(u)\,V(v)$ one obtains

$$(u^2-1)\frac{d^2U}{du^2} + (k^2L^2u^2 - d)U = 0 \tag{3.16}$$

$$(1-v^2)\frac{d^2V}{dv^2} + (d - k^2L^2v^2)V = 0 \tag{3.17}$$

where d is the separation constant. Because there is no line current along the axis, H_ϕ must vanish there or $V(\pm 1) = 0$. This condition determines d, the eigenvalue of equation 3.17. At large distances it is necessary that

$$U \to e^{ikr} = e^{ikLu} \quad . \tag{3.18}$$

Thus one picks the solution of equation 3.17 satisfying the condition $V(\pm 1) = 0$ and the solution of equation 3.16 satisfying equation 3.18 and sums over all the eigenfunctions to obtain the general solution for A

$$A = \sum_n a_n U_n(u) V_n(v) \quad . \tag{3.19}$$

Substituting into equation 3.13 one obtains

$$E_v = - \frac{i\eta}{kL^2} \left[(1 - v^2)(u^2 - v^2) \right]^{-1/2} \sum_n a_n U_n'(u) V_n(v) \quad . \tag{3.20}$$

The boundary condition at the surface of the spheroid is that the tangential electric field vanish

$$E_v(u_o, v) + E_v^a(u_o, v) = 0 \tag{3.21}$$

where u_o is the defining coordinate of the antenna and $E_v^a(u_o, v)$ is the applied field. Therefore,

$$- \frac{i\eta}{kL^2} \left[(1 - v^2)(u_o^2 - v^2) \right]^{-1/2} \sum_n a_n U_n'(u_o) V_n(v) = - E_v^a(u_o, v) \quad . \tag{3.22}$$

It can be shown (21) that the V functions are orthogonal.

$$\int_{-1}^{1} \frac{V_n(v)\, V_m(v)}{(1 - v^2)} \, dv = \begin{cases} 0 & n \neq m \\ N_n & n = m \end{cases} \tag{3.23}$$

Using equation 3.23 one finds

$$a_n = \frac{ikL^2}{\eta N_n U_n'(u_o)} \int_{-1}^{1} E_v^a(u_o, v) \frac{\sqrt{u_o^2 - v^2}}{\sqrt{1 - v^2}} V_n(v) \, dv \quad . \tag{3.24}$$

If one assumes an infinitesimal width for the applied field belt while allowing the applied field to become infinite in a way such that the applied voltage remains finite, one finds

$$a_n = \frac{ikL\, V_n(v_o)}{\eta\, N_n\, U_n'(u_o)}\, V^a \tag{3.25}$$

where V^a is the applied voltage and v_o is the position of the belt. Once the U and V functions and the eigenvalues have been computed, equation 3.20 is used together with equation 3.25 to obtain the field. Myers (9) has computed radiation patterns for the far zone for various values of u_o, v_o and kL.

3.2 The Thin Spheroidal Antenna

It can be shown that for the limit of an infinitely thin conductor the current distribution is sinusoidal (22). Thus the current on a prolate spheroid of eccentricity near unity is expected to be approximately sinusoidal. This can be seen very clearly from the expression for the current on the spheroid in certain important cases. These cases correspond to spheroid lengths of $kL = n(\pi/2)$ where n is an integer. For these special cases it can be shown that certain spheroidal functions can be expressed in closed form. Except for a normalizing factor, the functions that may be expressed in closed form for the particular values of $kL = n(\pi/2)$ are

$$\left.\begin{aligned} V_n(v) &= \cos\left(\frac{n\pi v}{2}\right) \\ U_n(u) &= \exp\left(i\,\frac{n\pi u}{2}\right) \end{aligned}\right\} \quad n = \text{odd integer} \tag{3.26}$$

$$\left.\begin{aligned} V_n(v) &= \sin\left(\frac{n\pi v}{2}\right) \\ U_n(u) &= \exp\left(i\,\frac{n\pi u}{2}\right) \end{aligned}\right\} \quad n = \text{even integer} \tag{3.27}$$

Thus if $kL = \pi/2$, the interfocal distance is $\lambda/2$ and since the total current on the spheroid is

$$I = \int_0^{2\pi} H_\phi(u_o,v)\rho\, d\phi = 2\pi A(u_o,v) \tag{3.28}$$

one obtains using equation 3.25

$$I = 2\pi \sum_{n=1}^{\infty} a_n U_n(u_o)V_n(v) = 2\pi\left[a_1U_1(u_o)V_1(v) + \sum_{n=2}^{\infty} a_nU_n(u_o)V_n(v)\right]$$

$$= \frac{i2\pi\, kLV_1(v_o)V^a U_1(u_o)V_1(v)}{\eta\, N_1\, U_1'(u_o)} + \frac{i2\pi\, kL\, V^a}{\eta} \sum_{n=2}^{\infty} \frac{V_n(v_o)\, U_n(u_o)V_n(v)}{N_n\, U_n'(u_o)}$$

$$= \frac{4kLV^a}{\eta N_1} \cos\left(\frac{\pi v_o}{2}\right)\cos\left(\frac{\pi v}{2}\right) + \frac{i2\pi kLV^a}{\eta} \sum_{n=2}^{\infty} \frac{V_n(v_o)U_n(u_o)V_n(v)}{N_n U_n'(u_o)} \quad . \tag{3.29}$$

However, v is directly proportional to the distance along the axis of the spheroid

$$v = z/Lu_o \tag{3.30}$$

and since $kL = \pi/2$, $u_o \approx 1$, $v = 2kz/\pi$,

$$I = \frac{4kLV^a}{\eta N_1} \cos\left(\frac{\pi v_o}{2}\right)\cos(kz) + \frac{i2\pi kLV^a}{\eta} \sum_{n=2}^{\infty} \frac{V_n(v_o)U_n(u_o)V_n(v)}{N_n\, U_n'(u_o)} \quad . \tag{3.31}$$

Thus the current is sinusoidal insofar as the quantity under the summation sign in equation 3.31 can be neglected. When the spheroid is very thin this is a good approximation because the derivative of the radial function $U'(u_o)$ becomes larger as u_o approaches unity and

the ratio $U_n(u_o)/U'_n(u_o)$ becomes smaller causing the quantity under the summation sign to decrease. Similar arguments apply to the other cases of $kL = n(\pi/2)$.

Even though mathematical simplification results by using a sinusoidal distribution of current, caution must be exercised in replacing the actual distribution by a sinusoidal approximation. In Fig. 3.3 are compared the radiation patterns for the actual and the sinusoidal current distribution for the case $u_o = 1.00001$, $L = 3\lambda/2\pi$ with the exciting gap a distance $.4L$ from the center of the antenna. The sinusoidal current for this case is shown in Fig. 3.4 and was constructed using the condition that the current vanish at the ends and be continuous at the gap. However, even though the spheroid is extremely thin, a length-thickness ratio of about 630, with the maximum diameter of the spheroid only about $\lambda/600$, the rigorous and the approximate patterns differ appreciably. The sinusoidal current results in a symmetrical lobe structure about the plane $\theta = \pi/2$, while the rigorous pattern has considerable asymmetry about this plane. The radiation pattern of a real linear distribution of current is always symmetrical about the plane $\theta = .\pi/2$ since the expression for the far zone field of a current $I(z)$ along the z axis of a spherical coordinate system is (23)

$$E_\theta = - \frac{i\omega\mu\, e^{ikr} \sin\theta}{4\pi r} \int I(z')\, e^{-ikz'\cos\theta}\, dz' \qquad (3.32)$$

and replacing θ by $(\pi - \theta)$ changes E_θ to its complex conjugate so that its magnitude remains the same. Thus the sinusoidal approximation can never be used if the asymmetry in the lobe structure is

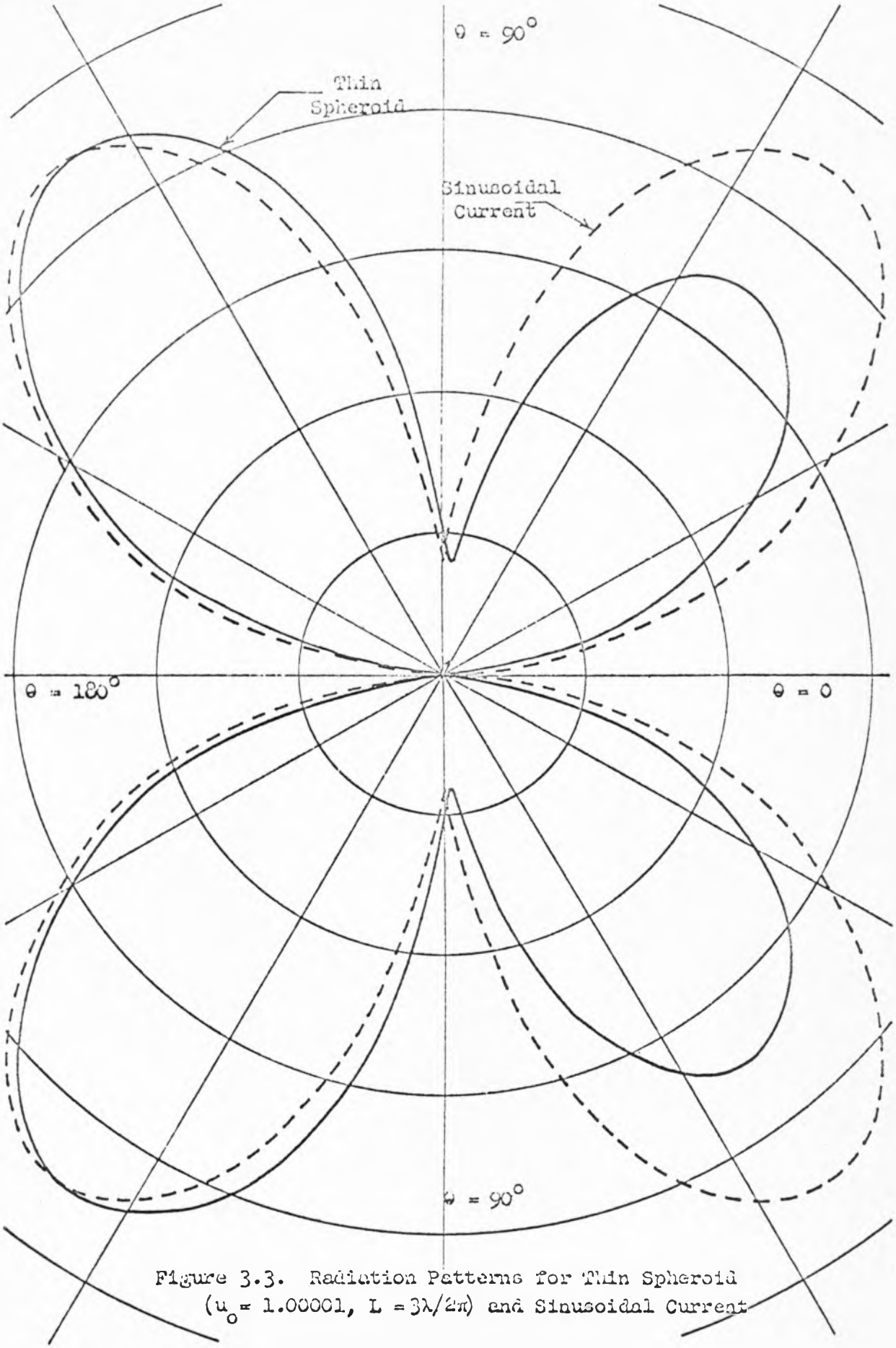

Figure 3.3. Radiation Patterns for Thin Spheroid ($u_o = 1.00001$, $L = 3\lambda/2\pi$) and Sinusoidal Current

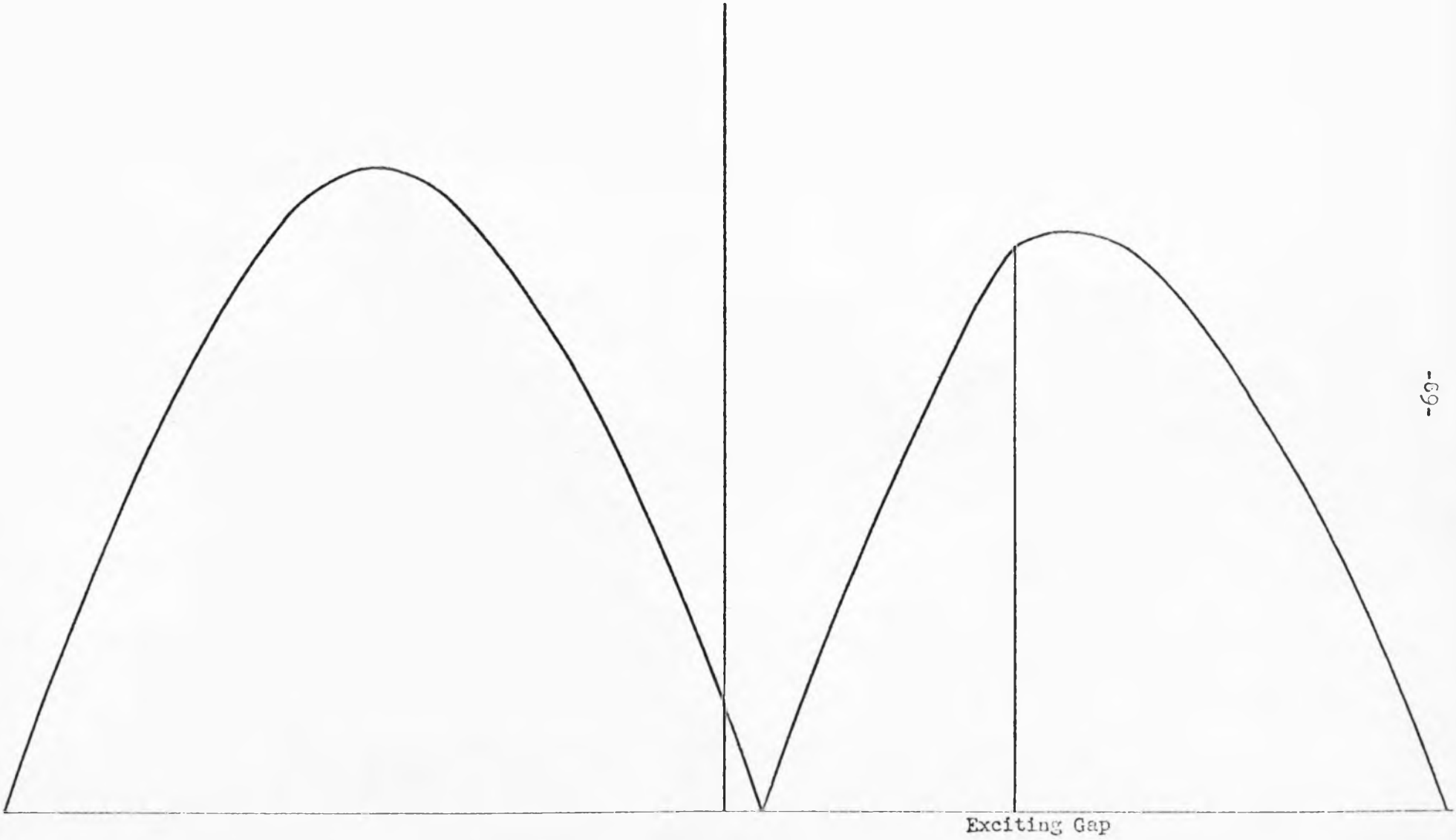

Figure 3.4. Sinusoidal Current used in Computing Radiation Pattern of Figure 3.3.

important. It can be used, however, if only the angular position and not the relative magnitude of the lobes is important.

4. FINITE CYLINDER EXCITED BY A RADIAL ELECTRIC DIPOLE; EXPERIMENT

The expressions for the radiation field of a radial dipole near a finite cylinder derived in Chap. 2 depend on the condition that the cylinder is not short and that the dipole is not close to an end of the cylinder. If these conditions are violated, ℓ_1 and ℓ_2 are small and the assumed current on the cylinder is no longer a good approximation. However, the complexity of the functions involved prevents setting a limit on ℓ_1 and ℓ_2 below which the analytically computed radiation pattern is in error by a given percentage. For this reason, measurements were performed and these are described and compared to the analytic results in this chapter.

4.1 Some Measurement Considerations

The technique of measurement is described in Appendix 1. The radiation patterns of cylinders of two different lengths were measured for the case of the radial dipole directly against the surface of the cylinder, i.e., b = a. With the dipole directly against the cylinder, the charge on the dipole nearest the cylinder causes currents on the cylinder whose field can be thought of as due to an equal and opposite image charge directly on the surface of the cylinder as shown in Fig. 4.1 at one instant of time. This image charge cancels the dipole charge so that the field is identical to that caused by the remaining charge alone and the original dipole current I as in Fig. 4.2. Because of this, in the experimental model the exciting dipole was an extension of the inner conductor of a coaxial line with the outer conductor connected to the cylinder as in Fig. 4.3. The coaxial line

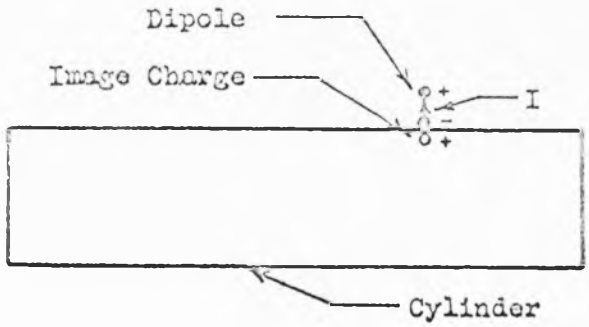

Figure 4.1

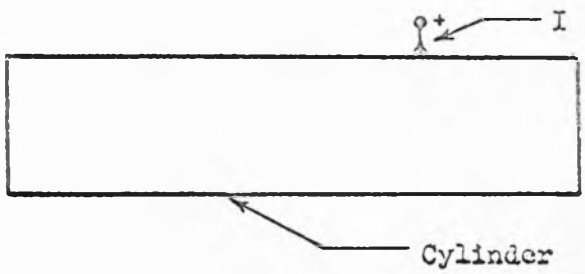

Figure 4.2

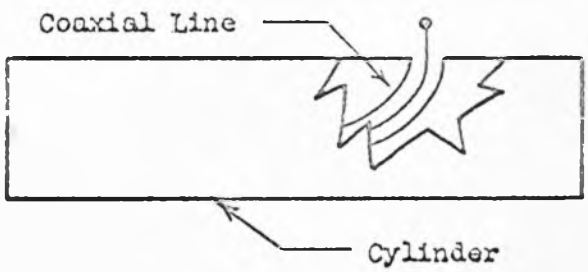

Figure 4.3

connects to the circuit described in Appendix 1. The configuration of Fig. 4.3 closely approximates that of Fig. 4.2 if the radius of the outer conductor of the coaxial line is small compared to a wavelength. This condition was satisfied since the outer diameter was approximately $\lambda/100$. A small metal ball was put on the end of the extended inner conductor to allow a greater lumped charge to collect at that end and make the current on the conductor more constant along the short extended portion, thus approximating the ideal dipole more closely. The length of the extended conductor was about $.12\lambda$. The experimental model is shown in Fig. 4.4.

It can be seen from equation 2.77 that in the half plane $\phi = 90^{\circ}$, the contribution to $E_{\theta TOT}$ by the dipole itself is zero. Thus the half plane $\phi = 90^{\circ}$ is the most desirable one in which to compare the theory to experiment since here $E_{\theta TOT}$ is due only to currents on the cylinder and has no component due to the known field of the dipole. Unfortunately, no such plane exists for $E_{\phi TOT}$ because the field due to the cylinder currents is zero in the only plane where the dipole field is zero. However, it is expected that $E_{\phi TOT}$ as computed from the approximate analysis of section 2.3 will be very accurate if the cylinder dimensions are such that $E_{\theta TOT}$ is accurate. This is due to the more rapid decrease of the ϕ-component of the cylinder surface current with z , which is the source of $E_{\phi TOT}$ on the cylinder. The z component of surface current decreases more slowly, and since it is the source of $E_{\theta TOT}$ on the cylinder, it is expected that $E_{\phi TOT}$ will be more accurate than $E_{\theta TOT}$ for a given cylinder. This was also shown to be true in section 2.1.

Figure 4.4. Experimental Model of Cylinder with Dipole

4.2 Cylinder Measurements

The measurements were performed on two different cylinders. They were made only in the half plane $\phi = 90^{\circ}$ because of the considerations of section 4.1.

The first measurement was made on a rather short cylinder in order to determine how well the expressions for the fields hold for short cylinders. The cylinder had $k\ell = 5\pi/4$, $k\Delta = 5\pi/12$, $ka = .632$. Thus the total length of the cylinder was $2\ell = 5\lambda/4$, the distance of the dipole from the nearest end of the cylinder was $\ell_1 = 5\lambda/12$ and $a = .101\lambda$. The experimental and theoretical patterns for this case are shown in Figs. 4.5 and 4.6. In Fig. 4.5 showing $E_{\theta TOT}$ for $\phi = 90^{\circ}$, the main lobe agrees quite well but the minor lobe in the theoretical case is split into two lobes experimentally. In Fig. 4.6, showing $E_{\phi TOT}$ for $\phi = 90^{\circ}$, the agreement is quite good and this component of field is seen to be roughly omnidirectional in this plane. Thus even though the cylinder is of the order of a wavelength, the predicted pattern agrees fairly well with experiment, the greatest error being in the minor lobes in the $E_{\theta TOT}$ pattern.

The second measurement was made on a longer cylinder which had $k\ell = 5\pi/2$, $k\Delta = 5\pi/6$, $ka = .632$. The total length of this cylinder was $2\ell = 5\lambda/2$, the distance of the dipole from the nearest end of the cylinder was $\ell_1 = 5\lambda/6$ and $a = .101\lambda$. The experimental and theoretical patterns are shown in Figs. 4.7 and 4.8. The shapes of the $E_{\theta TOT}$ patterns agree well. The major lobe and small minor lobes correlate quite well while the lobe at about 140° is about 30% larger in the theoretical case. In Fig. 4.8, the patterns for E_{ϕ} agree

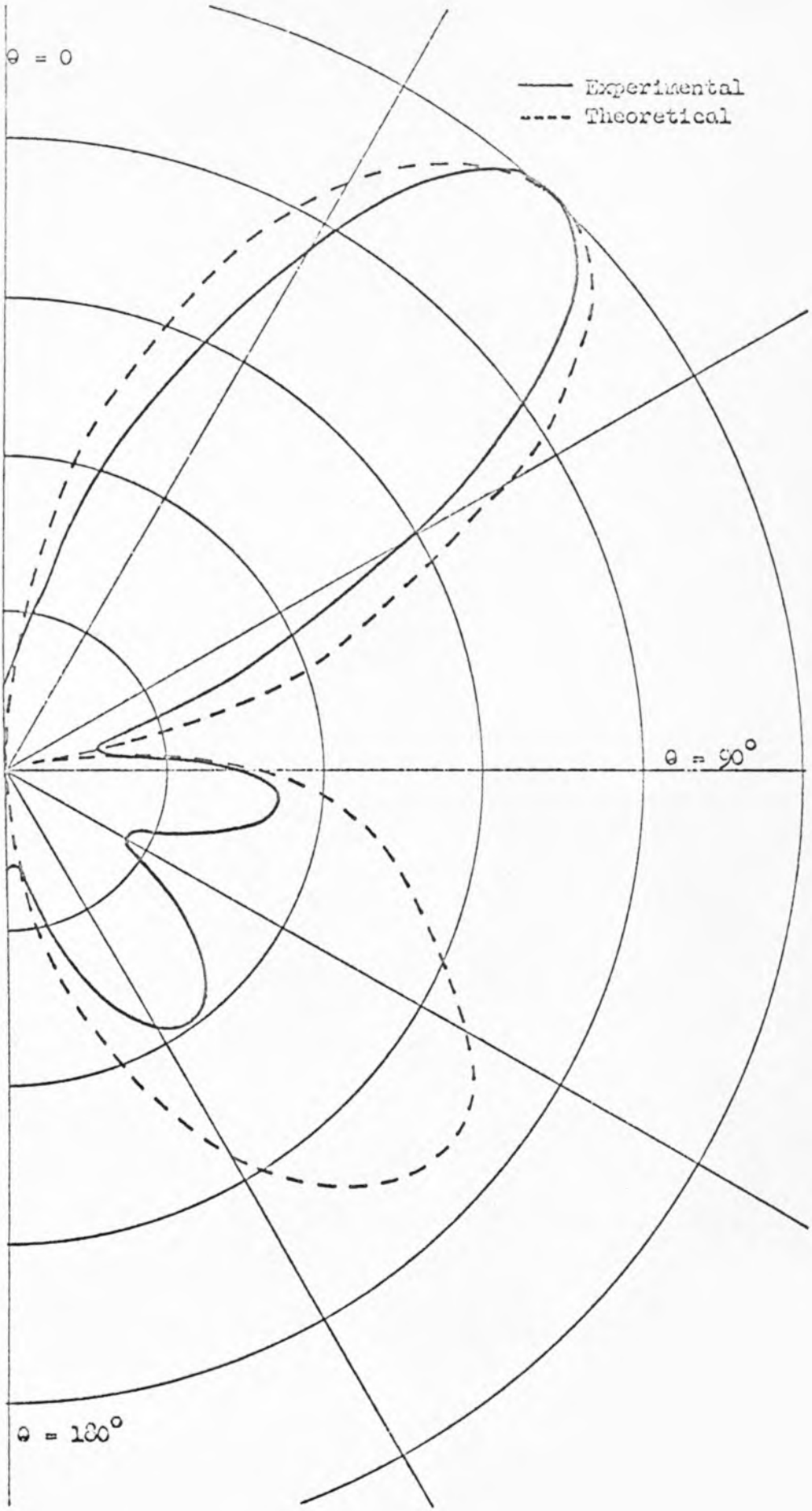

Figure 4.5.

$E_{\theta TOT}$ for
$\phi = 90^\circ$

$ka = kb = .632$,
$k\Delta = 5\pi/12$
$k\ell = 5\pi/4$

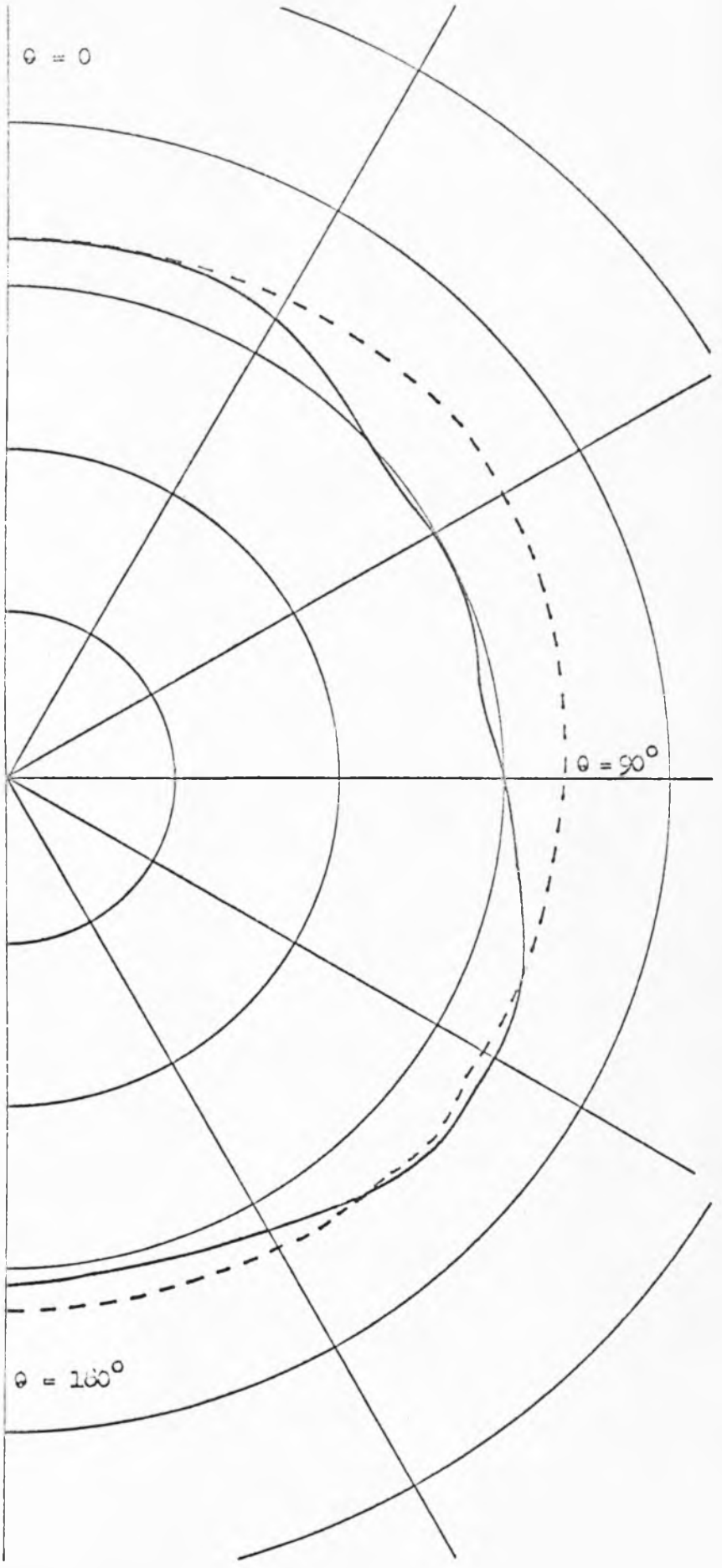

—— Experimental
---- Theoretical

Figure 4.6.
$E_{\phi TOT}$ for $\phi = 90^\circ$
$ka = kb = .632$
$k\Delta = 5\pi/12$
$k\ell = 5\pi/4$

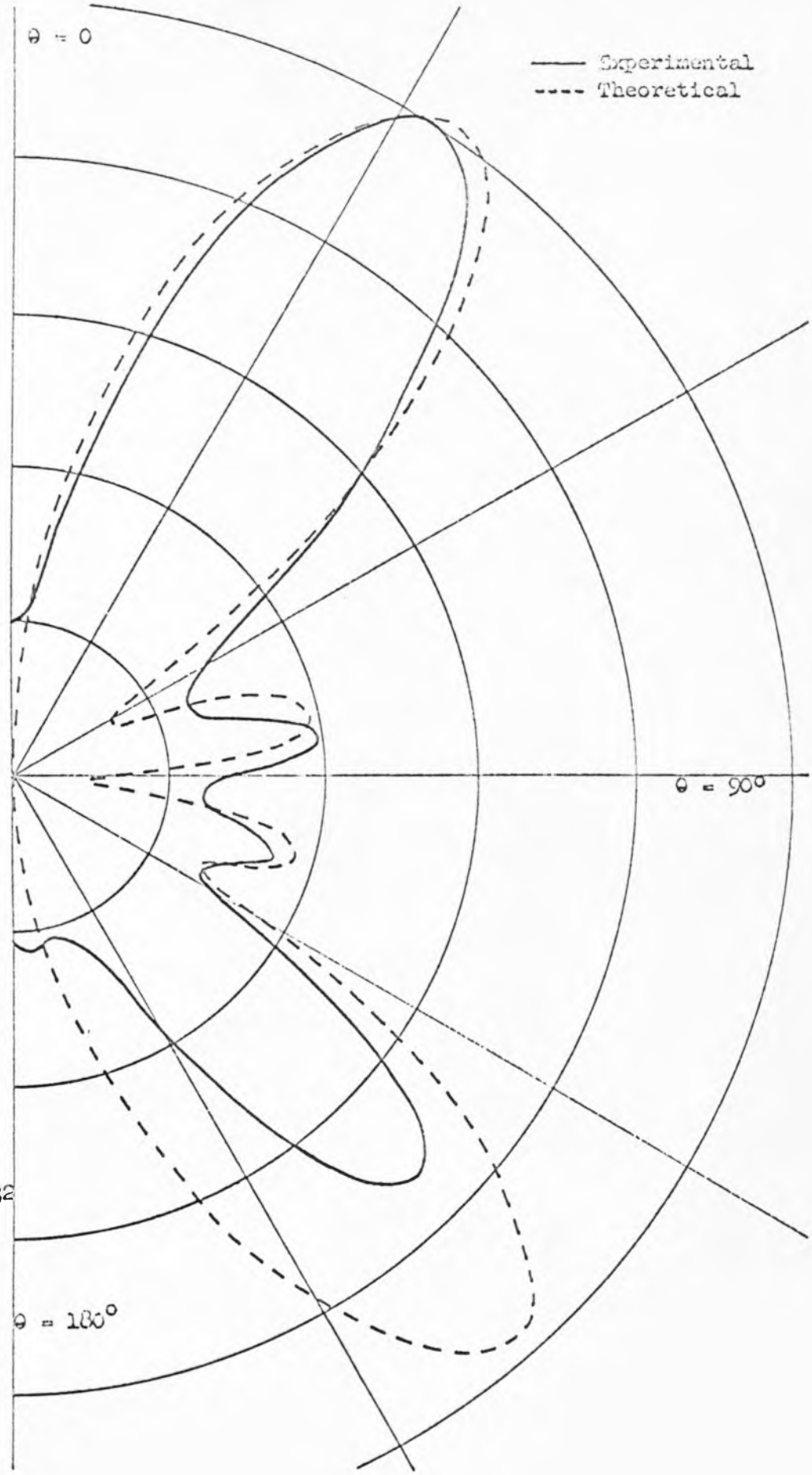

Figure 4.7

$E_{\theta TOT}$ for
$\phi = 90°$

$ka = kb = .632$
$k\Delta = 5\pi/6$
$k\ell = 5\pi/2$

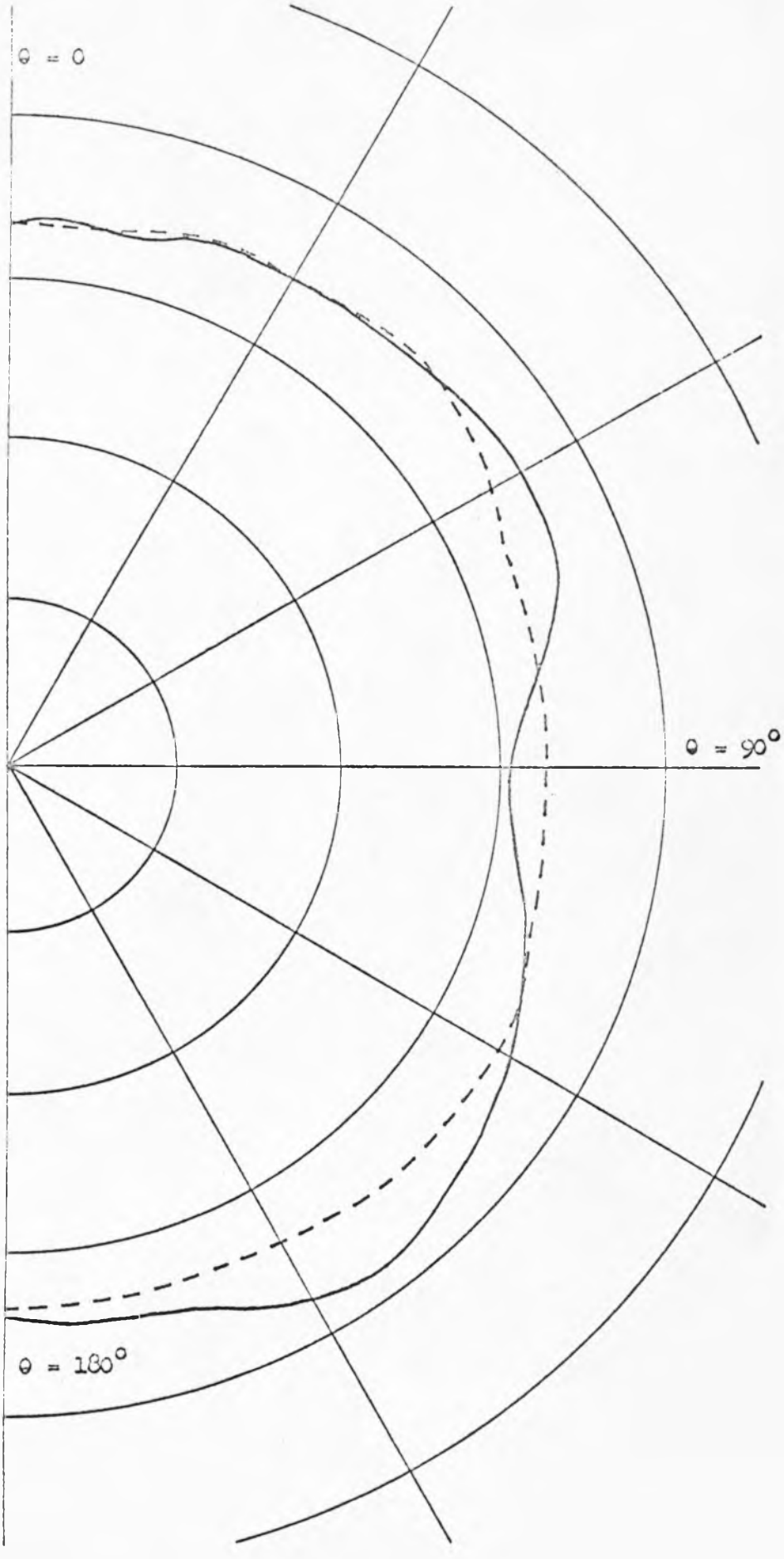

—— Experimental
---- Theoretical

Figure 4.8
$E_{\phi TOT}$ for $\phi = 90°$
$ka = kb = .632$
$k\Delta = 5\pi/6$
$k\ell = 5\pi/2$

within about 15%.

Thus in the case of a cylinder length of $5\lambda/2$, $\ell_1 = 5\lambda/6$, $a = .101\lambda$ the agreement between theory and experiment is good. The agreement should become better as ℓ and ℓ_1 become larger. It is difficult to obtain a quantitative idea of the behavior of the pattern error as the cylinder radius becomes larger. However, from equations 2.28 and 2.37, it is probably true that as a increases with all other parameters held constant, the error in $E_{\phi TOT}$ becomes larger since circumferential currents contribute to this field component. From equations 2.31 and 2.46, it is probably true that the error in $E_{\theta TOT}$ decreases as a increases, since axial currents contribute to $E_{\theta TOT}$. However, radiation from the end plates of the cylinder was neglected in the theory of Chap. 2 and this probably increases as a increases. The difference between theoretical and experimental patterns is thus a complicated function but it is expected that it will be small if $k\ell$ and $k\Delta$ are large and $ka \ll k\Delta$. Even if these conditions are not satisfied, useful qualitative results are obtained.

5. THE ASYMMETRICALLY FED PROLATE SPHEROIDAL ANTENNA; EXPERIMENT

In analyzing antennas mathematically it is usually necessary to replace a practical antenna structure by a structure capable of being analyzed mathematically. If an antenna does not have boundaries that are mathematically convenient, they are replaced by approximate boundaries which are necessary for a rigorous solution. For instance in analyzing a rather simple case, the cylindrical antenna, one should include the transmission line which feeds energy to the antenna in order to obtain an exact solution. However, from a mathematical point of view, the transmission line introduces great difficulties since the transmission line and antenna together cannot be represented simply in a coordinate system in order to treat the configuration as a boundary value problem. To obviate this difficulty the transmission line is not considered in the mathematical formulation and the mathematical solution is carried out. However, to be of practical value it must be known how closely the abstract configuration of mathematically convenient boundaries correlates with its experimentally practical counterpart. This may be done analytically, but this approach again leads to the same mathematical difficulties, since essentially the unsimplified configuration must be treated. Perhaps a better approach is to perform measurements on the actual practical antenna and compare the experimental and theoretical results. It is this approach that is followed here and is applied to the asymmetrically fed prolate spheroidal antenna.

5.1 Comparison of the Mathematical and Experimental Models

The mathematical idealization employed in Chap. 3 in the mathematical treatment of the spheroid is the method of excitation. It is assumed that the surface of the conducting spheroid is continuous, having no gap, and that by some unspecified means a belt of tangential electric field is applied at a certain location on the surface as shown in Fig. 3.2. Then in order to obtain a simple expression for the coefficients in the resulting series, the width of the belt is made infinitesimal, while allowing the applied field to become infinite in a way such that the applied voltage remains finite, i.e., the applied field is a delta function. In this way a relatively simple expression results for the field.

The experimental spheroidal antenna cannot be constructed in this manner. The applied field would have to be supplied by a continuous distribution of generators around the surface of the spheroid which is not possible from a practical standpoint. The practical configuration usually is a split conductor, the two portions being energized by a transmission line which impresses a field between the two portions of the conductor. Since an external transmission line would cause the field to be ϕ-dependent, the excitation must be from within. A convenient method is to use a radial transmission line and an internal generator as shown in Fig. 5.1 for a spheroid.

Some distinct differences between the mathematical and experimental structure are clear. The experimental structure has a gap or discontinuity in the conducting surface of the spheroid instead of

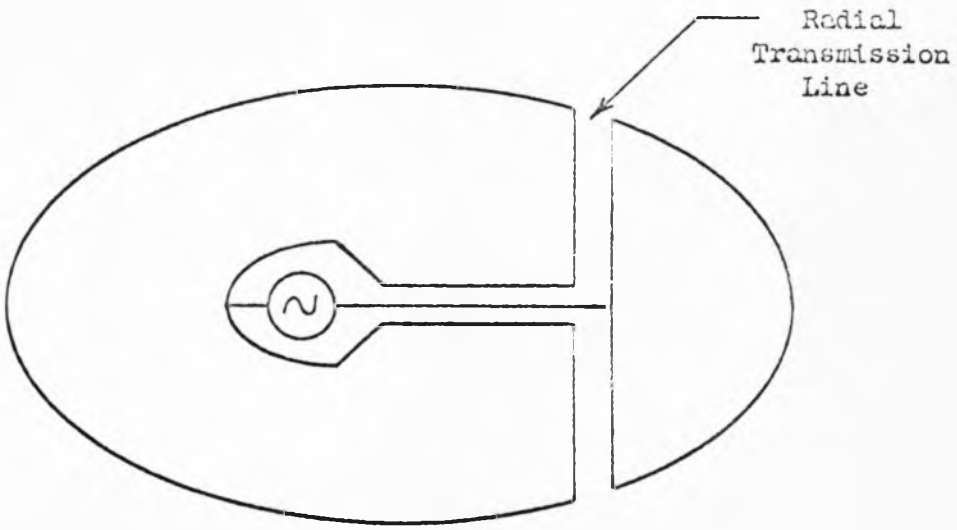

Figure 5.1. Prolate Spheroidal Antenna Showing Method of Excitation

the continuous surface of the mathematical model. This gap is necessarily of finite width as opposed to the infinitesimal gap of the mathematical model, since a very narrow gap permits a very small power flow which is a limiting factor in the practical case. The exact impressed field at the surface of the spheroid in the gap is not of a simple form because a discontinuity in the radial transmission line exists there and nonpropagating modes are excited near the discontinuity.

Because of these differences in the excitation of the spheroid one might well expect differences between the analytical and experimental radiation patterns. However, it is usually found that the far zone field of an antenna is quite insensitive to small errors in the source current. This is due to the fact that the far zone field is the result of an integration over the source current and the integral does not depend critically upon the details of the source current. The only regions where the effects of a somewhat incorrect current distribution become important are near the minima of the radiation pattern, since here even a small field change is a large percentage error.

5.2 Construction of the Asymmetrically Fed Spheroidal Antenna

To verify the preceding statements and also to give a quantitative idea of the error between the analytic and experimental radiation patterns, a spheroidal antenna was constructed on which measurements were performed. Since the measurement technique described in Appendix 1 is used, the spheroidal antenna is used as a receiver. A

schematic diagram of the antenna which is not to scale, is shown in Fig. 5.2. The "gap" is a polystyrene ring through which the impinging radiation travels. Two circular metal plates form a radial transmission line to guide the received energy to coaxial line, the inner conductor of the coaxial line being extended in tapered form between the radial line for a better transition. The signal is then fed into a circuit as described in Appendix 1. The audio signal is extracted through high resistance leads from the two terminals shown.

The spheroid was constructed so that the "gap" could be placed in three alternative locations. While the "gap" is in one location the other two locations are filled by metal rings so that the spheroid is electrically continuous everywhere except at the "gap". The "gap" is 3/4" wide or about $\lambda/30$ at 500 Mc, the frequency of measurement. The metal and polystyrene rings are threaded to make them easily removable.

The spheroid itself was constructed of wood and the outer surface was sprayed with copper. The thickness of the copper greatly exceeds the skin depth at the frequencies used so that electrically the spheroid body is solid copper. Figs. 5.3 and 5.4 show the spheroid and the internal components. One polystyrene and two metal rings are in place.

5.3 Radiation Patterns of Asymmetrically Fed Spheroidal Antenna

The spheroid tested had $kL = 3$ so that it is approximately a wavelength in length. The "gaps" were placed at $v = .1, .4, .8$ and

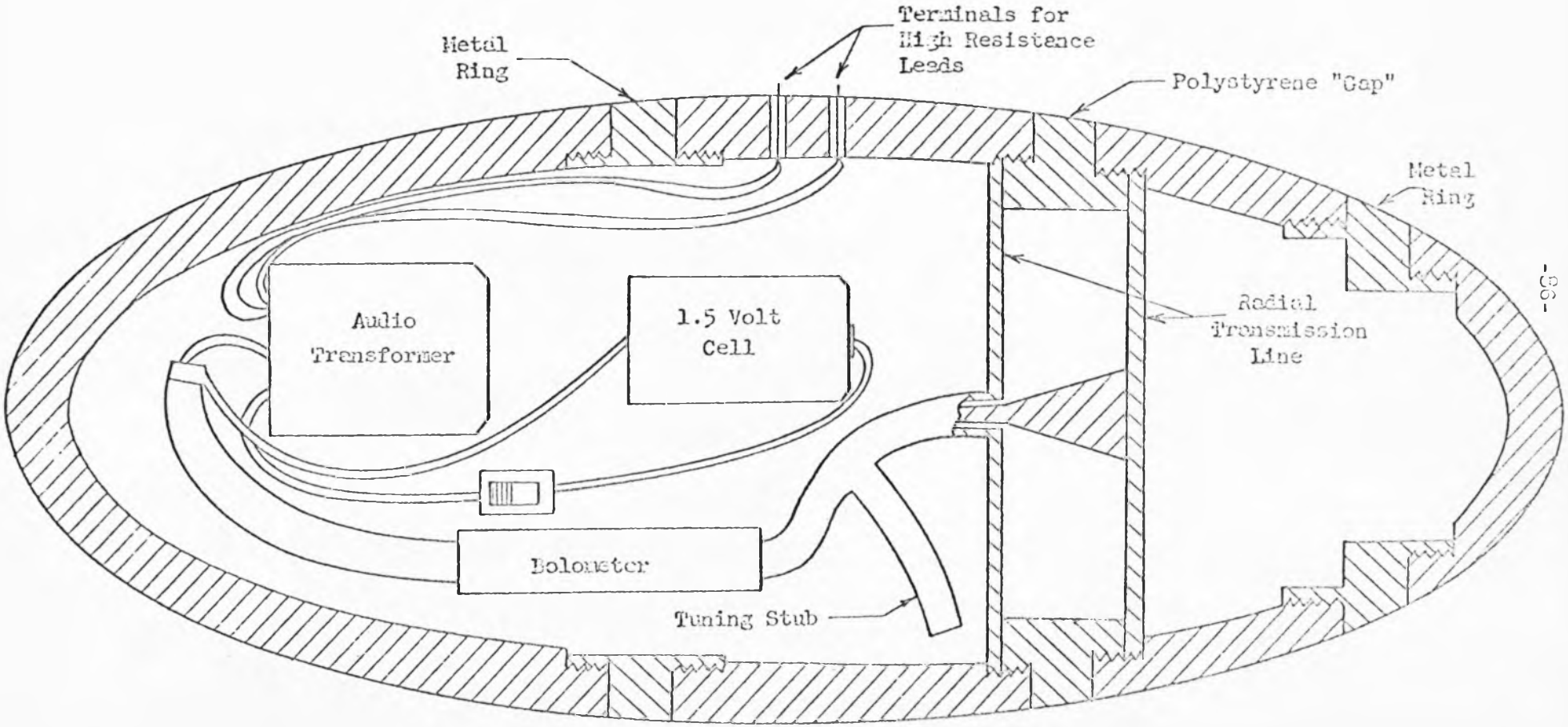

Figure 5.2. Schematic Diagram of Spheroidal Antenna

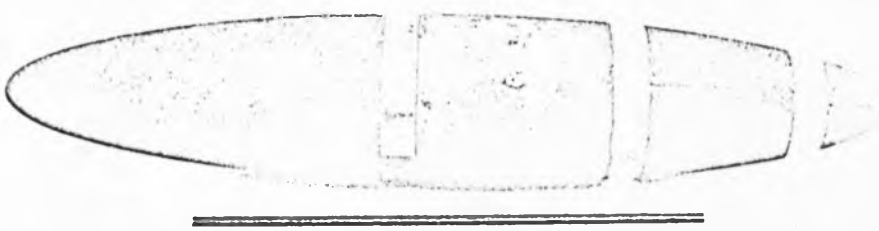

Figure 5.3. Spheroidal Antenna

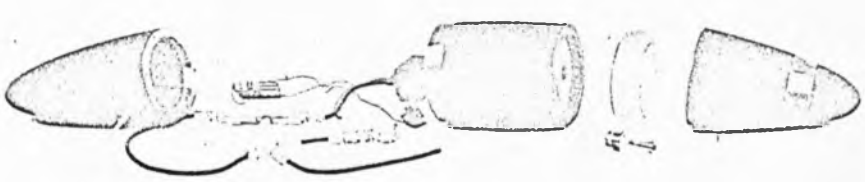

Figure 5.4. Exploded View of Spheroidal Antenna

the radial coordinate defining the spheroid was 1.02. The theoretical field patterns were taken from results furnished by Dr. Charles P. Wells of Michigan State University and are shown together with the experimental patterns in Figs. 5.5, 5.6 and 5.7 for the three positions of the "gap". In these figures the spheroid axis is along the direction of $\theta = 0$. The longer portion of the spheroid is always on the left. The patterns shown are plane sections of a figure of revolution around the spheroid axis.

It is seen in Figs. 5.5, 5.6 and 5.7 that the correlation between the theoretical and experimental patterns is quite good. The largest percentage error occurs near the minima of the patterns. In Fig. 5.5, $v_o = .1$, the minimum at about 55° is not as deep as the corresponding minima in the next two cases because the gap is not appreciably off center. The error near this minimum is about 7% in the first case. In the second case, Fig. 5.6, $v_o = .4$, and the percentage error at the minimum at about 85° is 10%. In the third case, Fig. 5.7, the error at the minimum at about 90° is 26%. In regions other than near the minima the agreement is very good. The experimental error in these measurements is estimated to be less than 2%.

It is evident from Figs. 5.5, 5.6 and 5.7 that the details of the excitation are not an extremely important influence on the radiation pattern. The theoretical and experimental structures result in very similar radiation patterns even though the excitation is somewhat different. The fact that the largest percentage error is near the minima is in agreement with the discussion of section 5.1. The

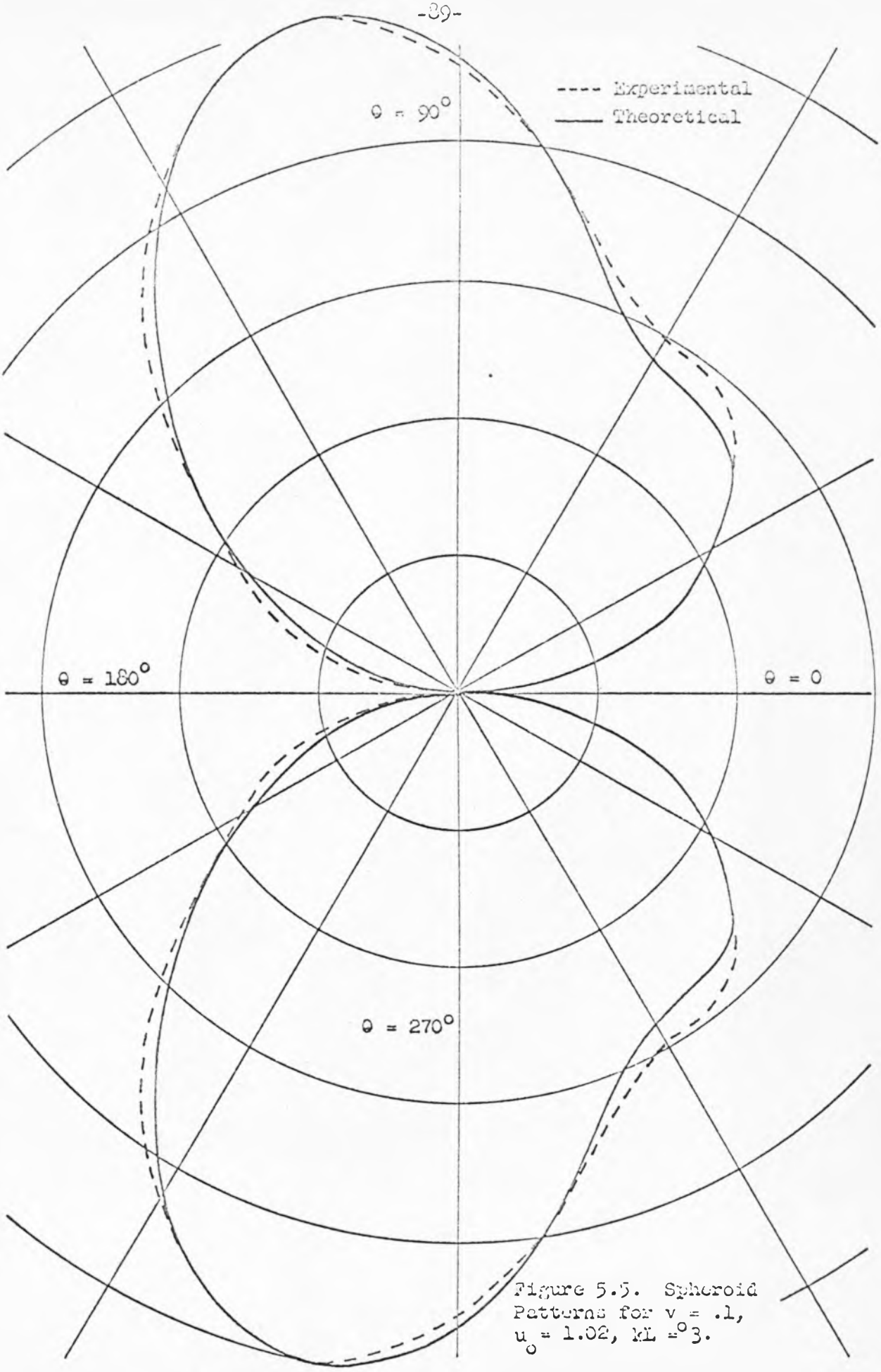

Figure 5.5. Spheroid Patterns for $v = .1$, $u_o = 1.02$, $kL = 3$.

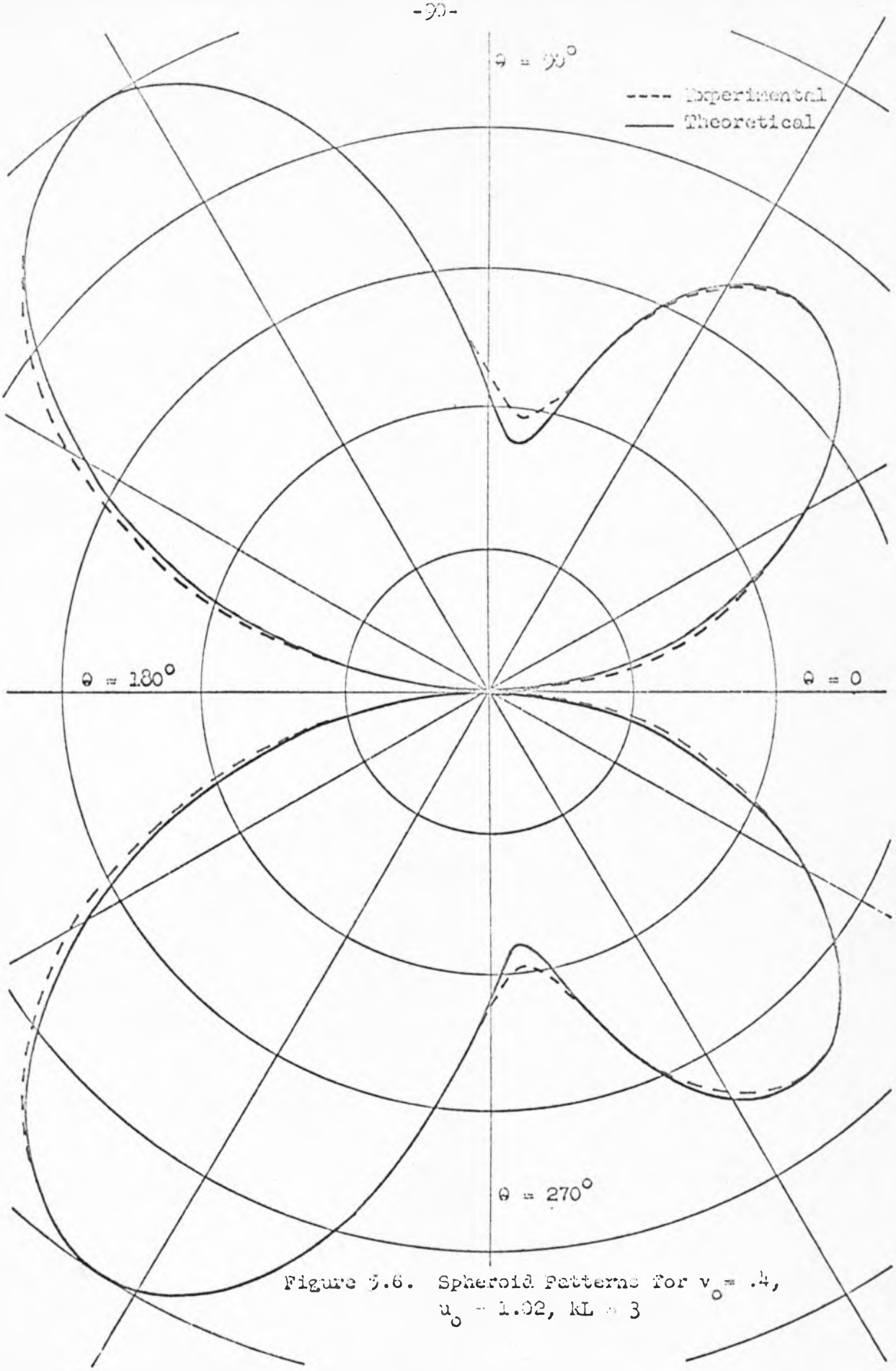

Figure 5.6. Spheroid Patterns for $v_o = .4$, $u_o = 1.02$, $kL = 3$

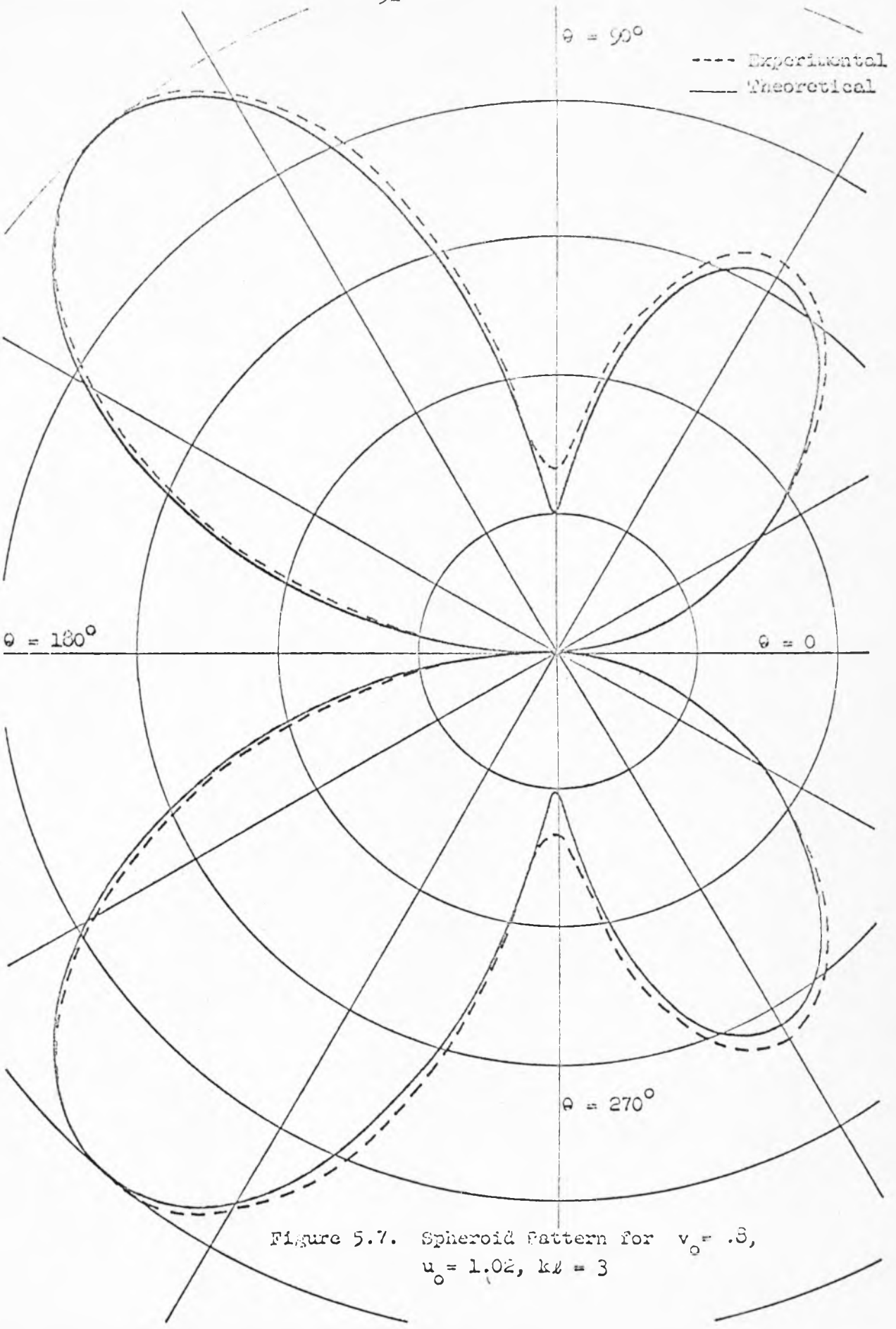

Figure 5.7. Spheroid Pattern for $v_o = .8$, $u_o = 1.02$, $k\ell = 3$

error is attributable to slightly different values for the constants, a_n, given in equation 3.25, giving rise to somewhat different amplitudes for the modes of equation 3.20. The theoretical solution should agree more closely if a delta function excitation is not assumed, using instead a finite field distributed over a finite gap width to agree more closely with the experimental model. However, in all regions except near the minima, the solution for the delta function excitation yields very close agreement to the experimental results for the small finite gap.

6. SUMMARY AND CONCLUSIONS

The far zone electromagnetic radiation from two asymmetrically excited systems is considered. In order to carry out an approximate solution to the problem of a finite cylinder excited by an asymmetrically located radial dipole, the analogous case of an infinite cylinder excited by a radial dipole is obtained. In addition to the far zone field, the current distribution on the infinite cylinder is derived.

It is shown that an approximate method can be used to calculate the radiation from a finite cylinder excited by a radial dipole. The method of approximation makes use of the fact that the currents on the finite cylinder are not greatly modified from those present on the infinite cylinder in the region near the dipole where the currents are large and are the sources of the largest part of the radiation. The approximation is better for the ϕ-component of the far zone electric field than for the θ-component because of the manner in which the currents decrease along the axis of the cylinder. In fact, a good approximation to the ϕ-component of the field can be obtained from the solution for the infinite cylinder. This approximation for the θ-component, however, can be in error by a large amount.

The far zone field of the finite cylinder excited by a radial dipole is derived using the approximation discussed above. The solution is obtained in series form in which the coefficients are certain definite integrals. The method of computing these integrals is discussed. Measurements on finite cylinders are compared to the

approximate analytic results and it is shown that fairly good agreement is obtained. The agreement improves as the cylinder length increases.

The field of a turnstile antenna mounted on a finite cylinder is derived and the modification of the radiation by the cylinder is exhibited.

The far zone radiation from an asymmetrically excited prolate spheroid is discussed and experiments on this antenna are compared to the theoretical results. Very good agreement except in the rather unimportant regions of the minima is obtained.

The radiating systems considered here have practical importance in the design of missile antennas because of the similarity between the exciting elements and the nearby conducting bodies to the missile antennas and the missiles themselves.

The method of approximation used here in the case of the finite cylinder is applicable to cylinders which are not very short. The expressions appear to yield good results for cylinders greater than about a wavelength or two in the cases examined. For very long cylinders these approximate expressions should yield very accurate results. However, because the time of computation of the definite integrals, ψ_m and γ_m, increases as the cylinder length increases, a limitation is imposed. For long cylinders it is thought that the approach of section 2.6 would prove fruitful. In this method the field of the currents beyond $z = -\ell_1, \ell_2$ is computed and subtracted from the field of the infinite cylinder to yield the approximate solution for the long finite cylinder. This is quite simple in the case of small ka

(section 2.6) but without this restriction the computation becomes more involved. It is thought, however, that this method will yield simpler expressions to compute than the method of section 2.3 in the special case of a very long cylinder.

APPENDIX 1. ANTENNA RANGE

In order to determine the radiation patterns of antennas experimentally, it is necessary to utilize a pattern range which consists, in the most simple case, of the antenna under study in a transmitting state and a pickup antenna which is movable about the transmitting antenna in order to sample the field at the desired points in space. However, for the antennas of interest here, this method must be modified. The reason is that the analytical formulation was carried through for the radiating system in free space. Thus if the radiating system under study is to transmit energy, the energy must be supplied through a transmission line and the induced currents on the line would perturb the field making the measurements inaccurate. Also, the structure which supports the antenna during measurements introduces similar errors.

In order to reduce the errors due to induced currents on the connecting transmission line, the following method was used. The antenna under test is operated in the receiving state. The receiving radiation pattern is measured which is a measurement of the signal received by the test antenna as it is rotated while it is immersed in the field of a transmitting antenna. However, the transmitting and receiving patterns of an antenna are identical (24) so that it is not necessary to distinguish between them. The advantage in using the test antenna in the receiving state arises from the method which can be used to guide the received signal from the antenna without disturbing the fields. The transmitting signal is square-wave modulated at 1000 cps and a detector is mounted inside the test antenna to

detect the received signal. A bolometer was used because of its reliable square law characteristics over a wide range of power. As shown in Fig. A1.1 the bolometer is in series with a small audio transformer and a 1.5 volt bias cell which are contained inside the antenna. The received signal heats the bolometer and the change in resistance varies as the absorbed power. Since the signal is modulated at 1000 cps the current in the bolometer circuit varies at 1000 cps with an amplitude proportional to the received signal. In order to measure this 1000 cps audio signal, it is fed along two special high resistance leads to a tuned amplifier and meter which are distant enough from the antenna to have negligible effect on the fields. The high resistance leads (about 20,000 ohms per foot) disturb the field very little since any impressed field causes negligible current to flow on these leads. To transmit the audio signal as efficiently as possible along these leads, it is necessary to use the audio transformer shown in Fig. A1.1 to raise the impedance levelto a high value to match the leads. 500 μμf feed-through capacitors were used to bring the lead terminals to the same r.f. potential as the test antenna body. At the end of the leads nearest the tuned amplifier an identical audio transformer was used to transform the impedance level back to a low value to match the input of the tuned amplifier. The output of the tuned amplifier is indicated by a meter and gives the amplitude of the received signal.

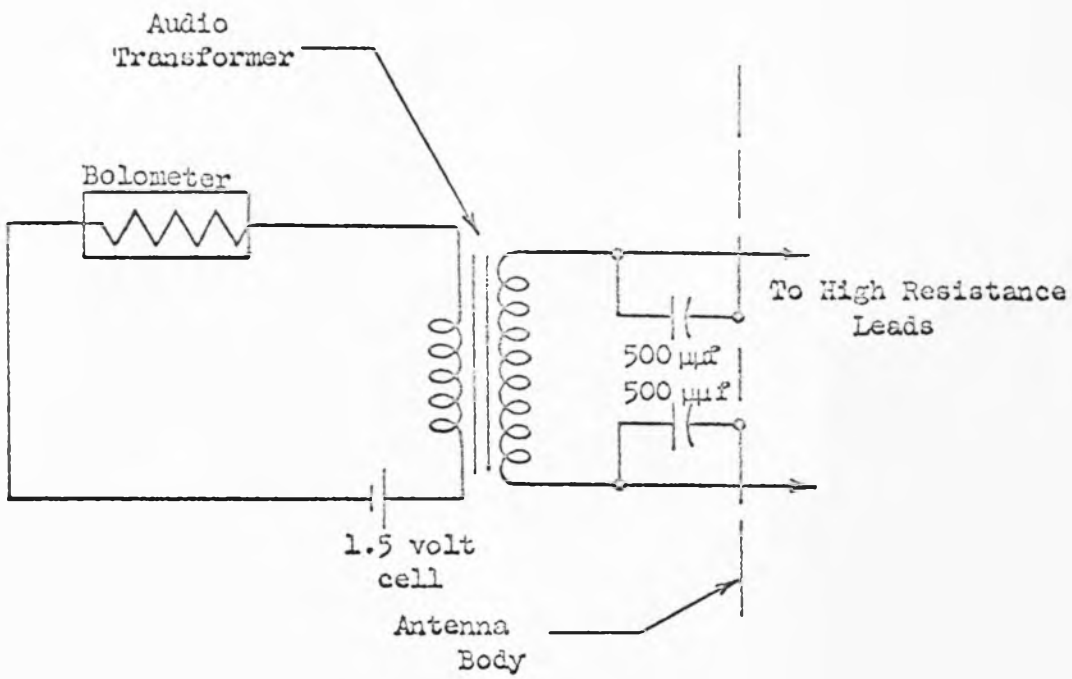

Figure A1.1. Circuit Used Inside Antenna Models

In order to eliminate the disturbance caused by the structure supporting the test antenna as much as possible, the supporting structure was a high tower constructed of polystyrene foam which has a relative dielectric constant of only 1.03. This value of dielectric constant is close enough to that of free space to make reflections from the support tower negligible. The polystyrene foam (styrofoam) construction yields more accurate measurements than the commercially available fiberglass construction because of decreased reflections.

During a pattern measurement the test antenna is placed on the support tower. The base of the tower is fastened to a metal table whose surface can be rotated by a system of gears. The transmitting antenna radiates in the direction of the test antenna at the desired frequency, while the turntable is rotated through the desired range of angle. The table is set at each intermediate angle at which a reading is desired and the signal from the test antenna is recorded. In this way a 360° pattern can be obtained in any particular plane by supporting the test antenna such that the desired plane of measurement is horizontal. A schematic diagram of the range is shown in Fig. A1.2.

To obtain an accurate pattern it is important to minimize reflections from nearby obstacles. For this reason it is desirable to make the measurements in a relatively open location. Thus the range was erected on the roof of a three story building which had no higher buildings in close proximity. Also a large paraboloid with a directional beam was utilized as a transmitting antenna so that the radiated energy in directions other than that of the test antenna is greatly reduced. Thus the energy in the directions of any reflecting

Figure A1.2. Schematic Diagram of Antenna Range

objects and simultaneously the reflected energy is reduced. By means of this method the only important reflection that remains is that from the roof, since the angle to be considered in roof reflection is within the region where the directional properties of the transmitting paraboloid have not reduced the radiated energy sufficiently. However, this reflection was largely eliminated by adjusting the height of the paraboloid and test antenna as shown in Fig. A1.3. Since the curvature of the transmitted wave is large at the roof, geometrical optics may be used, and the ray which would intersect the test antenna is shown. If the direction of this ray is made to coincide with a null of the paraboloid pattern, this source of error is greatly reduced. If θ is the angle of the null from the main beam, this requirement is satisfied if $h = (R/2)\tan\theta$. At a representative operating frequency, 500 Mc, $h = 22'$ which is the height used for the spheroid measurements described in Chap. 5. For other frequencies the null shifts and the height must be shifted accordingly.

The transmitting antenna is shown in Fig. A1.4 and the styrofoam support tower mounted on the turntable is shown in Fig. A1.5. The spheroid is shown under test and the high resistance leads are visible. The tuned amplifier and transformer are beside the turntable.

The transmitting antenna was fed by a commercially available power oscillator whose output is about 20 watts.

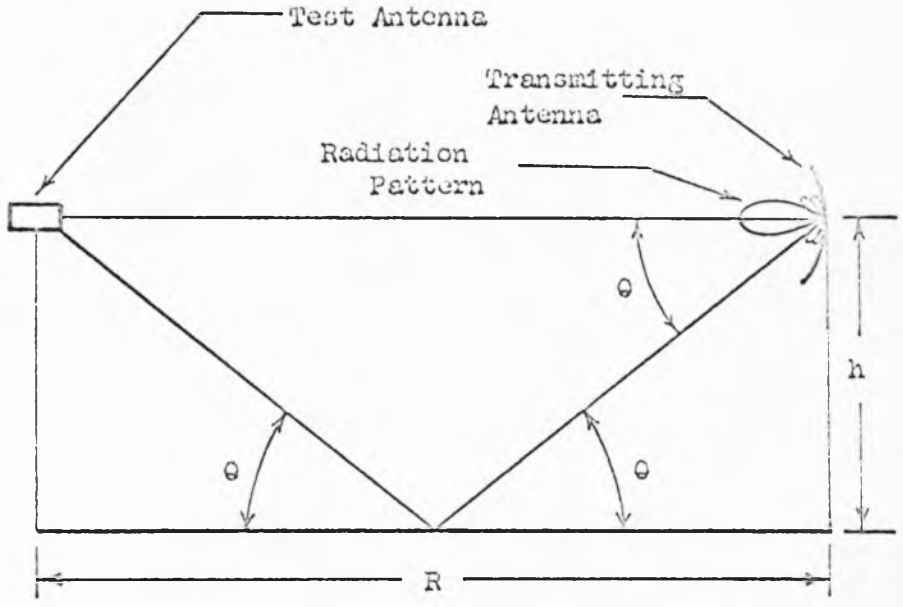

Figure A1.3. Adjustment for Minimum Reflection from Roof

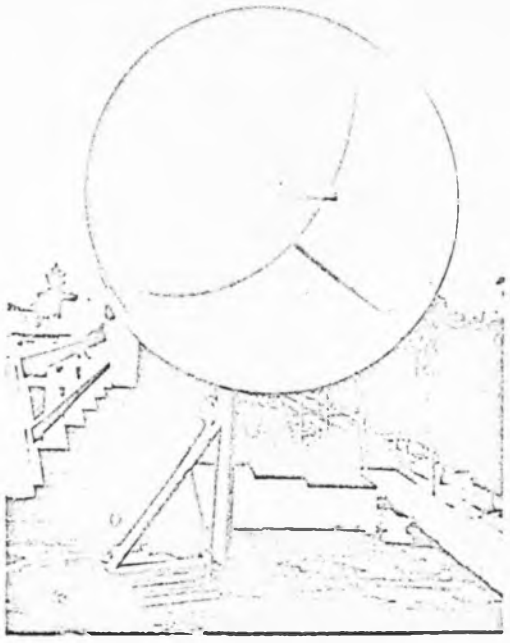

Figure A1.4. Transmitting Antenna

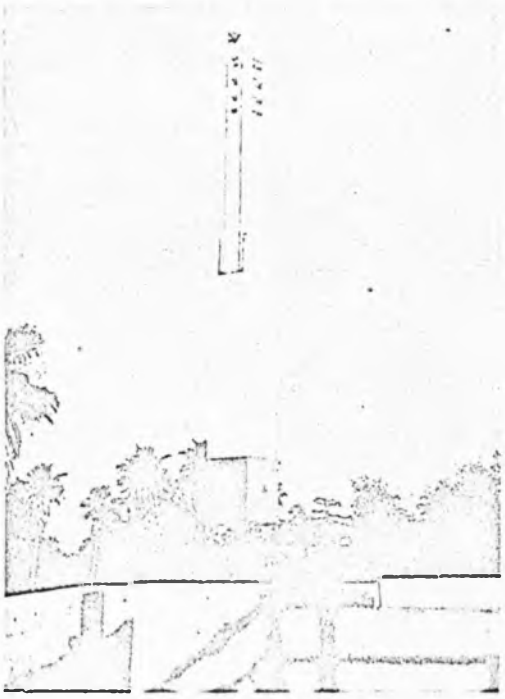

Figure A1.5. Support Tower

APPENDIX 2. COMPUTATION OF ψ_m and γ_m

The quantities $\psi_m(ka,kb,k\ell,k\Delta,\cos\theta)$ and $\gamma_m(ka,kb,k\ell,k\Delta,\cos\theta)$ must be evaluated in order to obtain numerical results from equations 2.64 and 2.77. Evaluation of these two definite integrals enables computation of $E_{\phi TOT}$ and $E_{\theta TOT}$ at any point in the far zone. Because of the difficulty involved in obtaining analytic expressions for these quantities, they were evaluated on a digital computer.

$\psi_m(ka,kb,k\ell,k\Delta,\cos\theta)$ will be considered first. It was evaluated only for the case of the dipole directly at the surface of the cylinder, i.e., $kb = ka$. In the following $\psi_m(ka,ka,k\ell,k\Delta,\cos\theta)$ will be shortened simply to ψ_m. From equation 2.61

$$\psi_m = \int_0^\infty \frac{H_m(ka\sqrt{1-h^2})}{\sqrt{1-h^2}\,H_m'(ka\sqrt{1-h^2})} \left\{ \frac{\cos(k\Delta h)\left[\cos(k\ell\cos\theta)h\sin(k\ell h)}{(h^2-\cos^2\theta)} \right.\right.$$

$$- \frac{\cos\theta\sin(k\ell\cos\theta)\cos(k\ell h)\right] - i\sin(k\Delta h)\left[\cos\theta\cos(k\ell\cos\theta)\sin(k\ell h)}{(h^2-\cos^2\theta)}$$

$$\left.\left. - \frac{\sin(k\ell\cos\theta)h\cos(k\ell h)}{(h^2-\cos^2\theta)} \right\} dh \quad . \qquad \text{(A2.1)}$$

The integrand of equation A2.1 is finite at all points in the region of integration. For brevity define

$$G_1(h,k\ell,k\Delta,\cos\theta) + iG_2(h,k\ell,k\Delta,\cos\theta)$$

$$= \frac{\cos(k\Delta h)[\cos(k\ell\cos\theta)h\sin(k\ell h) - \cos\theta\sin(k\ell\cos\theta)\cos(k\ell h)]}{(h^2-\cos^2\theta)}$$

$$- \frac{i\sin(k\Delta h)[\cos\theta\cos(k\ell\cos\theta)\sin(k\ell h) - \sin(k\ell\cos\theta)h\cos(k\ell h)]}{(h^2-\cos^2\theta)} \qquad \text{(A2.2)}$$

Then equation A2.1 becomes

$$\psi_m = \int_0^\infty \frac{H_m(ka\sqrt{1-h^2})\left[G_1 + iG_2\right]}{\sqrt{1-h^2}\, H_m'(ka\sqrt{1-h^2})}\,dh \qquad (A2.3)$$

For $h > 1$, the argument of the Hankel functions becomes imaginary and modified Bessel functions of the second kind arise. Separating A2.3 into separate integrals over the regions $0 \leq h \leq 1$ and $h \geq 1$, equation A2.3 becomes

$$\psi_m = \int_0^1 \frac{H_m(ka\sqrt{1-h^2})\left[G_1 + iG_2\right]}{\sqrt{1-h^2}\, H_m'(ka\sqrt{1-h^2})}\,dh + \int_1^\infty \frac{K_m(ka\sqrt{h^2-1})\left[G_1 + iG_2\right]}{\sqrt{h^2-1}\, K_m'(ka\sqrt{h^2-1})}\,dh \quad . \qquad (A2.4)$$

The second integral in equation A2.4 is already separated into real and imaginary parts, since $K_m(x)$ and $K_m'(x)$ are real functions of x. The first integral, however, must be separated by using the relation

$$\frac{H_m(x)}{H_m'(x)} = \frac{\frac{m}{x}\left\{[J_m(x)]^2 + [N_m(x)]^2\right\} - \left\{J_m(x)J_{m+1}(x) + N_m(x)N_{m+1}(x)\right\}}{[\frac{m}{x}J_m(x) - J_{m+1}(x)]^2 + [\frac{m}{x}N_m(x) - N_{m+1}(x)]^2}$$

$$- i\,\frac{2}{\pi x\left\{[\frac{m}{x}J_m(x) - J_{m+1}(x)]^2 + [\frac{m}{x}N_m(x) - N_{m+1}(x)]^2\right\}} \quad . \qquad (A2.5)$$

The Wronskian relation

$$J_m(x)\,N_{m+1}(x) - N_m(x)\,J_{m+1}(x) = -\frac{2}{\pi x} \qquad (A2.6)$$

has been used to simplify A2.5. Thus letting

$$\frac{H_m(x)}{H_m'(x)} = F_{1m}(x) + i\, F_{2m}(x) \tag{A2.7}$$

where $F_{1m}(x)$ and $F_{2m}(x)$ are defined in equation A2.5, equation A2.4 becomes

$$\psi_m = \int_0^1 (G_1 F_{1m} - G_2 F_{2m}) \frac{dh}{\sqrt{1-h^2}} + i \int_0^1 (G_1 F_{2m} + G_2 F_{1m}) \frac{dh}{\sqrt{1-h^2}}$$

$$+ \int_1^\infty \frac{K_m G_1}{\sqrt{h^2-1}\, K_m'}\, dh + i \int_1^\infty \frac{K_m G_2}{\sqrt{h^2-1}\, K_m'}\, dh \tag{A2.8}$$

where the argument of F_{1m} and F_{2m} is $ka\sqrt{1-h^2}$ and of K_m and K_m' is $ka\sqrt{h^2-1}$. These integrals were evaluated on a digital computer for various values of ka, $k\Delta$ and $k\ell$. Simpson's rule was used and ψ_m was evaluated for intervals of 7° in θ. The two infinite integrals in equation A2.8 were numerically integrated over the interval $1 \leq h \leq 10$. For $h > 10$ the nature of the functions allows analytic integration. The range of values of θ necessary for a complete determination of the radiation pattern is $0 < \theta < \pi$. However, the values of ψ_m for $\pi/2 < \theta < \pi$ are determined simply from the values in the range $0 < \theta < \pi/2$ because of the manner in which θ enters into equations A2.2 and A2.8. Replacing θ by $\pi - \theta$ in equation A2.2 leaves G_1 unchanged but multiplies G_2 by minus one. Thus if the components of equation A2.8 have been computed for a value of θ, it is necessary only to change the sign of the expressions

involving G_2 to obtain the value of ψ_m at $\pi - \theta$. This reduces the labor approximately in half.

$\gamma_m(ka, kb, k\Delta, k\ell, \cos\theta)$ will now be considered and with $kb = ka$ it will be denoted simply as γ_m. From equation 2.75

$$\gamma_m = \int_0^\infty \frac{h}{\sqrt{1-h^2}} \left[\frac{H_m'(ka\sqrt{1-h^2})}{H_m(ka\sqrt{1-h^2})} - \frac{m^2 H_m(ka\sqrt{1-h^2})}{(1-h^2)(ka)^2 H_m'(ka\sqrt{1-h^2})} \right]$$

$$\times \left\{ \frac{\cos(k\Delta h)[\cos(k\ell\cos\theta)\cos\theta \sin(k\ell h) - \sin(k\ell\cos\theta) h \cos(k\ell h)]}{(h^2 - \cos^2\theta)} \right.$$

$$\left. + \frac{i \sin(k\Delta h)[\cos(k\ell\cos\theta) h \sin(k\ell h) - \cos\theta \sin(k\ell\cos\theta)\cos(k\ell h)]}{(h^2 - \cos^2\theta)} \right\} dh$$

(A2.9)

Letting

$$G_3(h, k\ell, k\Delta, \cos\theta) + iG_4(h, k\ell, k\Delta, \cos\theta)$$

$$= \frac{\cos(k\Delta h)[\cos(k\ell\cos\theta)\cos\theta \sin(k\ell h) - \sin(k\ell\cos\theta) h \cos(k\ell h)}{(h^2 - \cos^2\theta)}$$

$$+ \frac{i \sin(k\Delta h)[\cos(k\ell\cos\theta) h \sin(k\ell h) - \cos\theta \sin(k\ell\cos\theta)\cos(k\ell h)]}{(h^2 - \cos^2\theta)}$$

(A2.10)

equation A2.9 becomes

$$\gamma_m = \int_0^\infty \frac{h}{\sqrt{1-h^2}} \left[\frac{H_m'(ka\sqrt{1-h^2})}{H_m(ka\sqrt{1-h^2})} - \frac{m^2 H_m(ka\sqrt{1-h^2})}{(1-h^2)(ka)^2 H_m'(ka\sqrt{1-h^2})} \right]$$

$$\times [G_3 + iG_4]\, dh \quad . \qquad \text{(A2.11)}$$

This is separated into real and imaginary parts with the final result

$$\gamma_m = \int_0^1 (G_3 F_{3m} - G_4 F_{4m})hdh + i\int_0^1 (G_3 F_{4m} + G_4 F_{3m})hdh$$
$$- \int_1^\infty \frac{h}{\sqrt{h^2-1}}\left[\frac{K_{m+1}K_{m-1}}{K_m K'_m}\right] G_3\, dh - i\int_1^\infty \frac{h}{\sqrt{h^2-1}}\left[\frac{K_{m+1}K_{m-1}}{K_m K'_m}\right] G_4 dh \qquad (A2.12)$$

where

$$F_{3m}(x) = \frac{ka}{x}\left\{\frac{m}{x} - \frac{J_{m+1}(x)J_m(x) + N_{m+1}(x)N_m(x)}{[J_m(x)]^2 + [N_m(x)]^2} - \frac{m^2}{x^2} F_{1m}(x)\right\} \qquad (A2.13)$$

and

$$F_{4m}(x) = \frac{ka}{x}\left\{\frac{2/\pi x}{[J_m(x)]^2 + [N_m(x)]^2} - \frac{m^2 F_{2m}(x)}{x^2}\right\} . \qquad (A2.14)$$

The argument of F_{3m} and F_{4m} in equation A2.12 is $ka\sqrt{1-h^2}$ and of K_{m+1}, K_{m-1}, K_m and K'_m is $ka\sqrt{h^2-1}$. Some of the integrands in equation A2.12 become infinite near $h = 1$ but the integral is finite. Near these points analytic integration is used. The range of γ_m is again $0 \leq \theta \leq \pi/2$ since only G_3 changes sign upon the substitution $\pi - \theta$ for θ .

Numerical values for ψ_m and γ_m were computed on a single computer program since many functions and combinations of functions are identical for each integral. In this way a complete set of values for ψ_m and γ_m can be run in a relatively short length of time.

Because ψ_m always appears multiplied by $mJ'_m(ka \sin \theta)$, the quantity $mJ'_m(ka \sin \theta)\psi_m$ was computed. Similarly the quantity $J_m(ka \sin \theta)\gamma_m$ was computed.

APPENDIX 3. DERIVATION OF THE FIELD FROM E_z AND H_z

It will be shown that all the field components can be determined from E_z and H_z and in particular, equation 2.19 for H_ϕ will be derived. The Fourier transforms with respect to z of Maxwell's two curl equations are

$$\frac{1}{\rho}\frac{\partial \bar{H}_z}{\partial \phi} - i\alpha \bar{H}_\phi = -i\omega\epsilon \bar{E}_\rho \tag{A3.1}$$

$$i\alpha \bar{H}_\rho - \frac{\partial \bar{H}_z}{\partial \rho} = -i\omega\epsilon \bar{E}_\phi \tag{A3.2}$$

$$\frac{1}{\rho}\frac{\partial(\rho \bar{H}_\phi)}{\partial \rho} - \frac{1}{\rho}\frac{\partial \bar{H}_\rho}{\partial \phi} = -i\omega\epsilon \bar{E}_z \tag{A3.3}$$

$$\frac{1}{\rho}\frac{\partial \bar{E}_z}{\partial \phi} - i\alpha \bar{E}_\phi = i\omega\mu \bar{H}_\rho \tag{A3.4}$$

$$i\alpha \bar{E}_\rho - \frac{\partial \bar{E}_z}{\partial \rho} = i\omega\mu \bar{H}_\phi \tag{A3.5}$$

$$\frac{1}{\rho}\frac{\partial(\rho \bar{E}_\phi)}{\partial \rho} - \frac{1}{\rho}\frac{\partial \bar{E}_\rho}{\partial \phi} = i\omega\mu \bar{H}_z \tag{A3.6}$$

where $\bar{H}_z = \int_{-\infty}^{\infty} H_z\, e^{-i\alpha z}\, dz$ and similarly for the other components. These equations may easily be solved for any component of the field in terms of $\bar{E}_z$ and $\bar{H}_z$. For example, by combining equations A3.1 and A3.5 the following equation for $\bar{H}_\phi$ is obtained.

$$\bar{H}_\phi = \frac{i}{k^2 - \alpha^2}\left[\omega\epsilon\frac{\partial \bar{E}_z}{\partial \rho} + \frac{\alpha}{\rho}\frac{\partial \bar{H}_z}{\partial \phi}\right] . \tag{A3.7}$$

Taking the inverse Fourier transform of equation A3.7

$$\frac{1}{2\pi}\int_{-\infty}^{\infty}\overline{H}_{\phi}e^{i\alpha z}\,d\alpha = H_{\phi} = \frac{i}{2\pi}\int_{-\infty}^{\infty}\frac{1}{k^2-\alpha^2}\left[\omega\epsilon\frac{\partial\overline{E}_z}{\partial\rho}+\frac{\alpha}{\rho}\frac{\partial\overline{H}_z}{\partial\phi}\right]e^{i\alpha z}\,d\alpha \quad . \tag{A3.8}$$

Letting $\beta = \sqrt{k^2-\alpha^2}$, equation A3.8 becomes

$$H_{\phi} = \frac{i}{2\pi}\int_{-\infty}^{\infty}\frac{1}{\beta^2}\left[\omega\epsilon\frac{\partial\overline{E}_z}{\partial\rho}+\frac{\alpha}{\rho}\frac{\partial\overline{H}_z}{\partial\phi}\right]e^{i\alpha z}\,d\alpha \tag{A3.9}$$

which is the desired relation for H_{ϕ} . The expression for E_{ϕ} is

$$E_{\phi} = \frac{i\omega\mu}{2\pi}\int_{-\infty}^{\infty}\frac{1}{\beta^2}\left[\frac{\alpha}{\omega\mu\rho}\frac{\partial\overline{E}_z}{\partial\phi}-\frac{\partial\overline{H}_z}{\partial\rho}\right]e^{i\alpha z}\,d\alpha \quad . \tag{A3.10}$$

REFERENCES

1. King, R.W.P., The Theory of Linear Antennas, Harvard University Press, Cambridge, Massachusetts, 1956, 403-407.

2. Morse, P.M., and Feshbach, H., Methods of Theoretical Physics, McGraw-Hill Book Company, New York, 1953, 1782-1789.

3. Carter, P.S., "Antenna Arrays around Cylinders", Proc. I.R.E. 31 (1943), 671-693.

4. Lucke, W.S., "Electric Dipoles in the Presence of Elliptic and Circular Cylinders", Jour. Appl. Phys. 22 (1951), 14-19.

5. Moullin, E.B., Radio Aerials, Oxford University Press, 1949, Chap. IV.

6. LePage, W.R., and Harrington, R.F., and Schlect, R.F., "A Study of Directional Antenna Systems for Radio D/F Purposes", Inst. of Industrial Research, Dept. of Elec. Eng., Syracuse University, Sept. 15, 1949.

7. Harrington, R.F., and LePage, W.R., "Directional Antenna Arrays of Elements Circularly Disposed about a Cylindrical Reflector", Proc. I.R.E. 40 (1952), 83-86.

8. Walsh, J.E., "Radiation Patterns of Arrays on a Reflecting Cylinder", Proc. I.R.E. 39 (1951), 1074-1081.

9. Page, L., and Adams, N.I., "The Electrical Oscillations of a Prolate Spheroid, I", Phys. Rev. 53 (1938), 819-831.

10. Chu, L.J., and Stratton, J.A., "Forced Oscillations of a Prolate Spheroid", Jour. Appl. Phys. 12 (1941), 241-248.

11. Ryder, R.M., "The Electrical Oscillations of a Perfectly Conducting Prolate Spheroid", Jour. Appl. Phys. 13 (1942), 327-343.

12. Page, L., "The Electrical Oscillations of a Prolate Spheroid, II and III", Phys. Rev. 65 (1944), 98-117.

13. Flammer, C., "The Prolate Spheroidal Monopole Antenna", Tech. Report No. 22, Contract AF19(604)-1296, Stanford Research Inst. (1954).

14. Hatcher, E.C.Jr. and Leitner, A., "Radiation from a Point Dipole Located at the Tip of a Prolate Spheroid", Jour. Appl. Phys. 25 (1954), 1250-1253.

15. Myers, H.A., "Radiation Patterns of Unsymmetrically Fed Prolate Spheroidal Antennas", I.R.E. Transactions on Antennas and Propagation AP-4 (1956), 58-64.

16. Stratton, J.A., Electromagnetic Theory, McGraw-Hill Book Co., New York, 1941, 466.

17. Borgnis, F.E., and Papas, C.H., Randwertprobleme der Mikrowellenphysik, Springer-Verlag, Berlin, 1955, 13-24.

18. Papas, C.H., "On the Infinitely Long Cylindrical Antenna", Jour. Appl. Phys. 20 (1949), 437-440.

19. Silver, S., Microwave Antenna Theory and Design, McGraw-Hill Book Co., New York, 1949, 87-90.

20. Jahnke, E., and Emde, F., Tables of Functions, Dover Publications, New York, 1945, 149.

21. Schelkunoff, S.A., Advanced Antenna Theory, John Wiley and Sons, New York, 1952, 102-127.

22. Smythe, W.R., Static and Dynamic Electricity, Second edition, McGraw-Hill Book Co., New York, 1950, 473.

23. Ramo, S., and Whinnery, J.R., Fields and Waves in Modern Radio, Second edition, John Wiley and Sons, New York, 1953, 505-508.

24. Carson, J.R., "A Generalization of the Reciprocal Theorem", Bell System Tech. Jour. 3 (1924), 393-399.